SEISMIC ANALYSIS AND DESIGN OF HYBRID CONCRETE TIMBER STRUCTURES WITH 2015 NATIONAL BUILDING CODE OF CANADA

by

Christopher Gregory Pieper

B.A.Sc., The University of British Columbia, 2014

A THESIS SUBMITTED IN PARTIAL FULFILLMENT OF

THE REQUIREMENTS FOR THE DEGREE OF

MASTER OF APPLIED SCIENCE

in

THE COLLEGE OF GRADUATE STUDIES

(Civil Engineering)

THE UNIVERSITY OF BRITISH COLUMBIA

(Okanagan)

October 2018

The following individuals certify that they have read, and recommend to the College of Graduate Studies for acceptance, a thesis/dissertation entitled:

SEISMIC ANALYSIS AND DESIGN OF HYBRID CONCRETE TIMBER STRUCTURES WITH 2015 NATIONAL BUILDING CODE OF CANADA

submitted by Christopher Gregory Pieper in partial fulfillment of the requirements of

the degree of Master of Applied Science.

Dr. Solomon Tesfamariam, School of Engineering (Civil)

Supervisor

Dr. Shahria Alam, School of Engineering (Civil)

Supervisory Committee Member

Dr. Kasun Hewage, School of Engineering (Civil)

Supervisory Committee Member

Dr. Thomas Johnson, School of Engineering (Electrical)

University Examiner

Abstract

The increasing use of timber for mid to high-rise structures fosters a need for high quality numerical modelling and modelling input parameters for timber and timber hybrid structural systems. Concrete is still a primary building material for mid to high-rise structures; however, designers seek to utilize timber, concrete, and steel to develop innovative structural systems.

Experimental timber connection data was used to validate Pivot hysteretic connection models. Results of validated tension-bolted timber connection parameters for timber column to foundation, timber beam to timber column, and timber beam to concrete core are provided for use with numerical models.

Experimental frame and connection data was used to validate connection and two-dimensional timber frame models. Similarly, results of hysteretic connection models for parametrized timber frame beam to column and column to base lagscrewbolt type connections are provided; as well, the numerical frame models developed demonstrate good agreeance with the experimental data.

Experimental results from full scale shake table testing were used to validate a two-storey concrete core with eccentric timber frame three-dimensional numerical structural model. With limitations noted, results somewhat predict response of the hybrid structure to cyclic ground motion. Critical parameters of hysteretic connection performance, damping, diaphragm stiffness, and core wall cracking are explored.

By extension of the experimental validations, a 12-storey hybrid concrete core timber frame numerical model was developed and analysed with equivalent static force procedure, modal response spectrum, linear response history and non-linear response history analysis. The selection and scaling of ground motions was completed following Method A from the newly released 2015 NBCC guideline; the selected scenario-specific ground motions, required processing, and individual and suite scaling factors are provided for three suites of five bi-directional ground motion pairs. Following Part 4, Division B, Section 4.1.8 of the 2015 National Building Code of Canada, the concrete core was designed for strength and drift using ETABS; further, the tension-bolted timber connections were able to sustain anticipated seismic shaking but not to contribute to the seismic force resisting system.

Lay Summary

Particularly in moderate to high seismic regions, earthquake engineering is required to ensure structures will withstand earthquake shaking without collapse. Seismic structural design has evolved significantly in the past 50 years such that desirable ductile (non-collapsing) failure modes under significantly large earthquakes can be achieved. Even more recently, timber is being viewed as a feasible building material for mid to high-rise structures; therefore, seismic timber and particularly timber hybrid (mixed timber-concrete and/or timber-steel) engineering has become an important topic for both research and professional practise in the analysis and design of structures.

One, two and three-dimensional numerical (computer) models of structures are developed. Experimental data is used to validate each model and results are provided for general use. Finally, experimental validations are extended to linear and non-linear analysis and design aspects of a 12-storey hybrid concrete timber structure following the 2015 national building code of Canada.

Preface

This thesis is original, unpublished work by the author under the supervision of Dr. Solomon Tesfamariam. Experimental results were provided by Dr. Tesfamariam to complete each of the experimental validations.

Table of Contents

List of Tables

List of Figures

Acknowledgements

I would like to acknowledge my supervisor Dr. Solomon Tesfamariam, P.Eng. for providing direction, knowledge, support, and patience throughout my graduate studies. I would also like to thank Mr. Tom Guenther, P.Eng. of Okanagan College and TWG Structural Consultant for guiding me to move forward with a bachelors program the opportunity to practise structural engineering throughout my college and bachelor studies; Dr. Rafiqul Haque, EIT (formerly of University of British Columbia) for his time in sharing his knowledge of finite element modelling techniques and seismic engineering which allowed me to progress through challenging aspects of the experimental validations; Mr. Tim Dunne, P.Eng. and Mr. Doug Clough, P.Eng. of Omega Engineering SA LLP for providing financial support and for the opportunity to grow and practise professionally during my studies; Dr. Stephen Halchuk of Natural Resources Canada for providing deaggregation plots and taking time to address my questions related to seismicity; Dr. Robert Tremblay of Polytechnique Montreal for his time in providing reference material and dialogue related to the selection and scaling of ground motions; The collaborators with Dr. Tesfamariam from the three experimental validation studies carried out in this thesis from which the experimental data was made available; NSERC and the UBC Work Study program for funding which facilitated my most preliminary studies of earthquake engineering and hybrid structures; and, the numerous friends and colleagues who have helped to develop my structural engineering abilities.

I would also like to acknowledge my family for their endless support during this thesis: My mom and dad who have devoted many hours to my family while I studied; my sister who first studied engineering and helped me believe I could as well; my loving children who step-up, provide balance and inspire me; my wife who continually encourages and whole-heartedly believes in me; my in-laws who help with the family while I focus; my grandfather who advocated for me to study engineering.

Without all of their support, this would not have been possible.

Dedication

In commemoration of their tireless support, this thesis is dedicated to my family.

1 Introduction

Modern building codes require numerical (computer) models for seismic design of mid to high-rise structures. The validity of such models is critical to gaining expected performance of constructed structures. Traditionally, concrete and steel structures dominated the mid to high-rise landscape; however, timber is increasingly being included. With the relatively new inclusion of timber in mid to high-rise structures, there is a need to develop accurate timber connection models and analysis techniques to provide both economical and safe designs. With high seismic demand in southwestern British Columbia, an abundance of timber as a construction material and a historical precedent of reinforced concrete (concrete) being used for seismic force resisting (core) systems, seismic structural design of hybrid concrete timber structures has become an important topic for structural engineers practising in this field.

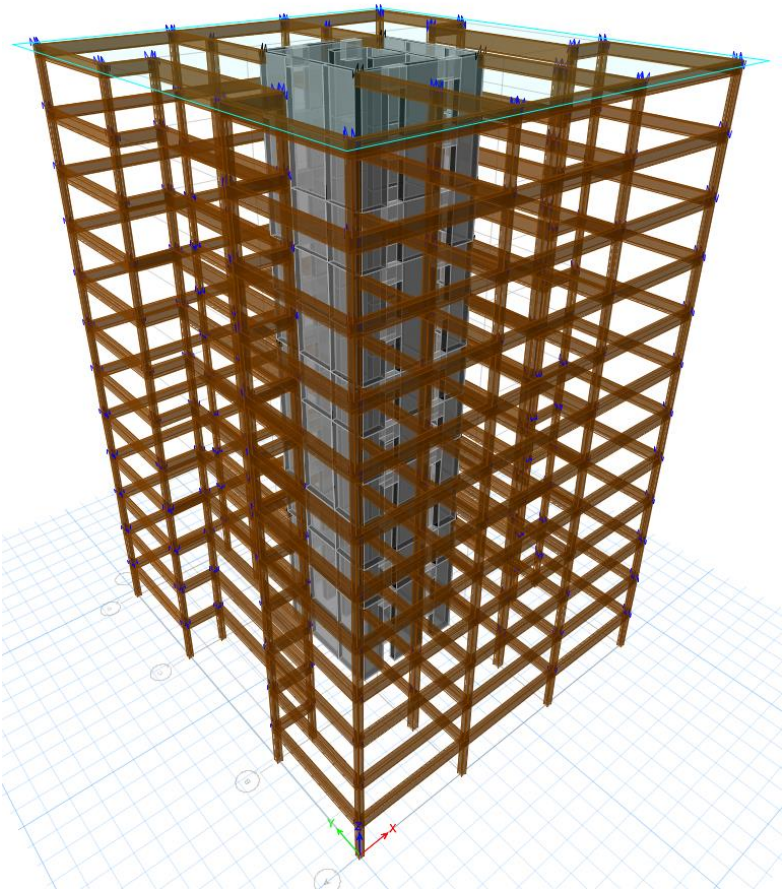

Figure 1-1 12-Storey concrete timber structure

1.1 Objectives

The objectives of this thesis are to:

1. Validate numerical hysteretic connection models, for timber and hybrid concrete timber structures under reverse cyclic loading, with experimental results.

2. Validate non-linear numerical frame models, which include calibrated hysteretic connection models, under non-linear static pushover analysis and reverse cyclic loading, with experimental results.

3. Validate a numerical 3D hybrid structure model, which includes calibrated hysteretic connection models, and variable damping, semi-rigid diaphragm, and cracked core stiffness parameters, to experimental results.

4. Implement the national building code of Canada (2015) to an innovative hybrid concrete timber structure numerical model to determine the effects of the timber frame semi-rigidities on the structural system performance and design criteria

5. Implement calibrated connection models and damping into a code-based study of a 12-storey hybrid concrete timber structure.

6. Implement code procedures for all four analysis types; equivalent static, response spectrum, linear and non-linear response history.

7. Implement the new guidelines for selection and scaling of ground motions.

1.2 Scope

Seismic structural analysis and design aspects are presented for a twelve-storey concrete-core timber-frame structure (see Figure 1-1) based on geometric plan layout and storey heights from comparable structures (MGB Architecture, and Equilibrium Consulting, 2012).

Numerical models of hysteretic connections, frame assemblies and a three-dimensional structure are fitted and validated with experimental data. Also using experimental results, structural modelling techniques are developed and validated connection parameters are presented. Aspects of seismic design are implemented in accordance with the 2015 national building code of Canada.

Recently, shake table tests were carried out and results obtained for a hybrid concrete-timber structure (Isoda, Kawai, Koshihara, Araki, & Tesfamariam, 2016). Presently, the structure does not appear to have been numerically modelled. Similarly, portal frame and timber lagscrewbolt connection testing has been carried out (Mori, Nakatani, & Tesfamariam, 2015) and timber tension-bolt connection testing has been carried out (Isoda et al., 2016; Isoda & Tesfamariam, 2016). Overall finite element models and their specific connection hysteresis models can be calibrated to experimental data which improves both prediction of structural behaviour and overall structural designs.

Experimental results were used to develop the baseline for an extended numerical study of a 12-storey concrete-timber structure.

The experimental validations conducted using ETABS were:

1) One-dimensional study – Pivot connection model parameters are validated for timber and timber-concrete tension-bolt connections using experimental results from reverse-cyclic load tests presented in Isoda and Tesfamariam (2016)
2) Two-dimensional study – Timber portal frames and their connections are validated using experimental results from monotonic static pushover and reverse-cyclic load tests (Mori et al., 2015)
3) Three-dimensional study – A two-storey hybrid concrete-timber structure utilizing the previously fitted tension-bolt connections is validated under lateral ground motion (acceleration) input using available shake table results (Isoda et al., 2016)

The extended study consists of the selected seismic analysis and design procedures for a 12-storey hybrid concrete timber structure following the national building code of Canada (2015) and implementing each of the four prescribed analysis procedures. Further, the concrete core primary seismic force resisting system is designed and influence of semi-rigid timber frames is determined.

A focus on code compliance and proper analysis steps is provided. In the equivalent static force procedure and response spectrum analysis, consideration of stability, torsion, regularity and capacity design are considered. Then, the primary seismic force resisting system is designed for strength and interstorey drift limit. For both the linear and non-linear response history analysis, the new (2015) NRC guidelines are followed to select and scale the ground motions for a three-dimensional simultaneous bi-directional analysis. Results of the linear response history analysis includes bi-directional pairs of major and minor demand for overturning as results from application of 100:30 rule. Results from both linear and non-linear response history analysis are averaged by scenario-specific suite such that design response can be selected based on critical suite(s) at each location.

1.3 Motivations

The primary motivations for this thesis were as follows:

1. Experimental validations of structures

Accurate analysis models are critical to enable creation of designs that are both efficient and safe for structures subjected to seismic loading. Experimental validations require that analysis modelling techniques be refined and provide a check for modelling techniques. With experimental validations not typically available in professional practice, the experimental validations provide an invaluable baseline for numerical modelling of structures.

2. Experimental validations of timber connections

As use of timber has increased in mid to high-rise buildings, various innovative timber connections are being created. Many timber connections are not yet codified and therefore designers must rely on experimental testing and calibration of test data to connection models - which is often not feasible to complete on a project specific basis. By providing connection values for various timber connection models, implementation will be facilitated.

3. Building code provisions and design methodologies

In professional practice, building codes provide structural design requirements. Aside from current and emerging research, the building code generally provides up to date and current state of the art

thinking. The 2015 national building code of Canada (NBCC) and supporting 2015 structural commentaries, including the new guidelines for the selection and scaling of ground motions, are likely to be enacted under a provincial version in British Columbia very soon; therefore, relevant building code provisions must be well understood.

4. New guidelines for selection and scaling of ground motions

While ground motions are typically a geotechnical engineers' responsibility, it is helpful for a structural engineer to have a good understanding of the geotechnical aspects that impact their work. The selection and scaling of historical ground motion records is currently the preferred method in the NBCC (2015) for load input when conducting the increasingly required non-linear analysis of structures.

5. Design of concrete core

Design of concrete core structures is well documented. For this prominent type of hybrid structure (concrete-core timber-frame) to be designed, it is critical for designers to both be able to design the core and determine the influence of the interacting timber components of the primary structural system.

6. Market demand

Climate change science has caused governments to increasingly demand sustainable structures. Further, global trends of urban densification promote construction of mid to high-rise structures. Governments also aim for economic diversification; in Canada, this includes fostering the use of timber and value-added timber products. Development of the timber and hybrid timber structural engineering practise will assist in meeting the emerging market demand.

7. Professional responsibilities

It is incumbent on the professional engineer to maintain current knowledge in the field and promote advances in their area of practice. Hybrid structures represent advances in building technology. Non-linear and code complaint analysis and design is also important as designers must safely design economical, sustainable and often intriguing structures.

1.4 Organization

In Chapter two, the literature review is presented. First, structural materials are discussed. Second, structural components are explored. Third, seismic design considerations are brought to light. Finally, code procedures for analysis and design are reviewed.

In Chapter three, the methodology is presented. A recap of the literature review findings, rational for the experimental validations, and need to proceed to the extended study is explained.

In Chapter four, the case details of each study conducted in the thesis are presented. First, the experimental validations are presented including one, two and three-dimensional studies. Next, the details of the extended study are presented including details of the reference structures and preliminary structural configuration adopted for analysis and design of the 12-storey structure.

In Chapter five, the procedures followed throughout the studies are presented. Each of the one, two, and three-dimensional studies procedures are provided. Next, the procedures followed for seismic analysis and design of the 12-storey structure according to the national building code of Canada (2015) are provided.

In Chapter six, the results are provided. The experimental validation results provide timber and timber hybrid tension-bolt and lagscrewbolt hysteretic Pivot connection parameters. Results of structural model validation are provided for the three-dimensional two-storey hybrid structure. Next, results from the numerical extension to analysis and design of a 12-storey structure are provided. The results come from each of the four prescribed analysis methods of the NBCC (2015) as well as the selection and scaling of ground motions.

In Chapter seven, the conclusions are presented. More precisely, this chapter includes conclusions, recommendations, limitations, and future work. The chapter first looks at the experimental validations then discusses the extended study.

2 Literature Review

This Chapter reviews 1) structural materials, 2) structural components, 3) seismic design considerations, then 4) building code procedures relevant to seismic analysis and design of hybrid concrete timber structures. This review also develops the rational for subsequent analysis and design decisions of the extended study.

2.1 Structural materials

Concrete, timber, and steel are typical materials that form structural systems. Steel is not investigated here except as reinforcing (rebar) in concrete and as connection material for timber. Each material has unique material design standards (CSA - CSA Standards, 2014a; CSA - CSA Standards, 2014b; CSA - CSA Standards, 2014c; Popovski et al., 2014). Reinforced concrete and timber can be used together to form a hybrid component, system or structure. (Abeysekera, 2015; Isoda et al., 2016; Schneider et al., 2015). A unique type of hybrid concrete timber system is a concrete timber composite; research of such composites is ongoing (Dias, 2012; Dias, Van de Kuilen, Lopes, & Cruz, 2007; Hehl, Tannert, Meena, & Vallee, 2014; Khorsandnia, 2015; Yeoh, 2011). Current research aims to identify promising hybrid systems (Abeysekera, 2015; Meleki, Asiz, Smith, Gagnon, & Mohammad, 2011; Schneider et al., 2015; X. Zhang, Fairhurst, & Tannert, 2015) and methods to accurately model hybrid structural systems.

2.1.1 Reinforced concrete

Concrete is strong in compression and weak in tension; therefore, concrete is typically reinforced for tension with steel (rebar). Flexural capacity of a section is developed through the composite action developed between the steel reinforcing and the concrete. Reinforced concrete is as composite material with typical compressive strengths from 25 MPa - 60 MPa; tension capacity of reinforcing is typically 400 MPa - 500 MPa. Reinforced concrete can also have prestressed tendons which can be much higher strength keeping significant tensile strains in steel tendons and out of concrete. Cracked concrete occurs when the cracking modulus is reached and at that point no concrete tensile capacity contributes to the strength and all tension is then carried by the steel.

Cracked concrete is significantly less stiff than uncracked concrete. This idea of cracked effective stiffness is expanded on in the seismic design considerations section.

Reinforced concrete can have a variety of failure modes varying from very brittle to very ductile, depending largely on the detailing of the reinforcing. As there has been much testing of reinforced concrete for seismic design, ductile details are fairly well understood and routinely implemented. One area of reinforced concrete detailing that is still an emerging technology is anchorage. The CSA A23.3-14 still has this section as an annex, not yet mandatory; however, the section does provide guidance and calculations to ensure ductility can be achieved in anchorage zones. Ductile joints, walls, beams, and columns have all been thoroughly tested and proven and they are used as required depending on the structural member being designed. Code prescribed ductility factors (R_d) range from 1.0 to 5.0.

Seismic design of reinforced concrete is fairly well understood (Park & Paulay, 1975). Numerical models can accurately predict global response of reinforced concrete structures (Lu et al., 2015). In capacity designed concrete structures, ductility is achieved by allowing reinforcing steel to yield in preferred locations, creating plastic hinges that will limit degradation of structural stability (Park & Paulay, 1975). Also, concrete can be confined with reinforcement to improve ductility when it is subject to crushing (SeismoSoft, 2014). Reinforced concrete non-linear behavior can be categorized as either shear or flexural non-linear response.

2.1.2 Timber

Timber is anisotropic and hygroscopic meaning the properties vary with grain orientation and moisture, respectively. Timber, as a material, can best be defined along three axes; longitudinal, radial and tangential; however, timber design codes (CSA - CSA Standards, 2014b) do not differentiate between the similar tangential and radial axis.

Timber can see 30 percent expansion radially and/or tangentially to a unit of longitudinal strain; however, transverse strain in the longitudinal-radial or longitudinal-tangential plane results in almost negligible (0.03) longitudinal strain (Green et al., 1999). For typical analysis, Poisson's ratio is taken as 0.3 because primary bending couples and/or axial compressive stresses will generate this type of strain. It becomes increasingly important to consider Poisson's ratio

variability in problems such as timber joinery where intimate wood contact is relied upon for resistance or where unaccounted for wood strains may result in increased stresses that could lead to brittle failures.

Shear modulus of timber in the longitudinal-radial plane is quite similar to that in the longitudinal-tangential plane and is about a sixth of the longitudinal elastic modulus. The shear modulus in the radial-tangential plane is much weaker and is only about 1/50-1/175 of the elastic modulus in the longitudinal direction. While the stiffness is much lower in this direction, this plane does not typically present a brittle failure mode. Shear in the radial-tangential plane would intersect the wood fibres and result in wood crushing whereas shear in the other two planes would result in slip between adjacent wood fibres which typically results in a brittle failure mode. Another potential failure mode is rolling shear where wood fibres roll relative to one another under transverse shear.

Raw harvested timber has inherent variabilities. If a high grade of timber is desired, glue laminated or other engineered wood products can be used to allow poor material to be removed and more consistent quality materials to remain.

A distinction between light wood framing compared with heavy and mass timber is made. Light wood framing covers the typical plywood or oriented strand board (OSB) and dimensional lumber framing systems including light wood frame trusses and I-joists, typical for residential and other low to mid-rise structures. Heavy timber typically refers to post and beam systems that are usually either sawn timber or glue laminated or structural composite lumber. Mass timber typically includes panelized products such as nail laminated timber, cross laminated timber or other panelized structural composites. This study of hybrid concrete timber primarily focusses on mass and heavy timber systems coupled with concrete as primary lateral system components; however, one study includes a plywood diaphragm which falls into the light wood framing category.

Timber failure modes can be brittle under tension parallel to grain, tension perpendicular to grain, and shear parallel to grain (CSA - CSA Standards, 2014b); therefore, timber connections, rather than the timber itself, are typically desired to be primary sources of ductility (Braconi et al., 2007; Fragiacomo, 2003; Ibarra et al., 2005; Schneider et al., 2015; Shen et al., 2013).

A high strength to weight ratio (FP Innovations, 2012) and increased damping characteristics (Booth & Key, 2006) are advantageous for timber in seismic design. Ongoing research investigates different types of wood materials including sawn (Chang et al., 2009), glue laminated (Popovski et al., 2014), cross laminated timber (Yasumura, et al., 2015), nailed shear walls (Li et al., 2014), and light wood framed diaphragms (He et al., 2011; C. Zhang, 2015). Code prescribed ductility factors (R_d) range from 1.0 to 3.0 for wood framed systems.

2.2 Structural components

Specific structural components of a building work together to form a primary structural system which carries the gravity and lateral loads. Lateral loads, particularly seismic induced lateral loads are the focus of this study. Under seismic loads, specific components and areas of a structure are designed to yield. Different seismic force resisting systems have unique costs and benefits. For example, greater ductility reduction values typically require more effort during construction. Also, components not part of the seismic force resisting system still require consideration with regards to seismic design; therefore, the desired structural components, and the desired seismic force resisting system structural components should be carefully selected.

2.2.1 Foundations and anchorage

Foundations and anchorage must be adequately designed and detailed, typically with reinforced concrete, to transfer earthquake forces safely to the soil from the structure. For simplicity of potential repair requirements, plastic hinges are often left to only form in the wall system, maintaining an elastic foundation (Boivin & Paultre, 2012); however, foundation components, such as a core wall extending into a basement, would still be subject to the ductile detailing requirements of the SFRS above. Force controlled foundations or foundations designed for the overstrength of their supported SFRS with capacity design principles may end up nearly twice as thick as those designed only for seismic design force requirements (Klemenic et al., 2007).

A special study and other specific measures (NRC - National Research Council Canada, 2010) may be required to better understand the interaction between the supporting soils and the foundation and to satisfy the design criteria as outlined in Part 4 of NBCC (2015). Non-linear foundation to soil interaction may need to be explicitly considered. Foundation-soil non-linearities

may include influences from both soils to footing and foundation to core. These non-linear influences may be modelled with a foundation system which includes a rotational spring under core elements, and a rotational and axial spring under basement walls (CSCE, 2008).

Foundations and soil interaction can play an important role in the performance of structures, including consideration of whether to allow a foundation to behave more as a pinned base or fixed. A footing which acts more as if were on pinned base supports has historically been referred to as a rocking footing (Ventura, 2005). A rocking footing may reduce the force demand on a structure but also increase drift. No rocking in the foundation is typically considered because the soil is stiffer than the structure (Klemenic et al., 2007) and because many typical foundations will be constrained in some way (Canadian Commission on Building and Fire Codes National Research Council of Canada, 2015). Rather than rocking, foundations designed to CSA A23.3-14 are currently classified as either capacity protected (fixed) or not capacity protected (rocking). Foundations must be designed to remain elastic based on the capacity of the seismic force resisting system (SFRS) unless specific detailing is provided to permit ductile rocking (Canadian Commission on Building and Fire Codes National Research Council of Canada, 2015). Soil interaction is typically covered in design by implementing site specific criteria that can be determined based on geotechnical investigation.

In this study, implementation of site criteria rather than soil interaction will be carried out; no special consideration of soil interaction is given beyond creating a site-specific response spectrum. It is assumed that the foundation will provide a rigid base for the structure. The foundation and anchorage design have been left for future study. Foundation displacements would need to be added to the design drifts to determine if the superstructure design, coupled with the foundation design, are to meet the performance criteria stated in the building code.

2.2.2 Timber frames

Timber sections are difficult to fix at the ends compared to leaving them with pin-end boundary restraints except where they are continuous through multiple storeys. If fixing at ends is required, timber will typically require some embedment into concrete or substantial steel fasteners. Timber composite beams have been achieved with studs, screws, steel mesh or groove type connections

(Zhang et al., 2015). Timber in tension is a brittle failure mode and care must be taken to ensure the capacity is not exceeded. Timber beams should be detailed to provide energy dissipation at the connections.

In analysis of structures, if timber frame semi-rigidity increases the overall system stiffness by more than 15 percent they must be included in the determination of the fundamental period; whereas, if they are less than 15 percent, their contribution may be omitted. Two models must be used to compare and determine whether semi-rigid timber frames should be included for period calculations and to see if their performance helps reduce overall system requirements. Note that even if they are not part of the SFRS, they still must be able to undergo system deformations that are expected to occur during and after a design seismic event. Overstrength (R_o) and ductility (R_d) factors for moderately ductile timber frames designed and detailed in accordance with CSA O86-14 are $R_d = 2.0$ and $R_o = 1.5$. The intent of inclusion of semi-rigidity of timber frames in this study is to see the impact of these frames and determine the most appropriate way to consider their contribution (if any) to the SFRS.

2.2.3 Timber floor diaphragms

Diaphragms can be classified as rigid, flexible, or semi-rigid. Their classification impacts analysis procedures, design requirements, and performance expectations. A rigid diaphragm may be an appropriate assumption for a CLT floor system which is fairly stiff and may further have a concrete topping; however, depending on the stiffness of the supporting shearwalls and connection detailing, this may not always hold true. A flexible diaphragm would typically be considered if a light wood framed diaphragm assembly is used without concrete topping (CSA, 2014), again depending on the stiffness of supporting shearwalls. Detailed consideration of flexible plywood diaphragms is provided in (Kleven & Noras, 2011). A semi-rigid diaphragm may be appropriate classification for a CLT floor diaphragm; however, the computational efficiency is significantly reduced when semi-rigid diaphragms are applied to a structural model (Computers and Structures Inc., 2016).

Plywood and oriented strand board (OSB) diaphragms provide some rigidity. Envelope approaches are recommended when stiffness cannot be accurately determined due to finishing such as concrete

toppings or ceiling materials. CSA O86-14 provides deflection equations for blocked shearwalls (cantilevered vertical diaphragm) and simply supported horizontal diaphragms. These mechanics-based approaches include contributions from chord elongations and slip, hold down slip, bending, nail slip and panel shear (Association of professional engineers and geoscientists of British Columbia (APEGBC), 2015). It is not typical to include the complexities of nailing and individual panels into finite element models; however, Woodworks Shearwalls software for example will capture this level of detail in structural models. Finite element models often use envelope approaches, diagonal strut simplifications or other equivalent stiffness approaches. One approach endorsed by the Canadian Wood Council is to follow ASCE 41-13 guidelines which define the flexible versus rigid cut-off as when the maximum diaphragm deflection is more and less than twice the average displacement of supporting vertical elements, respectively.

Diaphragm classification impacts design procedures for torsional response (NBCC, 2015). Torsional response is increased with rigid compared to flexible diaphragms. As rigidity of a floor system increases, force imparted on connections typically increases. Diaphragms can be designed for inelastic performance but typically rigid diaphragms are not designed to yield. Classification of concrete topped diaphragms may be affected by detailing of the topping. Adequate separation should be provided to allow movement of the diaphragm or the topping must be designed to form a part of the diaphragm. When concrete is added or the timber floor is of mass timber, the floor system may be considered rigid (Isoda et al., 2016).

Mass timber floor products include nail laminated, cross laminated and structural composite lumber panels. For nail laminated floor systems, a rigid diaphragm model coupled with a flexible diaphragm approach to provide an envelope approach to lateral force distribution to vertical SFRS elements is prudent but may be overly conservative so engineering judgement may still be required to determine design forces (Binational Softwood Lumber Council, 2017). As the diaphragm forms a part of the seismic force resisting system, internal diaphragm stresses must be calculated and designed for as elastic components. Diaphragm to column connections must be checked to ensure adequate overstrength is present to facilitate yielding of ductile components.

2.2.4 Shear walls

Shear walls can be constructed of reinforced concrete or timber elements. Where timber-based shear walls are used, energy dissipation can occur within the shear wall boundary connections (Schneider et al., 2015) (along with in the panel nailing in light wood framed shearwalls). For timber shearwalls, boundary connection energy dissipation is desirable; however, current connection materials would likely need to be repaired or replaced after a major event (Fragiacomo, 2011). Concrete shear walls may be better suited to taller structures where drift is a concern because lateral displacement of a structure will be decreased when stiffer concrete shear wall elements are included.

Concrete shear walls may have elements designed as piers, and spandrels. Analysis can vary depending on if coupling, or partial coupling of piers is allowed and how involved of an analysis method is used. The design methodology is analogous to slab edge-spandrel (L) or slab band (T) beam design, where effective flanges of piers are considered in the design. Note the distinction in terms that a spandrel in lateral core design is the lintel or coupling beam between two shearwalls; whereas, a spandrel in gravity design typically refers to a slab edge (L) beam. Cantilever concrete wall piers can be designed and detailed for seismic loading using ETABS (Computers and Structures Inc., 2015) and design algorithms for CSA A23.3-14 are included in their shearwall design manual (2015) to check the calculations. Wall ductility is directly related to the vertical length of the plastic hinge, the horizontal length of the flexural compression zone, and the compression strain capacity of the concrete (Adebar et al., 2005). Concrete core non-linearities develop due to excessive strain in either material; the reinforcing steel or the concrete.

Appropriate modelling of concrete shearwalls may be achieved with link or fiber models. A concrete shearwall fiber model may include multiple layers for reinforcing along with in-plane shear and out of plane stiffness concrete layers, additional refinement of fibers near higher stressed wall ends, out-of-plane bending stiffness reduction to 0.33EI, updated elastic shear properties with assigned strengths, 25 percent increase for steel strain hardening, and 20 percent increase for concrete compressive strength (f'_c) due to confinement and other strengthening effects (CSCE, 2008). With a link model, automatic hinge properties can be defined according to ASCE 41 (Computers and Structures, 2015a).

2.2.5 Coupled shear walls

Coupled cantilever shear walls are cantilever walls connected by coupling beams. The coupling of shearwalls induces opposing axial forces in coupled cantilever shear wall segments; the coupling beam (also referred to as a spandrel or lintel) is the beam that induces these forces. The degree of coupling ratio is established based on total system rotational resistance divided by the resistance provided by uncoupled walls alone. The degree of coupling impacts the design ductility and overstrength criteria. Coupled walls are stiffer than individual piers but not as stiff as solid walls. Coupled walls are typical where door openings are required, such as in elevator cores. Diagonal reinforcement is often used within the coupling beams to resist the large shear forces at beam ends. Coupling beams with diagonal reinforcement have at times been found to be difficult to implement in practice; as well, challenges with confinement of diagonal coupling beam reinforcing exist (Klemenic et al., 2007). Quantifying elongation of diagonal coupling beam reinforcing for transient coupling effects is important in some situations (Fox et al., 2014).

Design considerations include, beam to wall strength ratios, sequence of hinge formation, and inelastic shear deformation of wall elements composing a wall system (Boivin & Paultre, 2012). Consideration should also be given to displacement compatibility criteria to determine the sequence of yielding and to provide a coupling beam stiffness of about 20 percent (Paulay, 2001).

One method to model coupling beam components includes definition of rigid end zones, shear hinges (displacement type elements to model inelastic deformation of the coupling beam with energy degrading hysteresis loops), and a vertical embedded beam element to transfer the coupling beam moment to the wall (CSCE, 2008). Coupling beam compressive strains are often underpredicted in NL-TH analysis so care in specifying ties for compression reinforcement is required (Klemenic et al., 2007). Coupling beams may be modelled as frame elements, in which case zero-length plastic hinge element equivalent to plastic hinge length for the beam-column assembly may be used (Mousseau et al., 2008). Alternately, a designated length of plastic hinge can be defined which helps to provide computational efficiency in some circumstances. Both zero and finite plastic element length are preferred to a complex diagonally reinforced fiber model approach (Wallace, 2012).

2.2.6 Non-components – components not part of the SFRS

Components not part of the seismic force resisting system (SFRS) either need to have sufficient clearances to allow design drifts to occur without being influenced by the non-SFRS components or the components must be able to serve their function during and after design drifts have occurred. The timber connections validated in this thesis are an example of a connection that are able to undergo significant drift and cyclic loading while maintaining some strength and stiffness. The lack of separation of the timber beams to the SFRS means that the timber frames must be able to maintain their function for gravity loads during and after predicted seismic induced displacements. There is an option to include the timber components in the SFRS; however, the decreased R_d and R_o factors will result in higher design forces. The higher forces would be required because NBCC requires the lowest R_d and R_o within the system, at location of interest, be used. This is where the force-based design methodology of the NBCC does not account for unique system interaction and provides a reason why studies of hybrid SFRS systems should be carried out. Other non-components would include the remainder of the gravity system and structural components that are not part of the primary structural system.

2.3 Seismic design considerations

In order to carry out appropriate analysis and design of the hybrid structure, specific seismic design considerations were investigated

2.3.1 Ductility and overstrength

Ductility (μ) is the measure of absolute maximums of elasto-plastic displacement (δ_u) divided by the yield deformation (δ_y) as shown in equation (2-1)

$$\mu = \frac{\delta_u}{\delta_y} \tag{2-1}$$

Ductility is the primary reason for reduction of earthquake design forces. A structure that is ductile will dissipate energy through non-linearity. This significantly reduces the force demand by applying the equal displacement rule (for low to mid-rise structures) and reducing the force applied but increasing the displacement incurred. Careful detailing is required to ensure ductility.

The experimentally verified timber frames of this thesis may be used as part of the SFRS if ductility and overstrength factors (R_d, and R_o) are adjusted from those of the concrete core. The appropriate R_d and R_o factors form a bit of a debate. The closest NBCC provided R_dR_o factors may be those that are designed and detailed in accordance with CSA-O86 classified as moderately ductile moment resisting frames with ductile connections. The timber frames are classed as much less ductile system compared to the central concrete core wall system ($R_d = 4$ compared to $R_d = 2$). It is not expected that including the stiffness provided by the perimeter timber frames will be sufficiently useful to warrant inclusion as part of the SFRS due to the required increased design seismic force on the structure as a whole; however, this will be explored. A fairly current resource for determining R_dR_o is FEMA 695 (Applied Technology Council, 2009).

2.3.2 Structural irregularity

Structural irregularity is classified and separated into nine types in the 2015 national building code of Canada. Each principal direction may exhibit a particular type of irregularity but not necessarily will both directions have the same irregularities. Assumptions and unknowns regarding irregularity are confirmed during the analysis and design procedures; however, to discuss by example how irregularity impacts a structure, initial consideration for the structure of the extended study (as shown in Figure 1-1) is provided as follows:

Type 1 – Vertical stiffness irregularity. The core walls (both coupled and uncoupled) have uniform vertical geometric characteristics. This means that as long as wall depth reductions are not too drastic moving towards the top, we should be able to meet the 70 percent of adjacent storey and 80% of adjacent three stories restrictions. Initial classification: Regular.

Type 2 – Weight (mass) irregularity. Our floors do not have weight irregularities and the slightly lighter roof need not be considered. Initial classification: Regular.

Type 3 – Vertical geometric irregularity. The 130 percent benchmark will not be exceeded because the horizontal dimensions of the shearwalls are equal moving through storeys and the storey heights are equal. Initial classification: Regular.

Type 4 – In-plane discontinuity in vertical lateral-force-resisting element. This does not exist since the SFRS is directly stacked. Initial classification: Regular.

Type 5 – Out-of-plane offsets - No out of plane offsets exist. Initial classification: Regular.

Type 6 – Discontinuity in capacity – weak storey. Since the capacity will only (if at all) decrease moving up, there are no weak storeys. The foundation design must account for the strength of the lowest storey or the foundation may become the weak storey. Initial classification: Regular.

Type 7 – Torsional sensitivity (to be considered when diaphragms are not flexible). With core wall structures (such as the one in this study), torsional sensitivity often exists even if the center of mass is reasonably well aligned with the center of rigidity. The torsional response occurs as a result of eccentricities. Once further analysis is done, the parameter B will be calculated in accordance with 4.1.8.11.10) NBCC, and if it exceeds 1.7, then then Type 7 irregularity would exist. Initial classification: Regular but pay attention for change in classification.

Type 8 – Non-orthogonal systems. Our SFRS systems in each principal direction are orthogonal; therefore, Type 8 irregularity does not exist. Initial classification: Regular.

Type 9 – Gravity-induced lateral demand irregularity. This irregularity type is newly introduced in the NBCC (2015). Essentially it reads as though inclined columns or floor cantilevers, if significant, can cause the structure to shake more in one direction than the other. This may result in increased drifts and likelihood of failure. Checks are further described in NBCC (A) - 4.8.10.5). This structure does not appear to have this type of irregularity. Initial classification: Regular.

2.3.3 Torsion

Torsional aspects can be classified into two general categories; 1) natural (inherent) torsion which is the eccentricity between center of mass and center of resistance or rigidity (plus dynamic amplification), and 2) torsional moments due to accidental eccentricity. If the parameter B is less than the limit of 1.7, equation 4-18 can be applied with the equivalent static force procedure; however, if the limit is exceeded, a dynamic analysis is required.

The center of mass must be calculated. For a reasonably symmetric structure, the center of mass is expected to be near the centroid in both x, and y coordinates. The center of rigidity must also be calculated. This is done by calculating individual SFRS component stiffness's and combining them in such a way that all the deflections are compatible.

The approach to include the effects of accidental torsion depend on whether the structure is torsionally sensitive or not. If B≥1.7 (torsionally sensitive): Two options exist in accordance with 4.1.8.12.(4)(a) NBCC 2015.

1) Shift the centres of mass of each diaphragm by $\pm(0.10)D_{nx}$ then superimpose the additional forces due to torsion to the unrestrained 3D model forces. Then, take the maximum values as elastic: storey shears, storey forces, member forces, and deflections.
2) Use the torsional moments calculated from the equivalent static force procedure but scale them by (R_dR_o/I_E) then superimpose them on the unrestrained 3D model. Then, take the maximum values as elastic: storey shears, storey forces, member forces, and deflections.

If B≤1.7 (not torsionally sensitive): The approaches presented for torsionally sensitive structures are still allowable; however, a shift by only $\pm(0.05)D_{nx}$ is required. Cases including those with centres of mass un-shifted (only natural torsion exists), centres of mass (cm) shifted by $\pm(0.05)D_{nx}$, and cm shifted by $\pm(0.10)D_{nx}$ are analysed in this study.

2.3.4 Stability

P-delta effects are those effects that cause lateral demand on a structure due to gravity loads. P-delta effects need to be accounted for in the design. Methodologies available are prescribed by the 2015 NBC. When gravity loads are also eccentric loads, P-delta effects increase significantly. P-delta effects cause a negative slope on a force displacement plot which can lead to structural instability if not effectively accounted for. Application of the stability coefficient (up to the maximum limit of 0.4 prescribed by the NBCC (2015) is intended to ensure the force demand does not exceed that of the resistance capacity, considering P-delta effects.

The relevant NBCC load combination for determining P-delta effects for seismic is given as

$$Case\ 5 = 1.0D + 1.0E + 0.5L + 0.25S + (1.0C\ if\ Crane\ exists) \quad (2\text{-}2)$$

Following the recommendation of Filliatrault et al. (2013), the average displacements for the P-delta check are to be considered (rather than the maximum); however, averages do include static torsional effects.

Subclause 4.1.8.3.(8).(c) of NBCC (2015) requires sway effects due to interaction of gravity loads with the displaced configuration of the structure to be included in the analysis. The NRC Commentary (NRC, 2010) provides a stability coefficient that can be checked to determine if P-delta effects can be ignored, shall be included, or if the structure is dynamically unstable. If the stability coefficient at any level is less than 0.1, P-delta effects can be ignored at that level. If the coefficient is greater than 0.4, the structure must be redesigned due to dynamic instability. The stability coefficient (θ_x) equation, for each level, is provided as

$$\theta_x = \frac{P_x \Delta_x}{R_o V_x h_{sx}} \quad (2\text{-}3)$$

The axial load, at the specific level, under the specified combination (P_x) is multiplied by the code specified drift limit (Δ_x) and is divided by the product of overstrength (R_o), shear force above and including at that level (V_x), and the storey height (h_s).

Notional loads (N_x) are those caused by initial material, section, and erection imperfections. The steel design code requires that they be considered but concrete and timber codes currently do not. As a hybrid structure, perhaps notional load inclusion would be prudent though it has not been extensively investigated for this study. Note that the concrete design standard does specify a minimum eccentricity for column loads (CSA - CSA Standards, 2014a); and the timber code also requires that eccentricities be considered (CSA - CSA Standards, 2014b). A typical value of eccentricity for a timber gravity loaded component would be 1/6 of the member width (Canadian Wood Council and American Wood Council, 2016). This eccentricity of members influence on global response is not investigated in this study. Notional loads (N_x) may be calculated as

$$N_x = 0.005(P_x - P_{x-1}) \quad (2\text{-}4)$$

By including notional loads separately and P-delta effects through the stability coefficient, structural stability is increasingly addressed.

2.3.5 Seismic weight

Weights of the various known superimposed loads and expected component self-weights are tallied in accordance with Sentence 4.1.8.2 NBCC (2015); including, 60 percent of the storage load, 25 percent of the snow load, and partition loads of 0.5 kPa (half the gravity design value). The weights are typically lumped at floor levels. The lowest storey requires some additional consideration because if the lower half of the lowest storey is lumped at the ground level, some weight and resulting base shear is not captured. This is more important, yet still often neglected, with heavy construction such as concrete or masonry (Drysdale, 2014); whereas, for a timber structure the lowest half storey of shear may be more appropriate to neglect due to its relatively low weight and increased flexibility.

2.3.6 Damping

Damping parameters need to be used with caution since there are many types of damping. Some types of damping include hysteretic, acoustic coupling, energy radiation, and viscous, to name a few (Irvine, 2016). Typically, for steel and concrete structures a damping value of five percent is a good initial estimate (Booth & Key, 2006; Irvine, 2016) and for timber, it can often be found to be much higher (Booth & Key, 2006). For a linear analysis, five percent damping is often what structural design codes are based on (NRC - National Research Council Canada, 2010).

A suitable damping model could be the initial stiffness-based Rayleigh damping which is specified at both first mode and mode number equal to N (Boivin & Paultre, 2012). There are varying degrees of damping that can be experienced by concrete structures. Damping is reduced with prestressing forces and increased with cracking of concrete (Booth & Key, 2006). A minimum value of 2.5 percent is recommended for tall buildings which typically have lower values than low to mid-rise buildings (Los Angeles Tall Buildings Structural Design Council, 2017).

For a non-linear response history analysis, damping may be calibrated experimentally from a structure, such as the one in the three-dimensional study in this Thesis; otherwise, damping is often set to two percent but should not exceed three percent of critical as per the NRC structural commentary (2015).

Experimentally monitored values have been found to be between one and two percent (Boroschek & Yanez, 2000). In this Thesis, for the shake table, three-dimensional experimental validation, the hybrid concrete-timber structure with prestressing tendons, minimally cracked concrete, and otherwise unfinished, damping was found to best fit near 2.2 percent (see Section 6.1.3, Three-dimensional study, page 95). Based on the upper/lower bound limits described and the experimental results noted, a reasonable definition of damping for a non-linear analysis of a mid-rise concrete-core hybrid structure is between two and three percent.

2.3.7 Hysteresis

Hysteresis measures energy dissipation of a system by tracing load displacement or moment rotation during cyclic loading. Typically, hysteresis is used at connection level but it can also be used at a more global level. The area within the hysteresis trace equals the energy dissipated. Energy dissipation is important in design of structures because energy dissipation reduces force (load) demand on the system.

Hysteresis plots help analysts quickly identify hysteretic behaviour of the component; stiffness, yield, plastic, and ultimate limits can be identified as well as degradation of stiffness through repeated cycles. Compressive versus tensile behaviours are readily distinguished. Hysteretic performance can be captured experimentally (Schneider et al., 2015) then numerically modelled to represent actual connection behaviour. To numerically model hysteretic behaviour, researchers use several different software packages such as SAP2000 (He et al., 2011; Meleki et al., 2011), OpenSEES (Shen et al., 2013), SeismoStruct (Latour & Rizzano, 2015), and MARC.MSC (Xu et al., 2009). When experimental results are well matched to a hysteretic model, the confidence of the hysteretic model is improved.

Starting with the most basic and increasing in complexity, some prevalent hysteretic models are reviewed. An elastic hysteresis model would simply follow a backbone curve over repeated cycles. This type of hysteresis acceptable only for elastic design. A kinematic hysteresis model allows loops to be formed. These loops indicate plastic deformation and energy dissipation. A degrading hysteresis model provides reduction of strength and stiffness over subsequent load cycles. The Takeda model allows for pinching. The Pivot model in and Pinching4 models provide similar pinched, degrading trace capabilities (see Figure 2-1 (a) and (b), respectively).

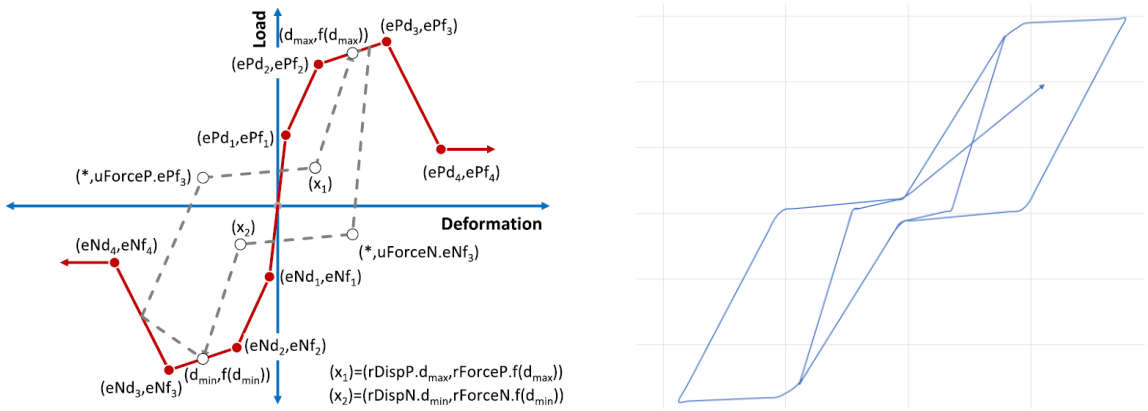

Figure 2-1 Hysteretic connection models (a) Pinching 4 [(Isoda & Tesfamariam, 2016) © with permission from ASCE]; (b) Pivot hysteresis segment from ETABS

The combined effects of plastic deformation are captured by hysteretic models such as the Pivot Hysteresis in ETABS and Pinching4 in OpenSEES. The Pinching4 model (Lowes et al., 2004) can show good agreement for hybrid timber structure connections and timber connections (Schneider et al., 2015) particularly when the ductility is expected to primarily occur in the timber and the connector. Calibration values have been provided for some hybrid systems such as timber infill frames using Pinching4 (Schneider et al., 2015; Shen et al., 2013).

Pinching in hysteresis is often recognized in timber systems. A cause for this behaviour is the plastic deformation of wood. For example, in a nailed shear wall system, the nails will yield and the wood will crush around the nails. The nails yielding is generally captured by a degrading model; however, the wood crushing causes a loss of stiffness near the origin. This loss of stiffness is due to the wood being fully crushed and not providing any load resistance within some region under a subsequent load cycle. If timber is undergoing plastic deformation, the hysteretic model chosen should include this pinching feature. Similarly, reinforced concrete exhibits pinching behaviour; as steel reinforcement yields, concrete can crush locally and reinforcement can slip.

By using hysteretic connection models, a numerical structural model can capture the overall picture of what is going on at specific connections without having to worry about capturing all the details. A limitation of this approach is that different failure modes are not separately input and assessed; proper connection design and detailing must be provided to ensure hysteretic behaviour

and subsequent failure modes are compatible. Pivot hysteresis is implemented with ETABS in this study.

2.3.8 Capacity design

A strength hierarchy should be established for failure modes to ensure that the yielding elements are able to provide the non-linearity required to provide adequate energy dissipation such that the forces to be resisted by the structure can be reduced by corresponding ductility and overstrength factors (R_d, R_o). The basic strength hierarchy or capacity design principles include prevention of shear, anchorage or other brittle failures, maintaining stability of the system once plastic hinges form, and protection of brittle regions of the system by ensuring their strength is greater than the load that could be imposed by yielding members (Park & Paulay, 1975; Paulay & Preistley, 1992). Material standards for both concrete and timber require that capacity design principles be followed (CSA - CSA Standards, 2014a; CSA - CSA Standards, 2014b). By designing and detailing specific elements and connections to behave in a ductile manner the designer can choose to maintain strength and stability where it is most critical for overall structure performance while allowing controlled yielding of specific structural elements and maintaining stability. Elastic (also called *capacity-protected* or *force-controlled*) members should be designed with as little overstrength as possible to ensure inelastic (also called *plastic* or *ductile-yielding* or deformation controlled) members can be designed to be as light (economical) as possible. The elastic components are designed to withstand probable forces that could be produced by inelastic (ductile) elements (Filliatrault et al., 2013). A basic application of this is in a multi-storey frame structure where the columns are designed as elastic elements and the beam is designed to yield. The yielding beam allows for stability to remain whereas if the columns were to yield, global stability may be lost, leading to collapse. This particular application of capacity-based design is known as the strong column, weak beam principle, which is well used in current seismic design.

Another situation that may occur is that with existing structures which may be designed and constructed prior to or not in accordance with modern seismic design codes. These structures will often have less resilient structural systems. Structures that do not comply with current building codes are more likely to have systems that take additional care and consideration to model. For example, the weak points that may cause failure prior to intended locations of ductility will need

to expressly be either included or upgraded. Inadequate shear transfer elements, drag struts, anchorage, or buckling failures may all lead to non-ductile failures that do not allow components to behave in-elastically as intended. Whether modelling an existing or proposed structure, it is important to ensure the likely failure modes are considered and the levels of ductility (or lack thereof) and overstrength are properly accounted for.

For a tall shear wall structure, the walls are typically designed to experience yielding in the lower (plastic hinge) portion. For a moment resisting frame, the beam will be designed to yield prior to columns to help maintain stability. For somewhat of a combined system, coupled shear wall assemblies use both flexural wall yielding (in the lower portion) and flexural coupling beam yielding to provide ductility to the system. Various material models can be used to implement non-linearity (Boivin & Paultre, 2012).

Alternately to determining forces on members that are designed to yield, the forces on non-yielding (capacity protected) elements shall be determined based on the probable force imparted on them by the yielding elements. For example, a building foundation will need to be designed to have capacity in excess of that of the structure base to ensure the structure base is able to yield as intended. In Canada, structural members will be either designated as force controlled or deformation controlled then designed for either the forces due to loads or capacity of connecting members and connections.

2.4 Code procedures and analysis methods

Non-linear behaviour of seismic force resisting systems (SFRS) plays an important role in modern earthquake engineering. The 2015 national building code of Canada (NBCC) has specific provisions and allowable methods for determining SFRS. Hybrid concrete-timber SFRS are not presently included in the current building code.

Analysis methods considered here are those allowed according to NBCC (2015), which are summarized in Table 2-1.

Table 2-1 Analysis methods prescribed in the 2015 national building code of Canada

Number	Category	Procedure	Method
1	Linear	Static	Equivalent Static Force
2	Linear	Dynamic	Modal Response Spectrum
3	Linear	Dynamic	Response History
4	Non-linear	Dynamic	Response History

As well, response history analysis methods require the selection and scaling of ground motions. This is an emerging science and for the first time the NBCC (2015) has included guidelines in the commentary. This guideline as well as other current relevant material related to the selection and calibration of ground motions is reviewed.

2.4.1 Equivalent static force procedure

The equivalent static force procedure (ESFP) is considered adequate for only limited structural configurations. It must be validated as being an allowable option prior to completing design (NRC - National Research Council Canada, 2010). The ESFP is a relatively simple static approximation of a complex dynamic problem. ESFP is typically conservative when used within the code specified limitations.

2.4.2 Modal response spectrum analysis

The elastic base shear is determined from the modal response spectrum method by combining (through SRSS) maximum modal response. The elastic base shear (V_e) must then generally be scaled to account for non-linearity (ductility) (Saaticioglu & Humar, 2003). This scaling will impact the results by decreasing the base shear (V) and increasing drift. More specifically, when using the NBCC (2015), further steps beyond just scaling for ductility are required to arrive at the design base shear (V_d) (Filliatrault et al., 2013). Considering the equal displacement rule which is generally relevant for short period structures (Filliatrault et al., 2013), scaling by overstrength and ductility values help to provide more realistic anticipated drift and force values to be considered in design (Canadian Commission on Building and Fire Codes National Research Council of Canada, 2015). For forces, only one step of scaling is required. For deflections, the first step is the same but an additional step of back scaling is required. The additional step is required because

deflections generally rebound and are therefore elastic. Residual (permanent) drift is not captured in this form of analysis. Conversion from the elastic base shear (V_e) to the design elastic base shear (V_{ed}) is required. Experience has shown that short period, ductile structures have an inherent ability to resist more load and further deformation, then that which is typically modelled (Canadian Commission on Building and Fire Codes National Research Council of Canada, 2015); therefore, the NBCC (2015) Clause 4.1.8.12.6 allows a reduction, provided the site class (soil conditions) is not F, and that SFRS ductility is greater or equal to 1.5 ($R_d \geq 1.5$).

For strength, Clause 4.1.8.11.3. of NBCC (2015) places upper limits on the fundamental lateral period (T_a) which are based on structural type. The limits are based on a series of tests and provide a generally conservative envelope. Often the period determined by dynamic modal analysis will be longer due to additional stiffening elements within the structure which are not part of the SFRS and are not easily modelled. The code specified period ($T_{a,emp}$) is determined empirically.

2.4.3 Linear response history analysis

It has been noted that some researchers, engineers, and research groups use the term response history and some use the term time history when discussing the same type of analysis. In this thesis, the seemingly more current *response history* convention is adopted. No distinction is made between the two. Response history analysis uses time-varying acceleration (ground motion) data to determine the time-varying response of a structure. Response history analysis requires complementary elements of structural and geotechnical engineering (CSCE, 2008). Geotechnical aspects include developing the most appropriate ground motions while structural aspects include predicting the influence of ground motions on the dynamic behavior of the structure.

A linear response history analysis carried out with ground motions tightly fit to the target response spectrum should produce very similar results to a modal response spectrum analysis with the key differences being that signs of forces are not lost. For example, combinations of axial and bending loads and their contributions can be directly added rather than statistically combined (Charney, 2015). Goals of a response history analysis often include determining; 1) component inelastic deformations, 2) design forces on force-controlled members, 3) storey transient and residual drifts, 4) floor acceleration and spectra, and 5) behavioral modes under significant non-linearity.

Component inelastic deformations, residual (permanent) drifts, and behavioral modes under significant non-linearity are better predicted with a non-linear response history analysis. Multiple response history analysis' can be used to develop average, variability or likelihood of failures over time. Goals can be evaluated either explicitly or indirectly (NEHRP, 2011). Intensity, scenario, and time (risk) based are the three types of performance assessment (PA). Intensity-based PA has: 1) drift, and 2) force intensity. Scenario-based PA is used for: 1) average, and 2) variability. Risk-based PA is a series of intensity-based results used to provide likelihood over time.

New guidelines for use with the 2015 NBCC for the selection and scaling of ground motions have recently been released by NRC (2015). From these guidelines, Method A which is acceptable and somewhat simpler than Method B1 and B2 may be used with response history analysis under the NBCC (2015). Review of this ground motion selection and scaling procedures is provided after the non-linear response history section to follow.

2.4.4 Non-linear response history analysis

Non-linear response history analysis allows for assessment of the local non-linearities and calculation of time varying structural loads and deformations under cyclic input ground motions (shaking). Response history analysis are typically used, along with peer review, to satisfy the NBCC (2015) *special study* requirement which applies to systems not included in the list of code defined seismic force resisting systems. This would apply to a hybrid concrete timber SFRS. Key elements of a special study can be generalized to include compatibility of seismotectonic time history, compatibility of inelastic properties, and interpretation of response.

Typical parameters of interest from a non-linear response history analysis include global response parameters (shear, overturning and drift), and component responses such as moment/curvatures, coupling beam rotations, permanent drift(s), changed periods of vibration due to non-linear response, extent of damage and structural stability, ductility demand of local yielding elements, and forces on non-yielding (elastic) components. Results from non-linear response history analysis do not generally need to be scaled because they already should represent the non-linearities associated with the structure (Filliatrault et al., 2013). The ability to more directly interpret results from a non-linear response history is a key advantage to understand local performance, predict

order of failures, capture changes in fundamental period during non-linear response, and to better predict stability under significant non-linearity.

Potential dynamic shear amplification caused by higher mode effects may not be fully captured in results of a non-linear response history analysis. Additional allowance for increased shear demand compared to that provided directly from interpreting the results of a non-linear response history analysis can be critical to prevent un-anticipated brittle shear failures (Klemenic et al., 2007); (Tremblay et al., 2001). This under-estimated shear demand is also common to modal and static methods when predicting shear demand in tall shear wall structures (Panneton, Leger, & Tremblay, 2006).

The results obtained from a non-linear response history analysis should be reasonably similar to those obtained from a properly conducted linear time history or linear response spectrum analysis. Some software such as ETABS (CSI, 2015) have built-in post processing functions; however, Matlab (Mathworks, 2017) or MS Excel (Microsoft, 2017) still may be useful for post processing multiple analysis results (Boivin & Paultre, 2012). Post processing of results typically is required or at least helpful to an analyst who must interpret non-linear response history analysis results. A critical aspect of a non-linear response history analysis is peer review. A current consensus for selection of peer review qualifications is provided by the Los Angeles Tall Building Structural Design Council (Los Angeles Tall Buildings Structural Design Council, 2017).

2.4.5 Ground motion selection and calibration

Sourcing of ground motions, either historical or synthetic, is required for response history analysis. Response history inputs must be pre-processed from their raw recorded data state then (typically) calibrated to be representative of the site-specific design spectrum. Earthquake ground motions are typically characterized by their frequency content, duration, intensity, and fault mechanism or scenario. Ground motions for use with engineering analysis must be pre-processed including for baseline correction and filtering and timestep (Bartlett, 2014; Boore, 2005; COSMOS, 2005; Guorui & Toa, 2015). Orthogonal pairs of ground motions are required for bi-directional analysis. Directionality and rotation to fault normal and fault parallel components is typically required when less than 5km from a fault (Reyes & Kalkan, 2012); however, directionality of earthquake ground

motions may have a significant effect on the results (Archila & Ventura, 2012) and should be considered with highly irregular or critical structures and those near to an active fault. Mainshocks and aftershocks have unique implications on loss estimation due to earthquakes (Tesfamariam & Goda, 2017) and aftershocks should not be used in isolation for a structural analysis but instead as a follow up to the mainshock, if at all.

The site in this study is located near to the Cascadia subduction zone where three scenarios, crustal, in-slab and interface, have been reported to contribute (Rogers et al., 2015). In-slab (within the subducting plate and under the continental plate) and interface (at interface of subducting and continental plate) events are part of the subduction process due to the Juan de Fuca plate subducting under the North American plate; whereas, the crustal events considered are shallow and typically within the North American plate. Data from Open File 8090 (Halchuk et al., 2016) is available which deaggregates the seismic hazard by the scenarios described.

In 2018, the (2015) commentary to the NBCC was released which contains new guidelines for selection and scaling of ground motions. Basically, Method A of the guideline requires that scenario-specific ground motions be linearly scaled over scenario-specific period ranges. While this new guideline is now released for Canada, a significant body of research is ongoing to develop most appropriate methods for selection and scaling of ground motions for seismic design of structures.

Historical ground motions contain real and ranging frequency content and represent real earthquakes; they often provide good damage reference to previously damaged or destroyed buildings; therefore, historical records are preferred when available (Naumoski et al., 2006).

Synthetic ground motions can provide a good spectral fit; however, they do not provide a historical reference for damage and their spectral content is not necessarily compatible with scenario-predicted events. The stochastic finite-fault method can be used to generate synthetic time histories. For example, Atkinson (2009) developed several synthetic ground motion time histories for uniform hazard spectrum (UHS) using this method. Lower period cut-off limits as specified in NBCC (2015) were captured in this work. The steps to match simulated records to a target uniform hazard spectrum are defined in Atkinson (2009).

Prior to even working on calibration of ground motions, it should be considered whether calibration to fit the uniform hazard spectrum (UHS) is appropriate. Baker (2011) notes that the uniform hazard spectrum can be overly conservative for ground motion calibration due to the requirement to calibrate over the entire enveloped (worst case) acceleration response. Instead, the conditional mean spectrum (CMS) may be more appropriate. This method scales back the UHS to provide a more probabilistic scaling baseline for seed ground motions. Baker (2011) defines the procedure to implement the CMS approach.

Calibration of ground motions refers to aligning aspects (e.g. PGA, S(T), etc.) to fit a specific site; including both soil characteristics and nearness and directionality to various seismic hazards (faults). It is agreed among researchers that ground motion characteristics used in analysis should be calibrated to location or hazard specific conditions. It is not well agreed as how best to do the calibration. Generally, there are two categories of calibration methods: 1) "scaling" (intensity-based or weighted), or 2) "matching" (spectral).

Typically for ground motion calibration, matching refers to spectral matching; whereas scaling refers to scaling some aspect of a ground motion to better match a component. A key limitation of spectral matching is that you can only get a mean not a distribution (because the variability is reduced during matching), this means that risk cannot be directly obtained (NEHRP, 2011, pp. 64). ETABS Software (Computers and Structures Inc., 2015) can be used for matching by both frequency and time domain; ETABS documentation (CSI Inc.,) provides scaling methodology and discusses input options for historical time history files. Some specific scaling and matching (calibration) techniques include:

1. Linear scaling (LS) – Uniformly scales the ground motion; types include:
    a. PGA scaling – Scales the peak ground accelerations but neglects structure dynamics
    b. $Sa(T_1)$ scaling – Scales to fundamental period but neglects higher mode response
    c. $S(T_{rsi})$ scaling – Scales to scenario-specific period ranges of interest
2. Sla Scaling – Scales to integrated response spectrum over a period range of interest
3. ASCE Scaling – As SIa except greater, rather than equal, integrated area is required
4. ATC Scaling – Procedure to eliminate variability between ground motions and account for target spectrum and structural period (Applied Technology Council, 2009).

5. ATK Scaling – Initially selects the best naturally fitting ground motions then adjusts based on target spectral acceleration divided by the response (Atkinson, 2005).
6. MSE Scaling – Minimizes mean square error between seed and target spectrum.
7. Modal-pushover based scaling – Considers structure strength (Kalkan & Chopra, 2010)
8. Frequency domain matching – Provides good spectral fit but poor dispersion of results; also, alters non-stationary ground motion characteristics (CSI Inc., 2017; (Michaud & Léger, 2014).
9. Time domain matching – Adds wavelets but keeps phase of seed ground motions
10. Hilbert-Huang transform – A spectral variability transform that preserves non-stationary characteristics (Michaud & Léger, 2014; Ni et al., 2013; Barnhart, 2011)

One final type of ground motion scaling is scaling for importance. Importance of the system is typically accounted for in a design model by increasing the seismic mass or by scaling the intensity of the ground motion; this is a separate procedure entirely that happens later in the analysis procedure.

3 Methodology

The results of the literature review indicate that hybrid concrete timber structures are increasingly being sought and that a gap in meeting the demand exists. Further, for such structures, core wall and coupled core walls with timber frame is a predominant structural form. Seismic analysis and design are critical to developing new hybrid systems. Appropriate seismic analysis and design requires consideration of individual structural components, and how to include the elements selected. Factors such as ductility and overstrength, irregularity, torsion, stability, seismic weight, damping, hysteresis and capacity design must be well implemented to develop a realistic numerical model and resulting design. For such designs to go to construction, the relevant building code must generally be followed. The national building code of Canada (2015) provides analysis methods and guidelines which facilitate earthquake resistant design. Beginning with a linear static analysis and moving to linear dynamic analysis methods then finally non-linear dynamic analysis improves confidence in the results as the overall analysis progresses.

For hybrid concrete timber structures, there are no pre-defined and code specified hybrid seismic force resisting systems. Some researchers are presenting suggested ductility and overstrength factors for specific hybrid and timber systems; however, this is not the aim of this study. Instead, this study aims to implement hybrid systems and look at the requirements to develop numerical models that reasonably represent the structures as well as demonstrate analysis and design procedures that are required and or recommended by the building code.

An appropriate way to demonstrate reasonableness (or correctness) in numerical modelling is through examples where known quantities are validated. Software analysis reference manuals are a good example of this methodology where numerous examples are verified to demonstrate capabilities of the software. Similarly, experimental results from testing provide opportunity for experimental validations. Many researchers use experimental data to fit hysteretic connection models because connection hysteresis is a critical parameter in non-linear response of a structure.

A logical progression from simple connection validations to mid-rise structures includes incrementally increasing the difficulty of the problem. For this reason, a two-dimensional study was sought to ensure the model was behaving as expected when hysteretic connections were included into a structural system. Next, a three-dimensional study was sought to establish

connectivity and dynamic properties. With all of these studies undertaken, the ability to develop an extended study was realized. The extended study represents a possible structural system to meet market demand for innovative hybrid concrete timber structures.

Based on the literature review, the aim of this research is to develop connection hysteresis for timber and timber hybrid connections with an appropriate hysteretic connection model, develop numerical modelling abilities adequate for two and three-dimensional structures, and finally to extend the work to a useful type of in-demand mid-rise hybrid structural system.

3.1 Research planning

ETABS is a commercially available finite element software capable of implementing hysteretic connection models and providing design information for structures. This software is used by many researchers and for professional practice in this field; finally, an educational version was made available; therefore, ETABS was selected to carry out the studies.

The experimental data was selected based on availability and meeting the research objectives. The objectives being to incrementally move from connection calibration, to two-dimensional study, to three-dimensional study, to application of the building code to an innovative mid-rise hybrid concrete timber structure.

3.2 Examples chosen

Hysteretic connection performance was determined to be a critical parameter for non-linear analysis of structures; the one-dimensional study provided opportunity to calibrate a hysteretic model.

Interstorey drifts were determined to be a critical parameter determining structural response; therefore, the two-storey model allowed for fitting of experimentally determined interstorey drifts to a numerical model.

Damping and member stiffnesses were determined to have critical influence on structural response; therefore, the three-dimensional study allowed for exploration of damping, diaphragm

stiffness and core wall stiffnesses while including hysteretic connection models for unique connection types.

Following the building code was determined to be a critical requirement for structural analysis and design; the extended study provided opportunity to apply the building code through analysis and design iterations in developing an in-demand structural form.

3.3 Data collection

Data was collected through analysis of models developed in ETABS and post-processed in MS Excel. Numerical models were saved uniquely at key steps in each process; this allowed a collection of models to be kept for reference to critical phases of each procedure.

3.4 Importance and limitations

The importance of this research is that first connection models' parameters are provided, second, numerical modelling is demonstrated against experimental results, and third a structural design is provided for an in-demand novel hybrid structure. Limitations are that the results are specific to the exact arrangement studied and the work has not been parametrized to allow developing of more broad conclusions

3.5 Proposed analysis

Based on similar research reviewed and discussed in the literature review, connection validations will be carried out with a hysteretic connection model. Also, based on the literature review, two and three-dimensional studies will be undertaken to implement seismic modelling approaches as well as to ensure results are reasonably fitting the experimental data. Seismic analysis and design steps were developed based on the seismic design flow chart provided in Figure 6.42 of Filliatrault et al. (2013) including application of the NBCC (2015). Application of the NBCC (2015) is appropriate because it reasonably represents the current state of the art, less the ongoing research. In this study, basic minimum code procedures are followed but also the more extensive code procedures that are optional but becoming more prevalent are followed which brings current research in line with the code. Particularly with innovative structures, such as hybrid structures, performing analysis beyond just the code prescribed minimums is recommended if not required.

3.6 Summary

The research methodology has been explained. The literature review identified key aspects to be implemented including component types, seismic design considerations, and building code analysis methods. The experimental validations provide a baseline for the extended study. The extended study develops a seismic design of an innovative hybrid structure.

4 Case Details

Case details of the experimental validations and extended study are presented. These case details form the basis of the remainder of work in this thesis.

4.1 Experimental validations

Case details for the one, two and three-dimensional experimental verifications are presented. Experimental validations provide both a baseline for the numerical analysis (extended study) as well as provide universal calibrated connection results for stand-alone use.

4.1.1 One-dimensional study

Reverse cyclic testing was carried out for timber connections by (Isoda & Tesfamariam, 2016). The experimental apparatus with a representative timber beam is shown in Figure 4-1.

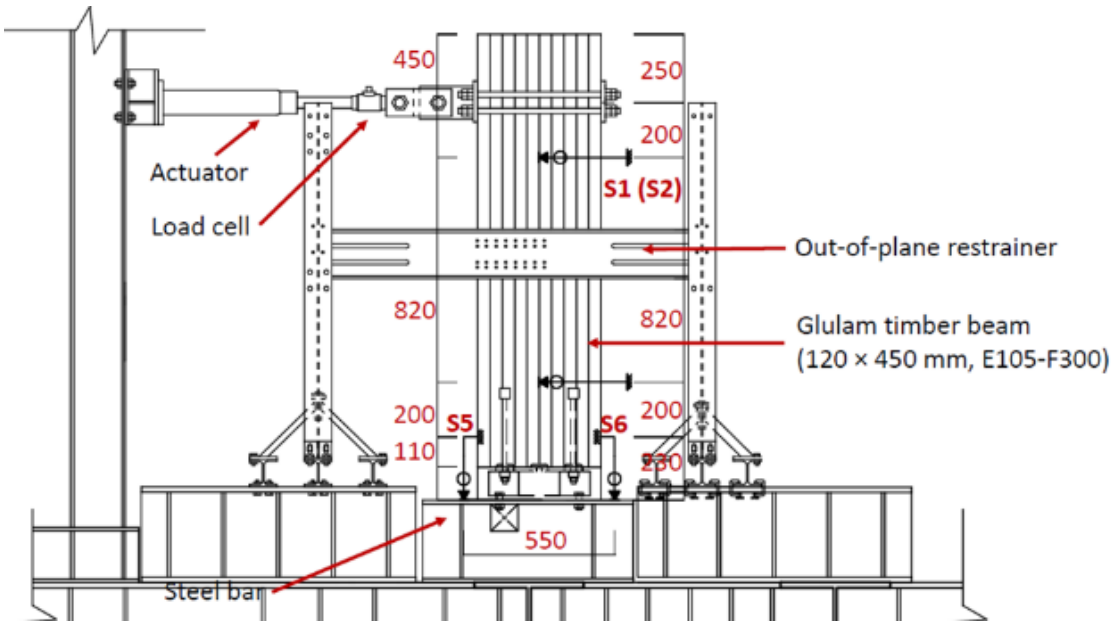

Figure 4-1 Experimental apparatus for connection testing [(Isoda & Tesfamariam, 2016) © with permission from ASCE]

The input load protocol was defined as a function of yield rotation as shown in Figure 4-2.

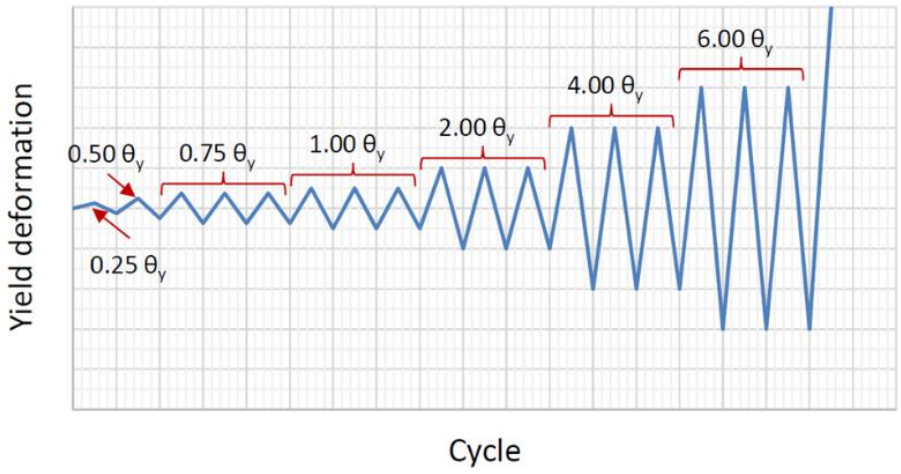

Figure 4-2 Load protocol [(Isoda et al., 2016) © with permission from ASCE]

The tension bolt moment-resisting joint assembly includes a 38 mm x 38 mm steel square bar embedded in timber with an end distance adequate to prevent pull-out. The three connections are concrete core to timber beam, timber beam to timber column, and timber column to base. The concrete core connection had a steel box at the core to receive the moment resisting joint. The column base connection bolt went directly into a steel base plate and the beam column joint used a steel bearing plate to prevent local crushing. The beam to core and beam to column connections used (1) 16 mm bolt top and bottom; the timber base had (1) 16 mm bolt centred. The beam to core and beam to column connections had three split rings while the column to base had just one. All bolts were 450 MPa and timber was 10,500 MPa Young's modulus, 30 MPa bending strength glue laminated timber. Column sections were 170 mm square; beam sections were 120 mm wide by 450 mm deep. General arrangements of the beam to core, column to base, and beam to column connections are shown in Figure 4-3 (a), (b), and (c), respectively.

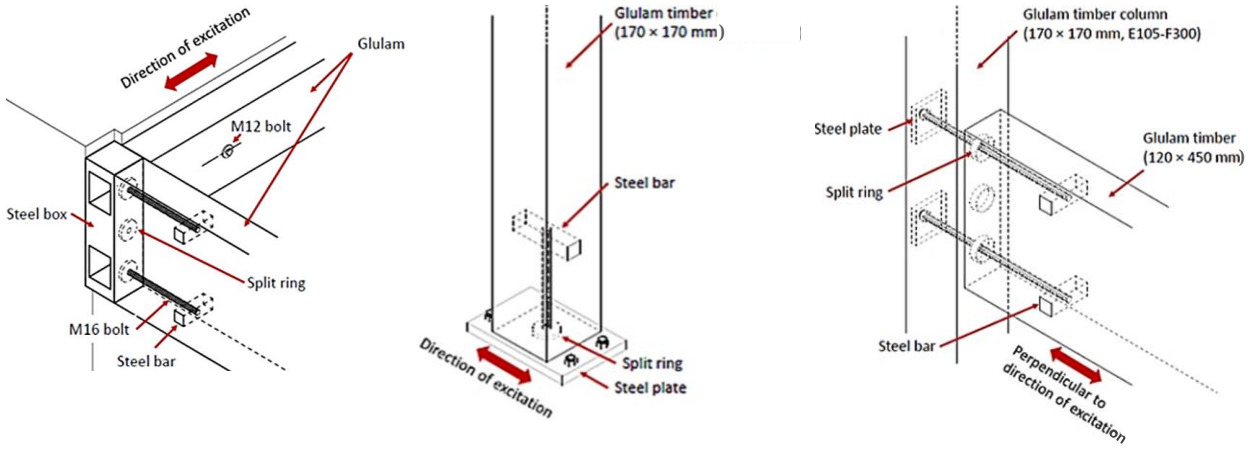

(a) (b) (c)

Figure 4-3 Connections (a) timber beam to concrete core, (b) timber column to steel base, (c) timber beam to timber column [(Isoda et al., 2016) © with permission from ASCE]

4.1.2 Two-dimensional study

A two-dimensional semi-rigid parametric portal frame and its individual connections were experimentally tested by (Mori et al., 2015). Their frame study was parametrized by beam depth. The portal frame experimental test apparatus and reverse-cyclic load input is shown in Figure 4-4 (a) and (b), respectively.

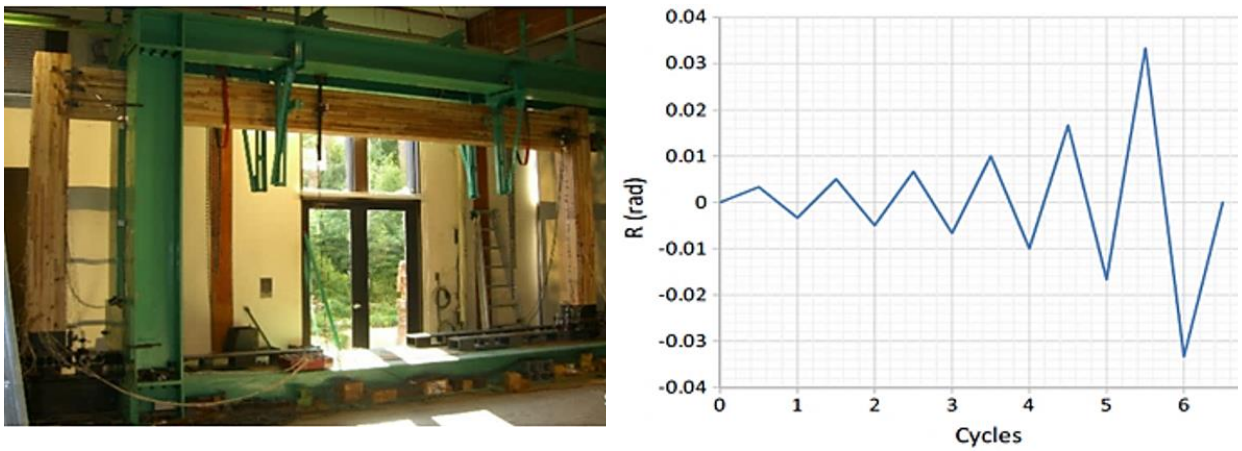

(a) (b)

Figure 4-4 Portal frame study (a) portal frame experimental apparatus, (b) reverse-cyclic load protocol [(Mori et al., 2015) © adapted for brevity with permission under creative commons license (http://creativecommons.org/licenses/by/4.0/)]

Timbers were glue laminated Japanese cedar with Young's modulus of 6500 MPa and bending strength of 25.5 MPa. Column sections were 300 mm x 300 mm; beam sections were 240 mm wide by 400 mm, 500 mm, and 600 mm deep. The portal frame had a 6000 mm beam span and 3140 mm column height.

Lagscrewbolt (lag-screw-bolt) fasteners were used. The lagscrewbolt fasteners consist of tubular (hollow) lagscrews with coarse timber threads on the exterior and hex bolt threads on the interior. Proprietary dovetailed steel plates were bolted to the lagscrewbolts. Beam to column and column to base connection general arrangements are shown in

Figure **4-5**. Static pushover analysis was used to verify global performance of the frames and reverse cyclic loading was used to calibrate hysteretic connection performance.

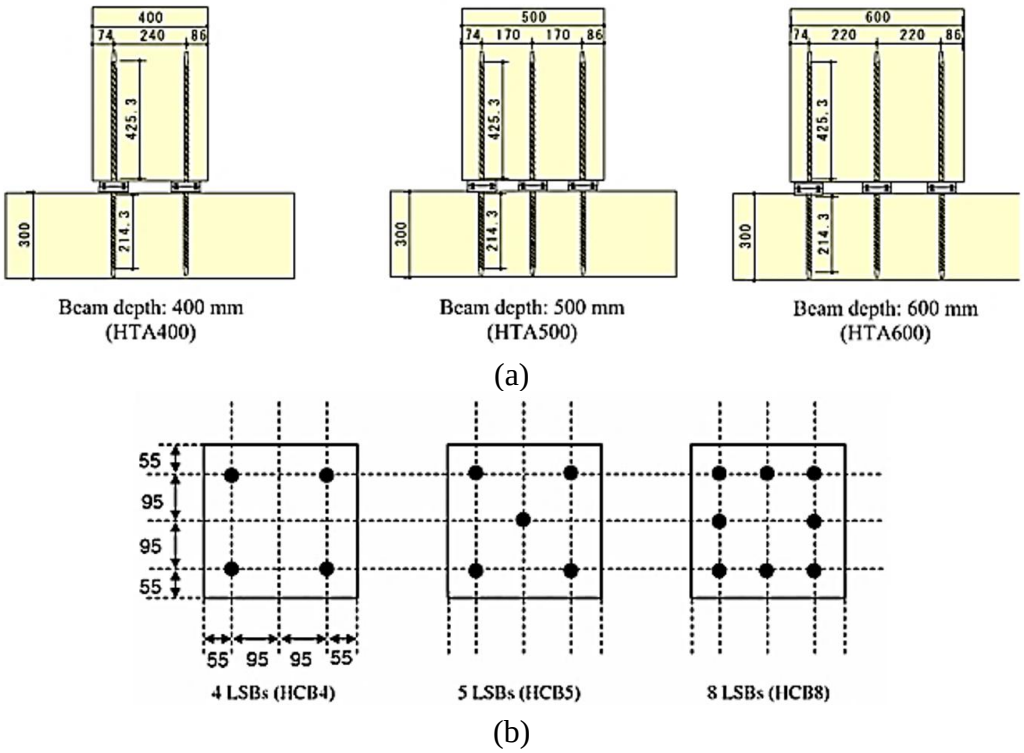

Figure 4-5 Portal frame lagscrewbolt connections (a) beam to column connections, (b) column to base connections [(Mori et al., 2015) © adapted for brevity with permission under creative commons license (http://creativecommons.org/licenses/by/4.0/)]

4.1.3 Three-dimensional study

Full scale shake table testing was carried out on hybrid concrete timber structures (Isoda et al., 2016). The testing parametrized the structure by number of storeys and diaphragm type. For the three-dimensional study here, the two-storey concrete-core timber-frame hybrid structure from (Isoda et al., 2016) was selected.

This two-storey structure utilized connections that were tested by (Isoda & Tesfamariam, 2016) and are calibrated in the one-dimensional study in this Thesis. The general arrangement of the structure is shown in Figure 4-6. Then, Figure 4-7 (a) and (b) show the shake table and hybrid structure along with the load input to be considered, respectively.

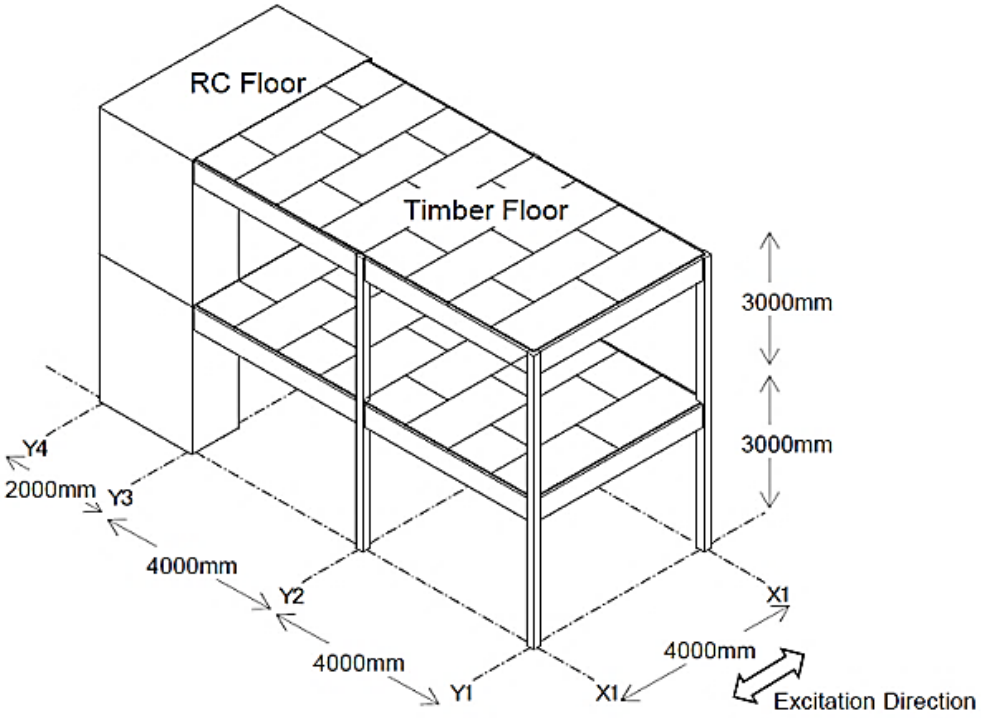

Figure 4-6 General arrangement of concrete-timber hybrid [(Isoda et al., 2016) © with permission from ASCE]

(a)

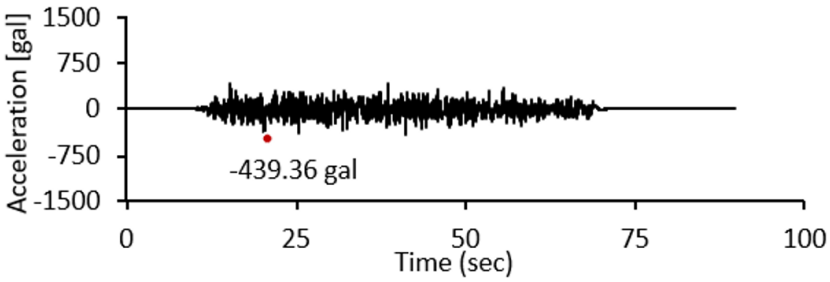

(b)

Figure 4-7 Three-dimensional two-storey concrete-timber structure (a) three-dimensional two-storey concrete timber structure experimental setup (b) input load protocol [(Isoda et al., 2016) © with permission from ASCE]

The shake table loads were generated by the ground acceleration input and masses from gravity loads of self-weight of the structural materials, an allowance for an 80 mm non-structural and structurally isolated concrete topping on the plywood, and a uniform live load of 1.1 kPa.

The concrete core walls were 180 mm thick with 2000 mm openings on two sides. The pre-cast concrete core was reinforced with 10 mm diameter, 400 MPa reinforcing spaced at 20 mm on centre on each face in both horizontal and vertical directions. The core was fastened to the base structure with four (4) and two (2) of 21 mm SBPR 930/1080 steel bars per wall with a prestress force of 257.5 kN located as shown in Figure 4-8. The concrete core dimensions are provided in Figure 4-8.

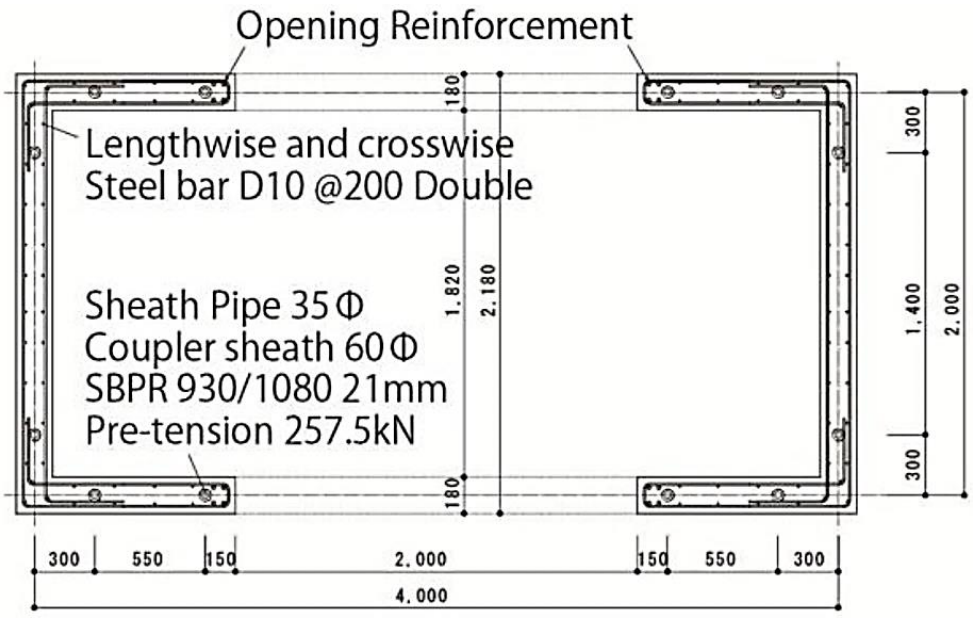

Figure 4-8 Concrete core section [(Isoda et al., 2016) © with permission from ASCE]

Timber beams, columns, and their connections were those defined already in the one-dimensional study. Additionally, timber purlins were required to provide support for the diaphragm. The purlins are estimated to be 120 mm by 300 mm placed at 1200 mm on centre. The diaphragm was 24 mm thick JAS second grade structural plywood nailed with CN75mm nails at 50 mm on centre.

4.2 Extended study

The extended study structure is based on structural plan layout and storey heights provided in the (MGB Architecture and Equilibrium Consulting, 2012) report *Tall Wood*. Elements of their 12-storey FFTT (forest through the trees) system along with elements of their concrete base structure are used to develop the preliminary structural system layout. Seismic design of buildings is iterative and solutions can vary based on starting point and design decisions. The design solutions of the extended study therefore do not match the design solutions of the original FFTT system but rather use it as a starting point for analysis or stepping stone for the hybrid concrete timber primary structural system of this study. Load conditions are also significantly different as the site of the extended study is on soft soil in Victoria under high importance, whereas the original FFTT system was for Vancouver on a rock site under normal importance. This difference results in roughly double the seismic loading due to soil amplification, high importance factoring and higher initial

spectral accelerations. Further, the high importance criteria limit the interstorey drift to less than half (2.5 percent is reduced to 1 percent) of that allowed under normal importance.

This section introduces the case details which were used to formulate the initial analysis model of the extended study. Final case details are updated based on the results of the analysis and design procedures.

4.2.1 Case details from 12-storey structural systems

Tall Wood (MGB Architecture and Equilibrium Consulting, 2012) presented a case for tall wood structures. The structural aspects were authored by Equilibrium Consulting while the architectural aspects were by MGB Architecture and Design. Equilibrium Consulting is a structural engineering firm based in Vancouver, BC at the forefront of innovative timber design. One of the FFTT structures in *Tall Wood* was the 12-storey timber structure. This structure also had a reference concrete structure. Aspects of the concrete reference structure and aspects of the timber FFTT structure were used to develop a starting point for analysis and design of the extended study 12-storey concrete-core timber-frame (hybrid) structure. Nominally, the overall dimensions of the structures allow for three 7.3 m bays in one direction and a 7.3 m, 9.9 m, and 7.3 m bay in the other direction. Twelve storeys at 3 m per storey was typical for both the concrete base and the Timber FFTT structures. Nominally 300 mm thick engineered timber slabs replaced 200 mm concrete floors in the base compared to FFTT system. The FFTT system housed the hallways surrounding the core within the core; whereas the concrete base building apparently did not require as large of an overall core size. An additional column line was provided on each end of the core in the concrete structure to carry gravity loads but the general layout of columns and beams was otherwise similar. Steel beams were used in the FFTT system with reduced beam sections to promote plastic hinging at preferred locations; primary non-linear response would however be expected to occur within the core via panel connections and hold-down assemblies. Hinging in the concrete base structure would presumably be limited to within the core coupling beams and lower segment of core walls. Structural integrity reinforcing would be provided to prevent catastrophic failures due to slab punching or other load effects. The general arrangement plans of the concrete base and timber FFTT structures are shown in Figure 4-9, and Figure 4-10, respectively.

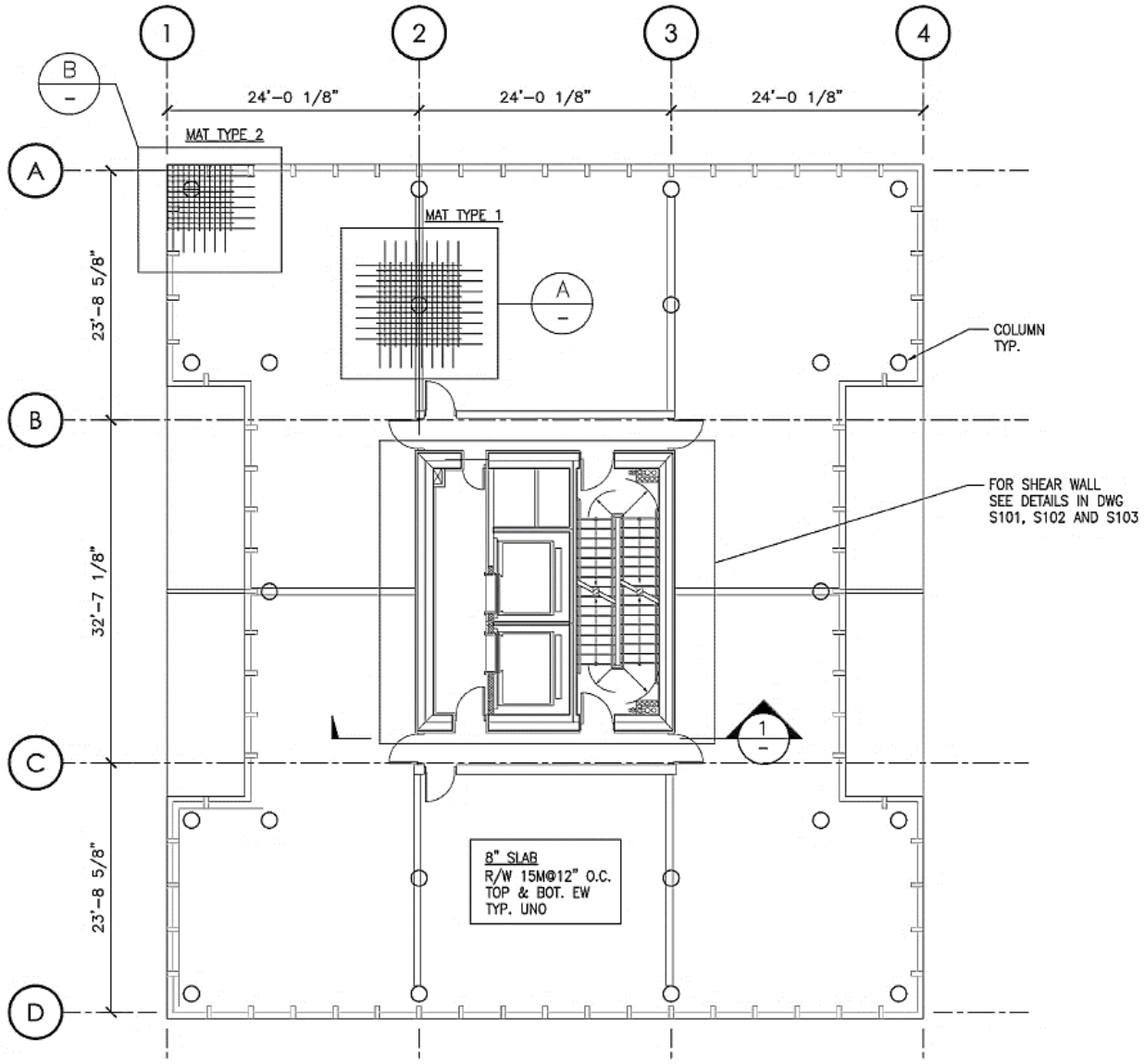

Figure 4-9 General arrangement plans (a) 12-storey concrete base structure [(MGB Architecture and Equilibrium Consulting, 2012) © adapted for brevity and provided with permission under creative commons license (https://creativecommons.org/licenses/by-sa/3.0/legalcode)]

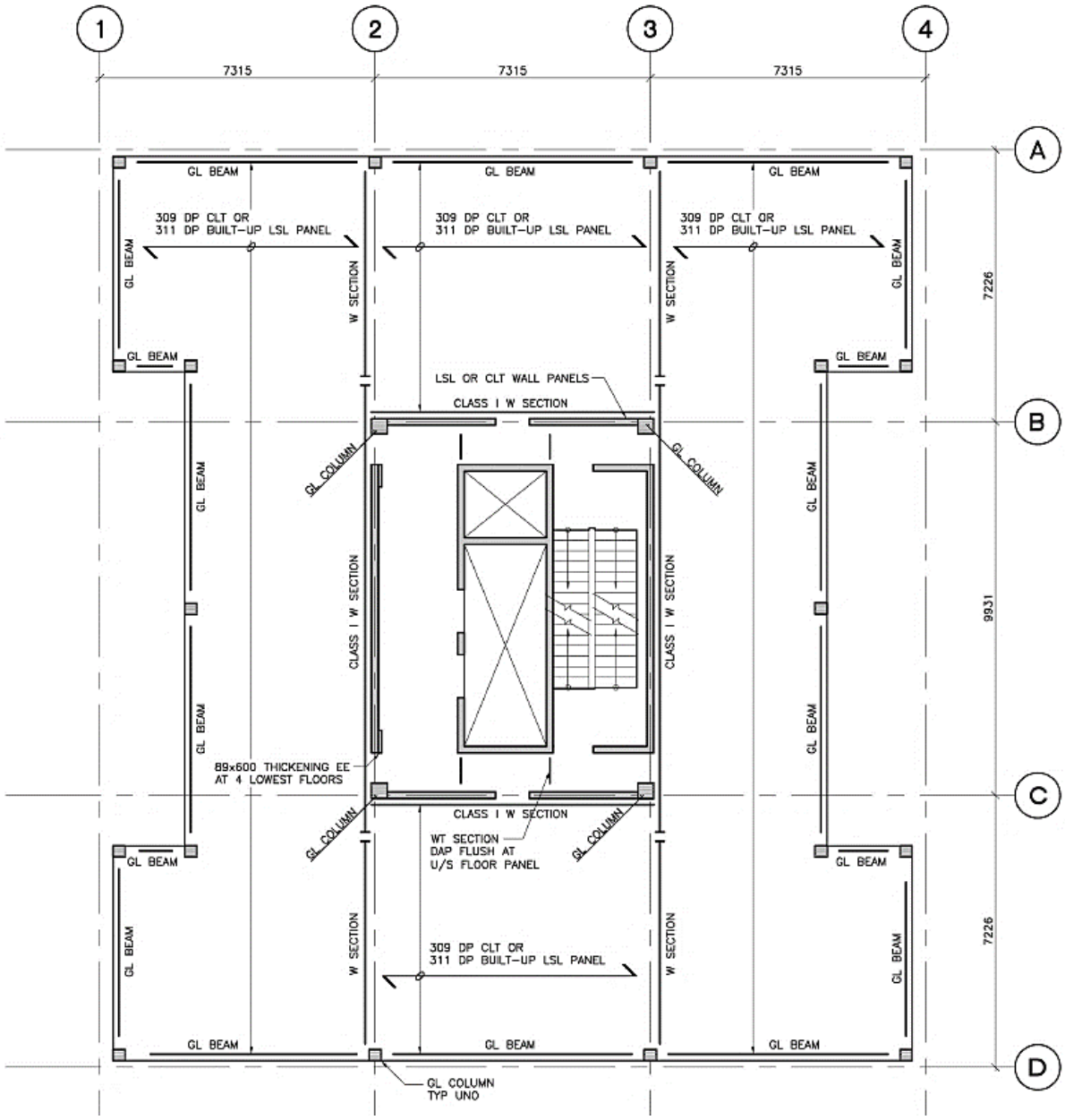

Figure 4-10 General arrangement plan of 12-storey FFTT timber system [(MGB Architecture and Equilibrium Consulting, 2012) © adapted for brevity and provided with permission under creative commons license (https://creativecommons.org/licenses/by-sa/3.0/legalcode)]

The concrete base core walls were 350 mm in the cantilever direction and 450 mm in the coupled direction, respectively. The cross laminated timber (CLT) core wall panels of the timber FFTT structure were not provided for comparison. A concrete core elevation and plan were provided and the core is shown in Figure 4-11. Loads considered for preliminary design in Tall Wood were

reasonably compatible with the loads required for the extended study; however, as discussed, the loading in the extended study is pushed considerably higher by proximity to seismic source hazards, soil conditions, and importance. The loading used for preliminary design in Tall Wood is shown in Figure 4-12.

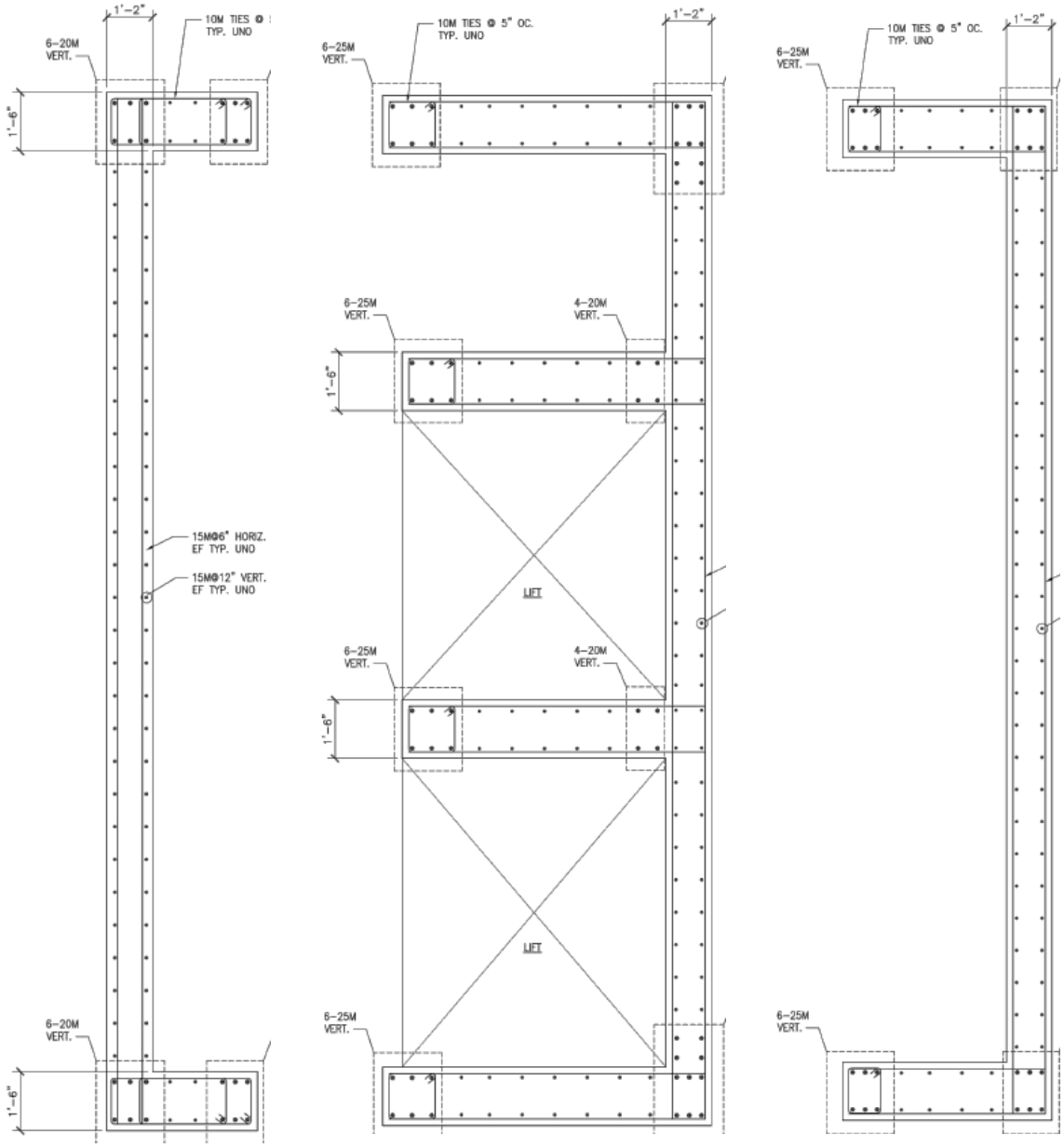

Figure 4-11 Core walls [(MGB Architecture and Equilibrium Consulting, 2012) © adapted for brevity and provided with permission under creative commons license (https://creativecommons.org/licenses/by-sa/3.0/legalcode)]

Importance Category	Normal
Climatic Design Data (per BCBC 2006)	
ULS importance factor for snow	Is = 1.00
Ground Snow Load	Ss = 1.80 kPa Sr= 0.20 kPa Plus snow built up where applicable
ULS importance factor for wind	I_w = 1.00
Hourly Wind Pressure	(1/10) 0.36 kPa
Hourly Wind Pressure	(1/50) 0.48 kPa
Seismic Design Data	
ULS importance factor for earthquakes	I_Q = 1.00
5% damped spectral accelerations	Sa(0.2)= 0.94 Sa(0.5)= 0.64 Sa(1.0)= 0.33 Sa(2.0)= 0.17

Peaked ground acceleration	PGA= 0.46
Assumed Site Class	C
Rd	2.0
Ro	1.5
Design Live Loads	
All floor and patio areas	1.90 kPa
Roofs	1.82 kPa Plus snow built up where applicable
Design Dead Load	(including partitions and 40 mm concrete topping)
Floors	4.00 kPa + perimeter wall weight
Roofs (includes allowance for rooftop units and screens)	3.00 kPa
Lateral Interstorey Drift Limit	
Wind	h_n/500
Seismic	h_n/40

Figure 4-12 Preliminary load criteria [(MGB Architecture and Equilibrium Consulting, 2012) © adapted for brevity and provided with permission under creative commons license (https://creativecommons.org/licenses/by-sa/3.0/legalcode)]

4.2.2 Case details for extended study initial analysis model

The initial analysis model for the extended study uses the same plan and storey dimensions as both the FFTT and concrete base structures discussed in the previous section. The concrete core has the same wall thicknesses as well. The timber connections are to utilize the connections from the one and three-dimensional experimental verification studies. The change in vertical shear due to beam spans and load change is assumed to have a negligible effect on the connection performance; however, in a real scenario, this would need to be investigated and accounted for. Timber sizes must be determined once the design process starts. A plan and isometric view of the initial analysis structure was developed in ETABS and are shown in Figure 4-13 (a) and (b), respectively. Loads for the preliminary design are provided in Table 4-1.

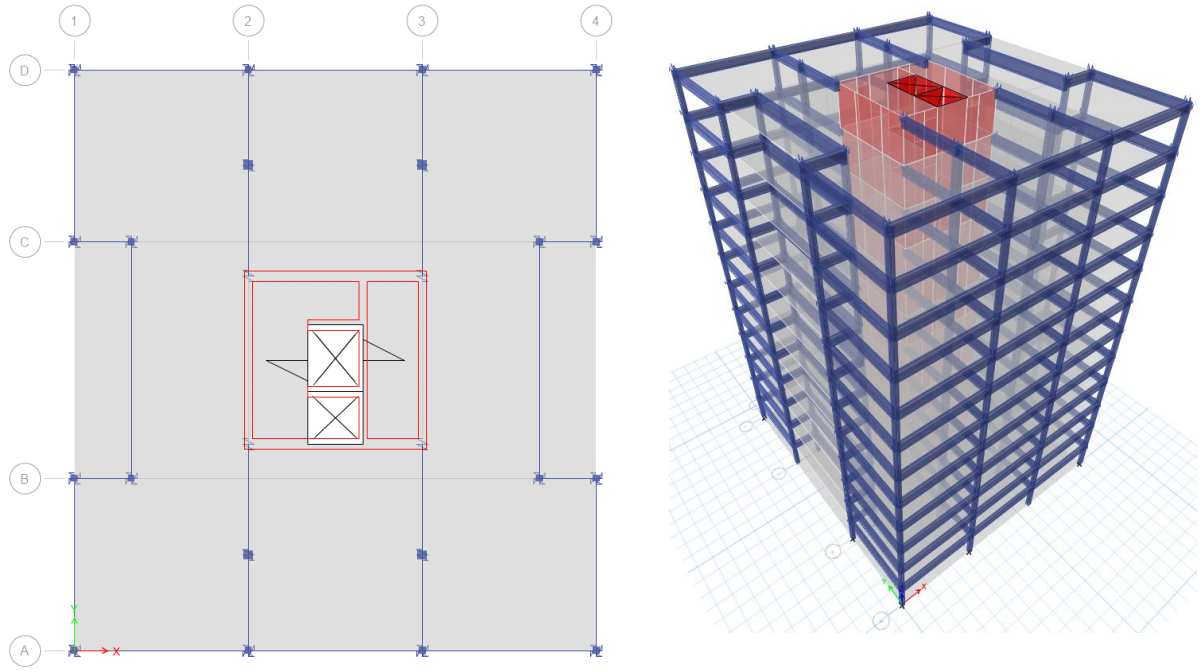

(a) (b)

Figure 4-13 Preliminary structural model (a) plan view with columns, beams, non-linear link elements, floor planks, core walls and openings, (b) isometric view of the 12-storey hybrid

Table 4-1 Structural loads and deflection criteria

Climactic design data (NBCC 2015 and NRC Commentary, I-1, I-15)		
Seismic	Victoria, BC; High importance; Site class E.	
Ground snow and rain load	S_s=2.2 kPa, S_r=0.1 kPa	
Hourly wind	$q_{1/50}$=0.40 kPa (pressures vary)	
Live and snow loads (NBCC 2015 and Table 4.1.5.3, NRC Commentary))		
Roof	S_{roof}=2.8 kPa	Roof area: $I_s[S_s(C_bC_wC_sC_a)+S_r]$
Floors 2-11	$L_{Flr2-11}$=4.8 kPa	(1.5[2.2(0.8)(1.0)(1.0)(1.0)+0.2)
Floor 1 (1st Storey)	L_{Flr1}=2.4 kPa	
Dead and super-imposed dead loads (SIDL)		
SIDL Roof	D_{roof}=1.5 kPa	
SIDL Floors 2-11	$D_{flr2-11}$=2.5 kPa	
SIDL Floor 1 (1st Storey)	D_{flr1}=2.5 kPa	
SIDL Cladding (all levels)	D_{clad}=2.0 kN/m (perimeter with jogs at balconies)	
Dead: All structural materials	Self-weight (CLT floors, core, beams, columns)	
Interstorey drift limit (NBCC, 2015)		
Wind	H_n/500	
Seismic	H_n/100 (with I_E=1.5), reduced from H_n/40 typically	

5 Procedures

This chapter outlines the procedures followed to complete the experimental verifications and extended study.

5.1 Experimental validations

Procedures to complete the one, two and three-dimensional studies are provided.

5.1.1 One-dimensional study

Fitted hysteretic models are required for non-linear analysis in accordance with the national building code of Canada (2015). Strength, stiffness, degradation and pinching parameters described in the literature review section are fitted using hysteretic plots. The procedure followed for the one-dimensional study of hysteretic connection calibrations is explained. A typical link and structural section object are shown in Figure 5-1; the link is tight to the left end (labelled as K1) while the remainder is the structural section (labelled as C1).

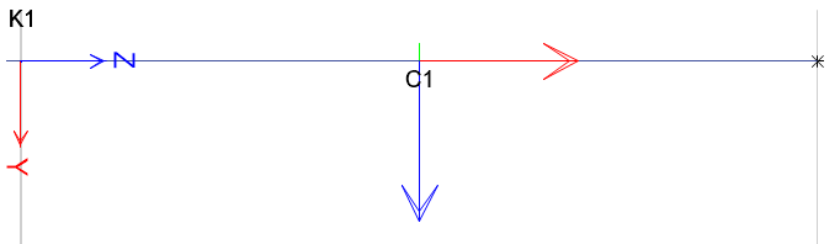

Figure 5-1 One-dimensional model with hysteretic spring (K1) at global origin and structural section (C1) with local axis extending from spring to joint restraint for rotational load input

The steps required to create the first analysis model are described then, briefly, the adjustments for the subsequent connection models are discussed. In the models, the concrete core to timber beam connection, loaded in the x and y-direction are noted as, BX and BY, respectively. For BX (strong axis bending), the reverse cyclic load protocol did not reach six times the yield rotation prior to failure; therefore, the models were calibrated to four times yield rotation only.

1. Create one-dimensional space with auto merge allowance for link elements

A typical cartesian (x,y,z) coordinate system was used and a grid in the z (global three) direction was created. The final grid spacing equal to the height from the actuator to concrete core interface (1330 mm) was achieved by first creating a 2 mm spacing then creating an adjacent 1328 mm spacing.

2. Create section and zero-length link

The software's auto merge tolerance was set to 3 mm to draw the link and elastic section. The software's auto-merge tolerance was reduced to 1mm forcing each end of the link to a single point resulting in a zero-length lumped plasticity model.

3. Apply restraints to section for application of ground displacement load

The section was restrained at the free end, away from the link, in all but one degree of freedom; namely, rotation in the direction of the applied load. This unrestrained rotation allowed rotation of the timber relative to the connection interface, as would be experienced by the cantilever timber (beam or column) in the test apparatus.

4. Create the load

A load pattern named displacement and a load case named non-linear direct integration history were created. An arbitrary load of 1 mm translation was applied as a ground displacement joint load to the top of the beam in the x (global one) direction. A time history function was defined with the reverse cyclic load protocol presented in Figure 4-2.

5. Scale the load

Because the load input is in terms of rotation and ETABS does not allow a rotation load to be specified, it was necessary to scale the load. For a small angle theta, the opposite side is a function of the adjacent; therefore, the height from actuator to base of connection multiplied by the rotation provided the displacement input required for the lateral movement of the restrained joint. Therefore, a scale factor of (14.4 mm) was calculated as the height (1330 mm) multiplied by the rotation at yield during the monotonic testing (0.0108 radians).

6. Define output time step and P-delta effects

P-delta effects were selected to contribute. The output time step was reduced to 0.01 seconds to provide clearer hysteresis plots for visual verifications

7. Define the non-linear link element

The link element was defined with no mass or weight, as it is zero length. All translational degrees of freedom were fixed because the connection was not allowed any gapping within the connection. Axial rotation (R1) was fixed. Initially, the minor rotational degree of freedom (R2) was fixed; however, when calibrating weak axis bending, this degree of freedom was modified. The major rotational degree of freedom (R3) was selected to have linear and non-linear properties.

8. Define initial parameters of link elements

Monotonic load test data (Isoda et al., 2016) provided a yield moment and rotation of 24 kNm and 0.09 radians, respectively; with this, an effective stiffness of 2667 kNm/rad was calculated. The value was decreased to 2600 kNm/rad after several fitting attempts were made and the connection model was refined. The backbone curve was defined with the values provided in Table 6-1 and the non-linear parameters were initially left as defaults.

9. Validate hysteretic model to experimental data through observation, trial and error

Post processing was done in MS Excel to allow overlay of test data and careful fitting of the results; observations from the first connection calibration were as follows:

a) Increasing α tended to increase the horizontal spread of the hysteresis loops. α is defined as a multiplier that locates the distance between the horizontal axis and the pivot point.
b) Increasing β tended to increase the pinching effect on the unloading of the hysteresis. β is defined as a multiplier that pushes the unloading. While maintaining the envelope curves, the energy dissipated in the connection is significantly decreased as pinching occurs. A fully pinched model would have the β parameter equal to zero.
c) η was primarily ineffective in calibrating the connection model.
d) the unloading stiffness could not be modelled to be as stiff as the reverse cyclic testing showed it to be. This is further discussed in the limitations section.

Final fitted parameters are shown in Table 6-1. In order to develop subsequent connection models, adjustments were made to the Pivot model inputs, restraints, load orientation and magnitude and section properties. Further observations made while fitting the remaining connection models were as follows:

a) The pivot point was similar for both the strong and weak axis for this connection type; possibly indicating the parameter alpha is constant for the connection type.
b) Pinching was less in the weak axis compared to the strong axis. The pinching is more of a gap and the reduced effective depth of the moment couple (between the steel rods) tends to require a smaller beta value.
c) The reloading stiffness of Pivot tends to degrade more than the experimental results.
d) The backbone curves match well.
e) The unloading stiffness heads through the axis using the Pivot point; whereas, the reverse cyclic load tests unload almost directly over their load path. The resulting un-matched unloading stiffness does not change the load envelope; however, the Pivot model would predict increased energy dissipation due to larger area under the hysteresis loops.

10. Output hysteresis best fits

While fitting the hysteresis plots was a visual exercise and it is part of the procedure, it is also part of the results; therefore, plots of best fit Pivot model hysteresis are shown in Figure 6-1 on page 91, for each of the four fitted connections, along with the tabulated results for connection parameter inputs in Table 6-1, respectively.

5.1.2 Two-dimensional study

A two-dimensional model was developed to ensure proper connectivity and modelling techniques were being achieved in two-dimensional space and to provide Pivot model parameters for the connections. Stiffness parameters for the backbone curves were developed from available reverse cyclic test results (Mori et al., 2015). Timber sizes and properties were defined for the various sections, connection types, and frame arrangements. Portal frame models were developed with hysteretic connection (K_i) and beam (B_i) and column (C_i) sections as shown in Figure 5-2.

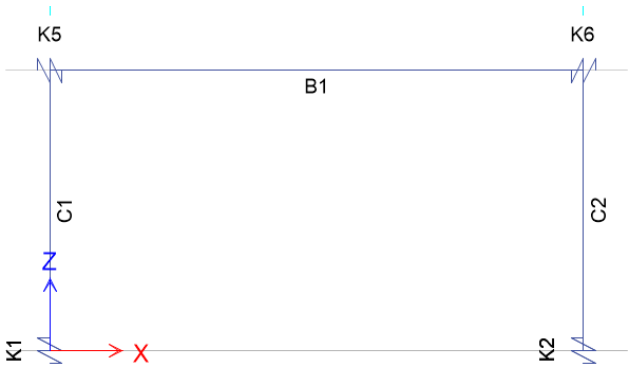

Figure 5-2 Two-dimensional non-linear portal frame model created with ETABS

First, individual components of the frame were calibrated according to experimental data (Mori et al., 2015). This was completed using a non-linear static pushover analysis to develop the backbone curves and with non-linear direct integration dynamic analysis to confirm the hysteresis. Because ETABS does not allow joint restraints to be specific to a load case and to facilitate the two pushover and response history analysis types, two separate models were created. Joint restraints were assigned in the direction of the displacement load. Joint displacement was used for the dynamic analysis because the load input is a time history acceleration. Conversely, the joint restraints were not applied for a non-linear static pushover analysis; the load input is defined as a force on the joint which was then scaled to achieve a predefined displacement. Initial calibration was estimated from backbone curve data then fine tuning of non-linear stiffness was carried out visually using MS Excel. Next, the static pushover curves for the frame were created. The frame height was reduced to 2640 mm, a 500 mm reduction from the full height of the column defined in the experimental model. This is acceptable because looking at the experimental setup, the top beam is mounted at about a beam depth below the top of column and the columns were said to be 3140 mm tall. This adjustment to the work point in the model brought the stiffness of the frame to good agreement.

Next, the non-linear dynamic analysis was considered. Here, the hysteretic properties of frame connections were compared. The ground displacement load was applied to both top joints of the portal frame with each of the top joints restrained in the direction of joint displacement. For final load scaling, the rotation of the link at the base of the structure was matched to the rotation applied to the connection calibration of the link element. An example of the hysteretic matching using

Pivot in ETABS is shown in Figure 5-3. With pushover analysis matching well, connection column base hysteresis matching and no change in non-linear parameters from the previously fitted connections, the goals of this study were achieved and so the remainder of the hysteretic fitting for the portal frame was left for future study.

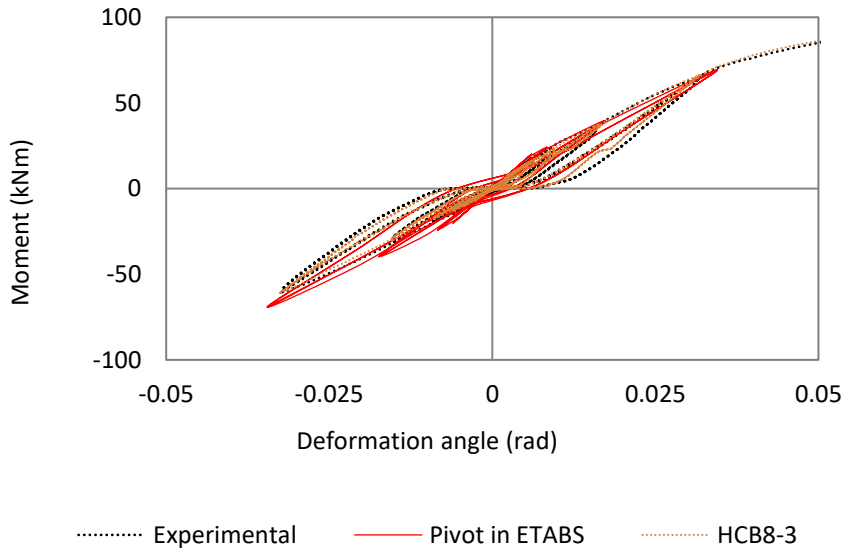

Figure 5-3 Hysteretic matching of column base in frame model

5.1.3 Three-dimensional study

A three-dimensional study was undertaken to develop proper modelling and analysis techniques; further, the three-dimensional study provided opportunity to implement fitted hysteretic connection models from the one-dimensional study, providing further validation. The procedure followed for experimental validation of the three-dimensional hybrid structure is presented in this section. An isometric view of the model developed in ETABS is provided in Figure 5-4.

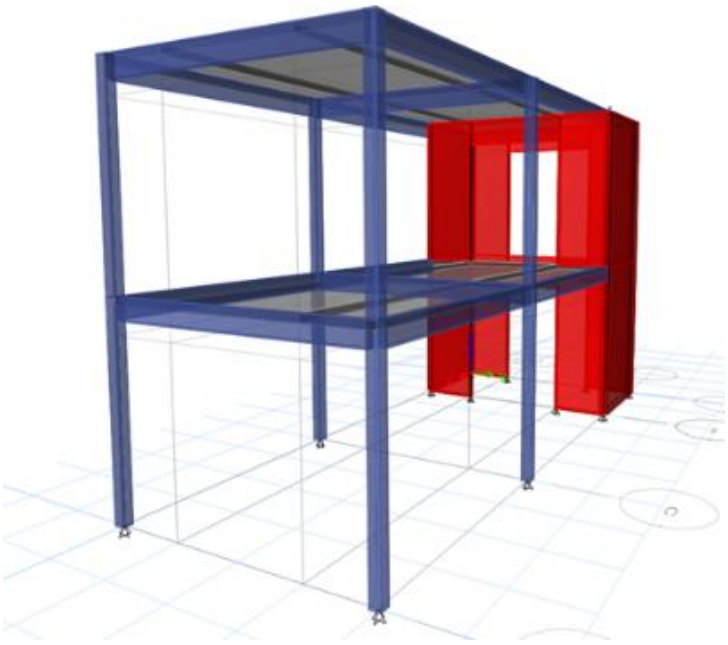

Figure 5-4 Three-dimensional model linear concrete core and non-linear timber connections

Concrete shear walls were modelled with linear shell elements and with pin connections to the ground. Timber beams and columns were modelled with general linear sections. The columns are continuous through the first level whereas the beams at the first level are not continuous. Connections of timber elements to concrete and timber to timber, and timber to ground were modelled with the Pivot multi-linear plastic element which were already calibrated in the one-dimensional study. The plywood diaphragm was modelled with a membrane thickness of 24 mm. The base acceleration was applied directly to all base nodes of the structure. The ground input file length was 89.99 seconds with a time step of 0.01 seconds.

To test how close matching of the experimental versus finite element model was, two initial target output variables were selected to match at the upper most nodes, furthest from the stiff concrete core. Parameters to match were absolute maximum displacement, and peak floor acceleration; as well, the dynamic response history of the structure was visually fitted considering phase and frequency of motion.

In ETABS, there are many options for specifying damping properties including by individual nodes. In this analysis, only the modal damping was adjusted. Based on the literature review, it

seemed reasonable to assume that the damping would be in the range of one to five percent for the bare hybrid concrete timber structure. To help better fit the damping, a brief parametric study was undertaken. Figure 5-5 shows the parametric study results and the matched floor displacement at approximately 2.2 percent damping. This is a reasonable estimate of damping because; 1) the structure is bare, 2) the bulk of the stiffness of the structure is due to the concrete core, 3) the concrete core in the experimental test had prestressed coupling forces applied.

More than 100 iterations were carried out in fitting the model. Primary variables were the diaphragm stiffness and damping of the structure. These variables would trade-off to achieve a closer fit. For example, a good fit of peak displacement and floor acceleration could be achieved with 0.6 percent damping and in-plane diaphragm modulus of elasticity of 6000 MPa; however, the dynamic response was obviously underdamped compared with the experimental results. This underdamping was apparent due to the excessive high frequency oscillations present in the acceleration history output.

In another trial, the damping was increased and the diaphragm stiffness adjusted which resulted in better matching dynamic response history and good matching peak displacement values but too low of floor accelerations and not well fitted phase and frequency of displacements.

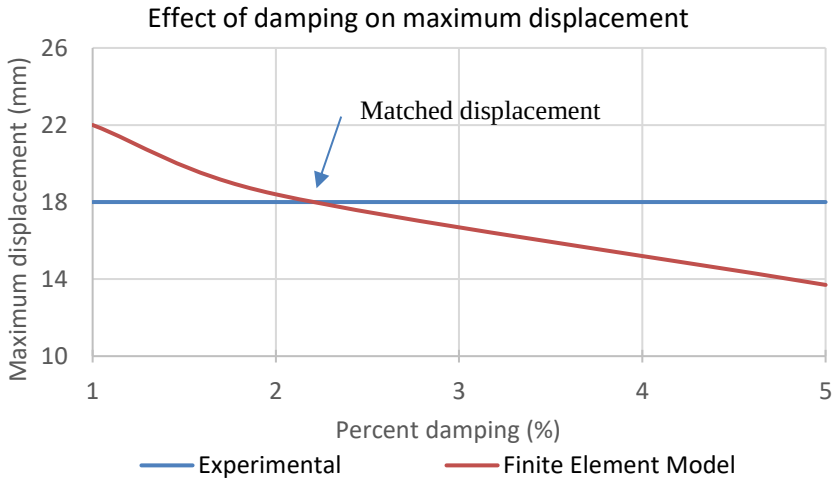

Figure 5-5 Parametric study of modal damping parameter

A secondary variable of concrete core cracking was introduced. Iterations with and without cracked core were carried out. Implementing a cracked core did not improve the overall fit which is consistent with the anticipated linear behaviour of the concrete core.

5.2 Extended study

Initial analysis and design steps the four (4) prescribed seismic analysis procedures of the national building code of Canada (2015) are demonstrated for the 12-storey hybrid concrete-timber structure considering material standards for concrete, timber, and steel (CSA - CSA Standards, 2014a; CSA - CSA Standards, 2014b; CSA - CSA Standards, 2014c). The general design procedures and steps are based on Filliatrault et al. (2013). Also, just before the response history analysis procedures, the procedure for selection and scaling of ground motions is demonstrated. This procedure follows Method A from the newly released guidelines from 2015 NRC Structural Commentary, Appendix to Commentary J.

5.2.1 Initial design steps

Prior to focussing in on any particular method of analysis and design, initial design steps are carried out.

1. Determine basic seismic and site data

The building is to be located in Victoria, BC. Victoria was selected due to the relatively high seismicity compared to many other regions in Canada (NRC - National Research Council Canada, 2010). The enacted building code for a site in Victoria, BC is presently the British Columbia building code (2012) with Part 4 of NBCC (2010) adopted by the BCBC (2012). The BCBC has not yet enacted a 2016 version; however, the 2015 NBCC is released and is being applied to this Thesis. It is expected that soon, the BCBC will release a 2016 version that will replicate the relevant section (4.1.8. Earthquake Load and Effects) of the 2015 NBCC. Two options are available to determine the five percent damped spectral response acceleration (S_a) values for the periods of interest at the site. They can be obtained from the NBCC (2015) Appendix C, or online from the NRC Earthquake hazards website (Natural Resources Canada, 2015). In this study, the parameters were obtained from the website because the exact latitude and longitude can be input

to provide an improved interpolation. The spectral accelerations for the code prescribed two percent in 50 years probability are provided in Table 5-1.

Table 5-1 2015 National building code interpolated seismic hazard values

2%/50 years (0.000404 per annum) probability										
Sa(0.05)	Sa(0.1)	Sa(0.2)	Sa(0.3)	Sa(0.5)	Sa(1.0)	Sa(2.0)	Sa(5.0)	Sa(10.0)	PGA	PGV
0.708	1.081	1.298	1.299	1.152	0.672	0.395	0.123	0.043	0.578	0.828

Assumed geotechnical parameters, averaged for the top 30 m of soil, include average standard penetration resistance corrected to a rod energy efficiency of 60 percent of the theoretical maximum (N_{60}), average undrained shear strength (S_u), and 3) average shear wave velocity (V_s) as shown in Table 5-2.

Table 5-2 Geotechnical parameters provided for the site

Geotechnical parameters considered in this study	
N_{60}	10
S_u	40 kPa
V_s	170 m/s
Site Class	E

The bearing capacity and other soil parameters such as susceptibility to liquefaction and lateral seismic soil loading on foundation walls shall be investigated during foundation design; however, these are beyond the scope of this study.

2. Definition of importance (risk) category

Assumed architectural requirements indicate that the use of the structure is to be for emergency services. This type of occupancy requires a seismic Importance (I_E) of 1.5 because the structure may be used in a post disaster situation. Note that while this classification requires an increase in the primary structural systems ability to resist severe loading conditions, it does not necessarily ensure operability and functionality for immediate occupancy (IO) which is the intent of the post disaster importance category. If the intent of the post disaster importance Category is to be met, other systems must adequately be designed to accommodate building movements under seismic

loading. The seismic importance factor (I_E) not only increases the base shear (strength requirements) but also tightens up interstorey drift (ISD, or drift) limits from 2.5 percent to one percent.

3. Determine unusual factors and/or constraints

It was assumed that this post disaster building is to receive funding from the provincial government which aims to increase the use of wood (timber) in public buildings (Government of British Columbia, 2009). Further, (Association of professional engineers and geoscientists of British Columbia (APEGBC), 2016) sustainability guideline requires that structural engineers consider sustainability goals in their work. Increased use of wood has been proven to be sustainable as a building material (Kremer & Symmons, 2015) so it ought to be considered for design; therefore, the structure is to make use of wood components where suitable. It is anticipated that a hybrid concrete timber structure may serve to meet the seismic demand requirement while simultaneously meeting the intent of the Wood First Act (Gov. BC, 2009). An open layout is sought to facilitate potential change in occupancy type and so a concrete core wall system with CLT floor panels and perimeter timber frames is selected.

4. Check applicability of simplified approach and define the design spectrum

An update from the previous 2010 NBCC to the new 2015 NBCC is the new Section 4.1.8.1 which allows a simplified approach to seismic design, given that certain criteria are met. This is the first check in the seismic section of the building code. The check, to see if the simplified approach is allowed, $I_E F_a S_a(0.2)$ and $I_E F_s S_a(2.0)$ must be less than 0.16 and 0.30, respectively. First though, the site parameter (F_s) must be calculated; Geotechnical parameters must be used unless the structure is to be founded on a rock site, as defined in NBCC 2015. F_s is determined with Equation 5-1.

$$F_S = \begin{cases} 1.0 \; if \; rock \; site \; of \; if \; N_{60} > 50, or \; S_u > 100kPa, \\ 1.6 \; if \; 15 \leq N_{60} \leq 50, or \; 50kPa \leq S_u \leq 100kPa, and \\ 2.8 \; for \; all \; other \; cases \end{cases} \qquad (5\text{-}1)$$

$$N_{60} \leq 15, and \; S_u \leq 50 \therefore F_s = 2.8$$

$$Check, \begin{cases} I_E F_s S_a(0.2) \leq 0.16s, and \\ I_E F_s S_a(2.0) \leq 0.30s, if \\ both\ true, use\ 4.1.8.1, \\ else, use\ 4.1.8.2 - 4.1.8.22 \end{cases} \quad (5\text{-}2)$$

$$= \begin{cases} (1.5)(2.8)(1.298) = 5.45 \geq 0.16s, and \\ (1.5)(2.8)(0.395) = 1.66 \geq 0.30s, \\ therefore \\ Use\ Article\ 4.1.8.2 - 4.1.8.22 \end{cases}$$

Because the criteria for the simplified approach are not met, the code stipulates to move onto Articles 4.1.8.2 to 4.1.8.22 of the NBCC (2015) to resolve the seismic force and force resisting systems. The site coefficient (F) for spectral acceleration S(T) is determined in accordance with Sentence 4.1.8.4.(4) NBCC (2015).

$$PGA_{ref} = \begin{cases} (0.8)PGA\ if\ \frac{S_a(0.2)}{PGA} < 2, \\ else \\ PGA \end{cases} \quad (5\text{-}3)$$

$$= \begin{cases} \frac{1.298}{0.578} = 2.14 > 2, \\ therefore \\ PGA_{ref} = 0.578 \end{cases}$$

Let F_a equal F(0.2), and let F_v equal F(1.0) in accordance with NBCC Sentence 4.1.8.4.(7). The values from Table 4.1.8.4-B NBCC were used and are provided in Table 5-3.

Table 5-3 NBCC (2015) Table 4.1.8.4.-B

Table 4.1.8.4.-B Values of F(0.2) as a function of site class and PGA_{ref}

	Values of F(0.2)				
Site Class	$PGA_{ref} \leq 0.1$	$PGA_{ref} = 0.2$	$PGA_{ref} = 0.3$	$PGA_{ref} = 0.4$	$PGA_{ref} \geq 0.5$
A	0.69	0.69	0.69	0.69	0.69
B	0.77	0.77	0.77	0.77	0.77
C	1.00	1.00	1.00	1.00	1.00
D	1.24	1.09	1.00	0.94	0.90
E	1.64	1.24	1.05	0.93	0.85
F	(1)	(1)	(1)	(1)	(1)

Notes to Table 4.1.8.4.-B: (1) See Sentence 4.1.8.4.(6).

Considering the PGA_{ref} value calculated earlier (0.578 g) and the Site Class (E), the value of F(0.2) is taken as 0.85. Note that interpolation may be required but is not used here because 0.568>0.5 which is the largest table value. The remaining F(PGA, PGV, and T) values are not explained here. Site specific spectral accelerations are calculated as shown in Equation 5-4.

$$S(T) = \begin{cases} largest\ of: F(0.2)S_a(0.2)\ or\ F(0.5)S_a(0.5), for\ T \leq 0.2s \\ F(0.5)S_a(0.5) \quad , for\ T = 0.5s \\ F(1.0)S_a(1.0) \quad , for\ T = 1.0s \\ F(2.0)S_a(2.0) \quad , for\ T = 2.0s \\ F(5.0)S_a(5.0) \quad , for\ T = 5.0s \\ F(10.0)S_a(10.0) \quad , for\ T = 10.0s \end{cases} \tag{5-4}$$

$$S(T) = \begin{cases} (0.85)(1.298) = 1.1\ or\ (1.17)(1.152) = 1.348 & \therefore S(0.2) = 1.348 \\ (1.17)(1.152) = 1.348 & \therefore S(0.5) = 1.348 \\ (1.39)(0.672) = 0.934 & \therefore S(1.0) = 0.934 \\ (1.58)(0.395) = 0.624 & \therefore S(2.0) = 0.624 \\ (1.84)(0.123) = 0.226 & \therefore S(5.0) = 0.226 \\ (1.79)(0.043) = 0.077 & \therefore S(10) = 0.077 \end{cases}$$

F(PGA), and F(PGV) are selected as F(PGA)=0.74, and F(PGV)=1.17 from NBCC Tables. The design spectral response acceleration S(T) is plotted in Figure 5-6.

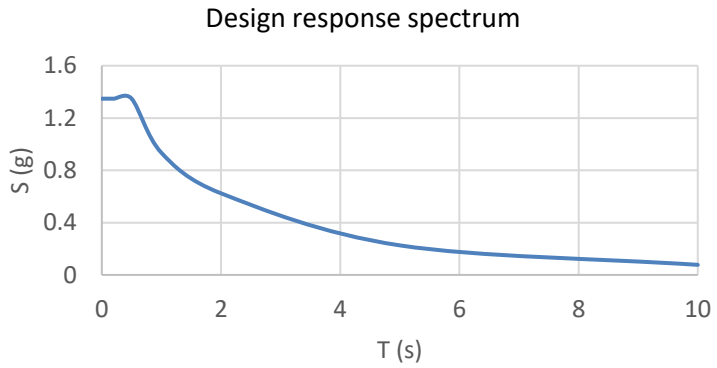

Figure 5-6 Design spectral response accelerations

5. Determine the design control parameters (DCP's)

Sometimes referred to as a seismic hazard index (SHI), design control parameters (DCP's) are code specified minimums used to trigger certain design criteria or system restrictions. The DCP's, and their limits for short and longer period accelerations (see Equation 4-5), are given in Sentence 4.1.8.6.(3), 4.1.8.10.(4) NBCC (2015), respectively.

$$DCP's = \begin{cases} I_E F_a S_a(0.2) \leq 0.35 \; then \; addt'l \; restrictions \; apply \\ I_E F_v S_a(1.0) \geq 0.25 \; and \; T_a \leq 1.0s \; then \; addt'l \; ... \end{cases} \quad (5\text{-}5)$$

$$DCP's = \begin{cases} (1.5)(0.85)(1.298) = 1.66 \geq 0.35 \; \therefore addt'l. restrictions \; apply \\ (1.5)(1.39)(0.672) = 1.40 \geq 0.25 \quad and \; Ta \; is \; unknown \; \therefore wait \; to \; see \end{cases}$$

Note that the DCP's are not always governed by the same limits; as stepping through the code provisions, one must specifically check the code to see which limits apply to which restrictions.

6. Load definition

With SFRS type defined R_d and R_o factors are initially assumed. Preliminary member sizing must be completed to determine starting weights for the system. Loads required for the preliminary gravity design are included in Table 5-4.

Table 5-4 Structural loads and deflection criteria

Climactic design data (NBCC 2015 and NRC Commentary, I-1, I-15)		
Seismic	See previous section	
Ground snow and rain load	S_s=2.2 kPa, S_r=0.1 kPa	
Hourly Wind	$q_{1/50}$=0.40kPa (pressures vary)	
Live and snow loads (NBCC 2015 and Table 4.1.5.3, NRC Commentary))		
Roof	S_{roof}=2.8 kPa	Roof Area $I_s[S_s(C_bC_wC_sC_a)+S_r]$
Floors 2-11	$L_{Flr2\text{-}11}$=4.8 kPa	(1.5[2.2(0.8)(1.0)(1.0)(1.0)+0.2)
Floor 1 (1st Storey)	L_{Flr1}=2.4 kPa	
Dead and super-imposed dead loads (SIDL)		
SIDL Roof	D_{roof}=1.5kPa	
SIDL Floors	D_{flr}=2.5kPa	
SIDL Cladding (All Levels)	D_{clad}=2.0kN/m (perimeter with jogs at balconies)	
Dead: All Structural Materials	Self-Weight (CLT Floors, Core, Beams, Columns)	
Interstorey Drift Limit (NBCC, 2015)		
Wind	H_n/500	
Seismic	H_n/100 (with I_E=1.5), reduced from H_n/40 typically	

It is recognized that the loads shown in Table 5-4 are simplified, other specific point loads, guard loads, etc. would need to be included during detailed design. For the design of the SFRS the loading shown is adequate. Since the focus of this thesis is on seismic design not wind, wind load is omitted but must be investigated for compliance with NBCC. Wind may govern either overall or in specific

storeys. Even if wind governs, seismic detailing must still be completed if one is to use the R_d and R_o factors used to reduce the design base shear.

7. Determine basic gravity and SFRS components

Results of preliminary checks for the gravity system suggest that timber component sizes as shown in Table 5-5 are adequate.

Table 5-5 Timber component sizes

Columns	
C1	315 mm x 315 mm Glulam D.Fir-L 16c-E
C2	400 mm x 400 mm Glulam D.Fir-L 16c-E
Beams	
B1	315 mm x 570 mm Glulam D.Fir-L 24f-E
B2	315 mm x 835 mm Glulam D.Fir-L 24f-E
CLT Floor and Roof	
F1	315 mm thick E grade

Notes:
1. The larger columns may require glue-up in the shop.
2. The column sizes can reduce moving upward through the building
3. The beam sizes can reduce where live loads are 2.4 kPa
4. CLT floor plates consider Crosslam CLT Design Guide (Structurlam, 2016) and EQ (2012) report.

Since gravity design is not the topic of this thesis, the preliminary timber sizes shown will be used for all levels. In a real design, it acknowledged that efficiencies should be realized.

8. Concrete core initial assumptions

Vertical SFRS components are of reinforced concrete. To account for decreased stiffness due to cracked properties, the effective stiffness of concrete shear walls was initially assumed to be 0.35Ig (as per the ASCE-7 requirement).

$$I_{cr} = 0.35I_g (\text{Initial Assumption to ASCE} - 7) \quad (5\text{-}6)$$

Further refinement considering axial load capacity demand ratio, in accordance with CSA A23.3 (Clause 10.14.1.2) was required and is carried out in subsequent iterations as follows:

$$Coupling\ beam\ conventionally\ reinf.: A_{ve} = 0.15A_g;\ I_e = 0.4I_g \quad (5\text{-}7)$$

$$Coupling\ beam\ diagonally\ reinforced: A_{ve} = 0.45A_g;\ I_e = 0.25I_g \quad (5\text{-}8)$$

$$Wall = A_{ve} = \alpha_w A_g;\ I_e = \alpha_w I_g, where\ \alpha_w = 0.6 + P_s/(f'_c A_g) \leq 1.0 \quad (5\text{-}9)$$

Note that two distinct reinforced concrete shear wall systems are initially assumed to form the primary vertical SFRS; ductile coupled walls and ductile shear walls. Ductility and overstrength factors for ductile coupled concrete shearwalls and ductile shearwalls designed and detailed in accordance with CSA A23.3-14 are R_d=4.0, and R_o=1.7, and R_d=3.5, and R_o=1.6, respectively. Note that the system benefits from coupling action under loading in the x-direction only whereas, in the y-direction, the core walls are not coupled but simply cantilevered. A check for degree of coupling is required and takes the form

$$\frac{(T)(l)}{M_1 + M_2 + M_3 + (T)(l)} \quad (5\text{-}10)$$

Where (T) is the axial tension and compression acting at the centroid of the coupled walls which is calculated as

$$\sum_{i=1}^{n} V_{fbi} = T \quad (5\text{-}11)$$

Where V_{fbi} is the sum of the upward storey shears at the coupling spandrel edges of a given pier and (l) is the distance between the centroids of coupled walls.

The degree of coupling must not be determined with a response spectrum analysis because the reactions are not in equilibrium. Instead, the equivalent static force procedure (ESFP) was used to complete and balance the check. It is presently assumed that full coupling action will arise from the design. This assumption will be checked during ESFP analysis.

9. Determine the seismic weight (W)

The building loads which are used to develop the seismic weights were summarized in Table 5-4. Note that the floor live load has been increased from 1.9 kPa for residential occupancy to 2.4 kPa to allow for flexibility in occupancy allowing for office space for all floors above the first. The first floor has been increased to 4.8 kPa to meet the lower storey office load requirement (NRC Commentary, 2015). Assuming the weights of the perimeter timber frames fit within the allowable 1.0 kPa cladding load, the seismic weights are provided in Table 5-6. Later, the self-weight of the timber frames is included.

Table 5-6 Preliminary seismic weights used for analysis

W_{roof}	
Area	(528 m^2)[(1.0)(3.0)+(0.25)(2.8)]=1954 kN
Perimeter	(92.8 m) (1/2(3)+1)(1.0)= 232 kN
Core	(384 kN/m) (3/2)=576 kN
Sum	W_{roof}=2762 kN
W_{floor}	
Area	(528m^2)[(1.0)(4.0)]=2112kN
Perimeter	(92.8m)(3)(1.0)= 278kN
Core	384kN/m(3)=1152kN
Sum	W_{floor}=3542kN

The total seismic weight of the structure was estimated to be 2762 + 11(3542) = 41,724 kN.

10. Set the period (T)

Either, the empirical period (T_{emp}) or a period (T) calculated according to mechanics in accordance with NBCC (2015), within a range from empirical to a code specified upper limit (T_{lim}), can be selected. There is a benefit to calculating the period (T), rather than simply using the empirical period (T_{emp}). If one assumes the analytical period is longer than the code specified period (T_{emp}), the preliminary base shear can be reduced. This is desirable because a lower starting point often leads to a more economical design after some design iterations. The upper limits on analytical periods (T), according to NBCC (2015) are provided to leave some allowance for stiffness contribution of non-structural elements with the system (Canadian Commission on Building and Fire Codes National Research Council of Canada, 2015). Where drift is governing, the period used for these calculations can be a shorter (stiffer) period to possibly limit drift or alternately a longer period to reduce force demand and also possibly reduce drift.

$$\mathrm{T}=\begin{cases} T_{emp}, or \\ T_{emp} \geq T \geq T_{lim} \end{cases} \tag{5-12}$$

$$\begin{cases} 0.05(h_n)^{\frac{3}{4}} = \ 0.735\ s, or \\ 0.735\ \mathrm{s} \leq T = 1.42\ s\ (uncoupled\ in\ x), 1.29\ s(coupled\ in\ y) \leq (2)T_{emp} = 1.47\ \mathrm{s} \end{cases}$$

Since the period calculated with ETABS is less than the limit of double the empirical period and less than an absolute value of four seconds, any value of period between the ETABS calculated

and empirical values can be used. It was anticipated that the perimeter moment frame may add more than the 15 percent allowable stiffness so the period was initially taken as 1.0 s, and 1.2 s for x, and y-directions respectively. The model for initial period determination was very limited, including only cracked core walls, rigid diaphragms, and seismic weight applied as dead load with the mass source switched to source the load patterns. Multipliers for the mass and weight of materials were used to avoid counting their weights twice. The first and second mode period were 1.4, and 1.2 seconds.

The equivalent static force procedure (ESFP) allows for consideration of T_{emp}, $T_{analytical}$, or T_{max}. A longer period helps to reduce the demand on this initial design iteration. The period was set to the maximum allowed based on the structure type and reduced drift limit of one percent for the importance type.

11. Determine initial design base shear (V)

First irregularity types were considered; Type 7 may exist; Type 1 can be mitigated with thoughtful design choices; and all other irregularities were not present in the structure. Note that according to 4.1.8.7.(1), if we cannot mitigate the torsional sensitivity (irregularity), the NBCC dynamic analysis procedure must be used. Also note that Type 7 irregularity is not allowed for post disaster structures, per 4.1.8.10.(2) NBCC. However, the ESFP provides a good initial starting point and provides the base shear (V) that is required for subsequent phases of design.

5.2.2 Equivalent static force procedure

The equivalent static force procedure is implemented as follows:

1. Calculate base shear and storey forces, shears and overturning distributions

$S(T_a)$ was interpolated for each direction (see Figure 5-6) and calculated as $S(T_{a,x}=1.0\text{ s})=0.934$ g and $S(T_{a,y}=1.2\text{ s})=0.872$ g. M_v and J were calculated based on table 4.1.8.11 in the NBCC. First, S(0.2)/S(5.0) ratio is found to be six. For the coupled system in the x-direction where $T_a=1.0$ s, $M_v=1.0$ and J=0.97. For the wall system in the y-direction with $T_a=1.2$ s, $M_v=1.01$, J=0.93.

$$V = S(T_a)M_v I_E W/(R_d R_o) \quad (5\text{-}13)$$

$$V_x = \frac{(0.87)(1.0)(1.5)W}{(4.0)(1.7)} = 0.192W = 0.19(41{,}724) = 8007\text{kN}$$

$$V_y = \frac{(0.93)(1.01)(1.5)W}{(3.5)(1.6)} = 0.24(41{,}724) = 10{,}014\text{ kN}$$

For walls and coupled walls, a lower limit is provided as

$$V = S(4.0)M_v I_E W/(R_d R_o) \quad (5\text{-}14)$$

$$V_x = \frac{(0.3)(1.0)(1.5)W}{(4.0)(1.7)} = 0.066W = 0.066(41{,}724) = 2{,}754\text{ kN}$$

$$V_y = \frac{(0.3)(1.01)(1.5)W}{(3.5)(1.6)} = 0.08(41{,}724) = 3{,}338\ kN$$

And since our system is ductile and soil seismic site class is E (better than F), an upper limit on the seismic base shear is given as the greater of:

$$V = \frac{2}{3}S(0.2)I_E W/(R_d R_o), \text{ and} \quad (5\text{-}15)$$

$$V = S(0.5)I_E W/(R_d R_o)$$

2/3(1.348)=0.899, and S(0.5)=1.348; therefore the second equation governs and V_{max}=(1.348)(1.5)W/(R_dR_o)=0.297W, and 0.340W for x and y respectively. These upper limits do not govern so the base shear of 8,007 kN and 10,014 kN were used for the initial ESFP procedure. The base shear (V) is distributed over the height of the structure per 4.1.8.11.(7) NBCC. The correction for taller structures (F_t) provided in the NBCC ESFP is calculated because the period is greater than 0.7 seconds. F_t=0.07T_aV giving 701 kN and 672 kN for x and y, respectively. Each storey is assigned a fraction of the base shear according to

$$F_x = (V - F_t)W_x h_x/(\sum_{i=1}^{n} W_i h_i) \quad (5\text{-}15)$$

Overturning effects are determined with the following equation. J is modified to become Jx where J_x=1.0 for $h_x \geq 0.6h_n$, and J_x=J+(1-J)(h_x/0.6hn) for $h_x < 0.6h_n$

$$M_x = J_x \sum_{i=1}^{n} (F_i - h_x) \quad (5\text{-}16)$$

Preliminary shear and overturning moment distributions, prior to inclusion of torsion and P-delta effects, are presented in Figure 5-7 (a) and (b) show the system in the coupled direction resulting in lower stiffness and lower loading whereas the y-direction (c) and (d) show increased storey shear and overturning due to the stiffer cantilevered core walls.

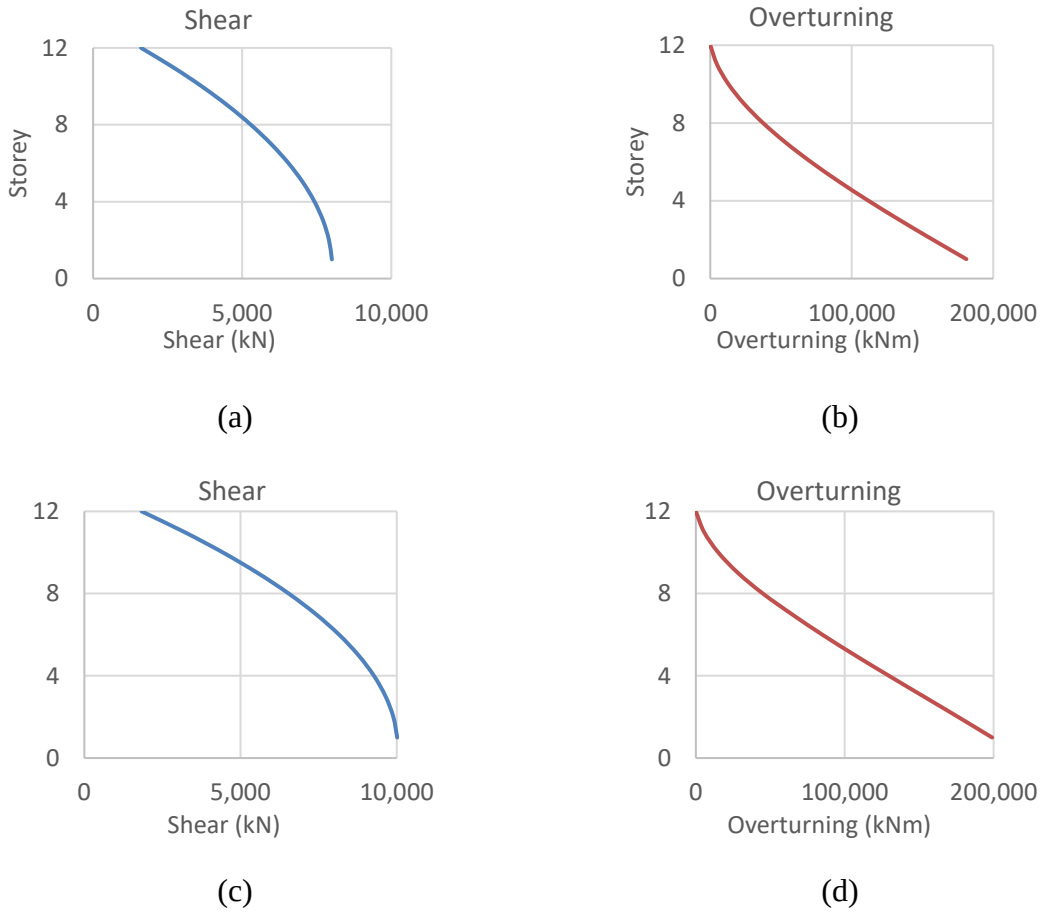

Figure 5-7 Preliminary shear and overturning results (a) shear in x-direction, (b) overturning in x-direction, (c) shear in y-direction, (d) overturning in y-direction

2. Consider accidental torsion, P-delta effects, notional loads and check drift limits

The eccentricity results and torsional characteristics of the structure as calculated with ETABS are provided in Table 5.7.

Table 5-7 Eccentricities and total static torsional moment

Eccentricities (m)	
e_x	Natural: $\|cm_x - cr_x\|$=0.03 m, Accidental: $0.1(D_{nx})$=0.1(22.0)=2.20 m, Max total: 2.23 m
e_y	Natural: $\|cm_y - cr_y\|$=0.00 m, Accidental: $0.1(D_{nx})$=0.1(24.4)=2.44 m, Max total: 2.44 m
Torsional Moments (kNm)	
T_x	$T=Ve_x$=(8007)(2.23)=17,856 kNm
T_y	$T=Ve_y$=(10,014)(2.44 m)=24,434 kNm

Note that the torsional moments are split into a per floor moment and applied at each level. For brevity here, only overall torsional moments are shown. Initially, the center of mass was displaced in both principal directions as shown in Equation 4-18.

$$T_x = F_x(\pm 0.10 D_{nx}) \quad (5\text{-}17)$$

Next, the parameter B_x was calculated

$$B_x = \frac{\delta_{xe,max}}{\delta_{xe,avg}} \; where: \delta_{xe,avg} = 0.5(\delta_{xe,min} + \delta_{xe,max}) \quad (5\text{-}18)$$

The model was first run with no eccentricities; then, the code specified eccentricity was applied. The results for the x-direction were most severe in the first storey, where maximum displacement was 2.4 mm and average was 1.3 mm, this results in

$$B_x = \frac{(2.4)}{1.3} = 1.85 > 1.7$$

When loaded in the y-direction, the second storey is the most critical storey, B_y is given as

$$B_y = \frac{(2.6)}{1.4} = 1.83 > 1.7$$

Based on these results, it is concluded that the preliminary structure is torsionally sensitive. Since torsionally sensitive structures are not allowed for post disaster NBCC (2015), some modification must be made. Maximum interstorey displacements were calculated as 12.3 mm and 13.7 mm in x, and y directions were on the 9th and 8th floor respectively. Dividing by storey height (eg. 12.3/3000) gives drifts of 0.4 percent and 0.5 percent, then amplifying for non-linear effects (R_dR_o-/I_E), brings the drifts to 2.25 percent and 1.6 percent, respectively for x and y; the post disaster limit of pne percent maximum drift was exceeded.

Stability coefficients were checked. Maximum stability coefficients occurred at ground level where they were 0.01 which is considerably less than the limit of 0.1. This indicates that P-delta effects need not be considered. While they need not be considered according to the code, it was of interest; therefore, the effects were considered. P-delta effects were included as a non-linear load case in ETABS such that all further analyses could then start from that point of P-delta modified stiffness including self-weight. Since compressive stresses in axial-lateral systems increase sway, the impact on the period provides a good point of reference. To illustrate the relative magnitude of P-delta effects of the fundamental period (T), a non-linear case was defined where the period calculation includes the P-delta effects. The results were that the period increased to 1.007 s from

1.000 s (less than one percent change). This small change in period helps further illustrates that global sway effects are negligible.

Note that just because P-delta effects are negligible for global sway, P-delta effects on individual members still need to be considered. Individual member design can typically use moment magnification methods (CSA - CSA Standards, 2014a; CSA - CSA Standards, 2014b; CSA - CSA Standards, 2014c) to account for lateral displacement of a member between its ends to account for local (member-specific) P-delta effects. Because notional effects are currently only required for steel, notional loads were not included in this analysis and are left for future study.

3. Wall coupling check

The wall base moments and the outermost couple are used to determine the percentage coupling achieved. To achieve this, a two-dimensional model was used of only the coupling walls. It was assumed that 0.3 of the ESFP loads were received for this check.

$$\frac{(10{,}123)(5.815)}{(2{,}515 + 10{,}383 + 2{,}520) + (10{,}123)(5.815)} = 0.79\ or\ 79\%\ Coupled \qquad (5\text{-}19)$$

Note that at least 66 percent is required to consider the concrete shear walls coupled (rather than only partially coupled).

4. Update model properties

Model updates for cracked stiffness's are calculated following A23.3 (2014),

$$Coupling\ beam\ conventionally\ reinf.: A_{ve} = 0.15A_g;\ I_e = 0.4I_g \qquad (5\text{-}20)$$

$$Coupling\ beam\ diagonally\ reinforced: A_{ve} = 0.45A_g;\ I_e = 0.25I_g \qquad (5\text{-}21)$$

$$Wall = \ A_{ve} = \alpha_w A_g;\ I_e = \alpha_w I_g, \qquad (5\text{-}22)$$

$$where\ \alpha_w = 0.6 + \frac{607{,}000}{30(350 * 1000)} = 0.64 \leq 1.0$$

Note that the case shown was worst case (heaviest wall loading) and is at the base of the wall (per A23.3); however, A23.3 allows averaging with less loaded walls. The parameter α_w was increased to 0.6 for all concrete core walls (as an average).

Revision requirements are gathered and implemented to analysis models from findings of this phase. A quick look at drift, torsional sensitivity, and period influence is provided in Table 5-8.

Table 5-8 Change in key parameters due to model update

Parameter	Initial	Updated
B_x	1.86	1.85
B_y	1.83	1.79
R_{dx}	4.0	3.5
Max ISD in x	2.25	3.1
MAX ISD in y	1.6	3.7
T_x	1.0 s	0.79 s
T_y	0.91 s	0.72 s

The fundamental period in each direction decreased by about 20 percent. It is noted that while stiffness' (EI_{eff}) increased, so did the load attracted by the stiffer structure which significantly increased predicted drifts.

5. Check if semi-rigid frames influence the SFRS

The semi-rigid timber frames were added to the model and checked for significant impact on the structural performance, keeping in mind the 15 percent code limit on increased stiffness for inclusion in the SFRS. It is assumed that construction detailing at the joints provides the same timber sizes resulting in the same performance and that the change in vertical shear due to gravity loads is negligible in the hysteretic performance of the connections. The addition of the semi-rigidity to the timber frames provided only a 2.5 percent decrease in fundamental period. This was lower than anticipated. It is noted that the 15 percent limit to additional stiffness is easily met; thus, inclusion of the timber semi-rigidity in the SFRS is not required. It is not desired either since the small additional stiffness will require approximately double the design force due to ductility R_d being reduced to maximum of R_d=2.0.

5.2.3 Modal response spectrum analysis

To achieve a passing design for global drift and shear in coupled beams, additional concrete core wall thickness was required and two additional blade walls were also included in the core region. The following steps were followed during the response spectrum analysis.

1. Perform response spectrum analysis

In each orthogonal direction and with the model restrained in the direction normal to the input, the design response spectrum (S(T)) was provided as a load. From this analysis, the fundamental lateral period (T_a), and the elastic base shear (V_e) for each of the two axes of consideration were calculated as shown in Table 5-9.

Table 5-9 Modal response spectrum elastic base shear and fundamental period

	x-direction	y-direction
V_e (kN)	47,616	50,087
T_a (s)	0.767	0.697

2. Adjust to an elastic design base shear (V_{ed})

The elastic design base shear (V_{ed}) was reduced by multiplying by two thirds of the response spectrum at a 0.2 seconds period divided by the response spectrum at the fundamental period ($S(T_a)$). Using the value of T_a calculated in the previous step, the following values of elastic design base shear were calculated. Note $S(T_a)$ is interpolated linearly based on the site-specific design spectral response accelerations as shown in Figure 5-6. $S(T_{a,x})$=1.127g, $S(T_{a,y})$=1.185g.

$$If \begin{cases} Site \neq F, and \\ R_d \geq 1.5, \end{cases} ; then\ V_{ed} = (V_{ed}) * greater\ of \left\{ \begin{array}{l} \left(\frac{2}{3}\right)\frac{S(0.2)}{S(T_a)} \leq 1.0 \\ \frac{S(0.5)}{S(T_a)} \leq 1.0 \end{array} \right\} \quad (5\text{-}23)$$

$$V_{ed,x} = (47{,}616) * greater\ of \left\{ \begin{array}{l} \left(\frac{2}{3}\right)\frac{1.348}{1.127} = 0.797 \leq 1.0 \\ \frac{1.348}{1.127} = 1.196 \ \leq 1.0 \end{array} \right\}$$

$$V_{ed,x} = 47{,}616kN; similarly\ V_{ed,y} = 50{,}087kN$$

Note that in the 2010 edition of the NBCC, the $S(0.5)/S(T_a)$ term was not included; therefore, the base shear would have been reduced in this step.

3. Determine the base shear (V); consider drift (T_{drift}) versus strength ($T_{strength}$)

For scaling, the NBCC (2015) equation used for calculating the minimum lateral earthquake force (V) (Note: $V=V_{ESF}$) is used with unique period values for drift compared to strength calculations. The base shear (V) has been calculated already in the initial design steps. For strength and drift, the periods (T_a) are allowed to vary as $T_{a,drift}$ and $T_{a,strength}$. In effort to not be overly conservative, the period may be adjusted as follows for strength and drift calculations. Since T_{emp}=0.735 s, and T_x=0.767 s, T_y=0.697 s, use T_x=0.735 s, and T_y=0.697 s for both strength and drift calculations. Therefore, $S(T_{a,x})$=1.154, and $S(T_{a,y})$=1.185. Finally, V_x=10,621 kN, and V_y=12,760 kN.

4. Calculate the scaling factor (V_d/V_e)

First, the design base shear (V_d) is calculated as shown in Equation 4-25.

$$V_d = V_{ed}\frac{I_E}{R_d R_o} \leq \begin{Bmatrix} 0.8V \text{ if regular or irregular but ESFP allowed} \\ V \text{ if dynamic analysis is required} \end{Bmatrix}$$

$$V_{d,x} = 47{,}616\frac{1.5}{(3.5)(1.7)} \leq \{10{,}621\} = 12{,}004\ kN \qquad (5\text{-}24)$$

$$V_{d,y} = 50{,}087\frac{1.5}{(3.5)(1.6)} \leq \{12{,}760\} = 13{,}416\ kN$$

Then, the scaling factors $(V_d/V_e)_{x,y}$ are calculated as 12,004/47,616 = $(V_d/V_e)_x$ = 0.252, and similarly $(V_d/V_e)_y$ = 0.268. These scale factors were applied to values obtained from the dynamic analysis with unrestrained floors including: elastic storey shears, storey forces, member forces, deflections. Deflections were also scaled once more.

5. Include effects of accidental torsion

Because the structure has B>1.7 in both x, and y-directions, and for simplicity, superposition of the torsional moments due to $\pm(0.10)D_{nx}$ was used. Figure 5-8 demonstrates the effects of shifting the centres of mass and the amount of inherent (natural) torsion. Note that there is negligible inherent torsion. This is because the structure is very symmetric with centres of mass and rigidity aligned. In this particular case, it is demonstrated not to be necessary to superimpose the $0.10D_{nx}$ values to the restrained model because the restrained model is equal to the zero-eccentricity model.

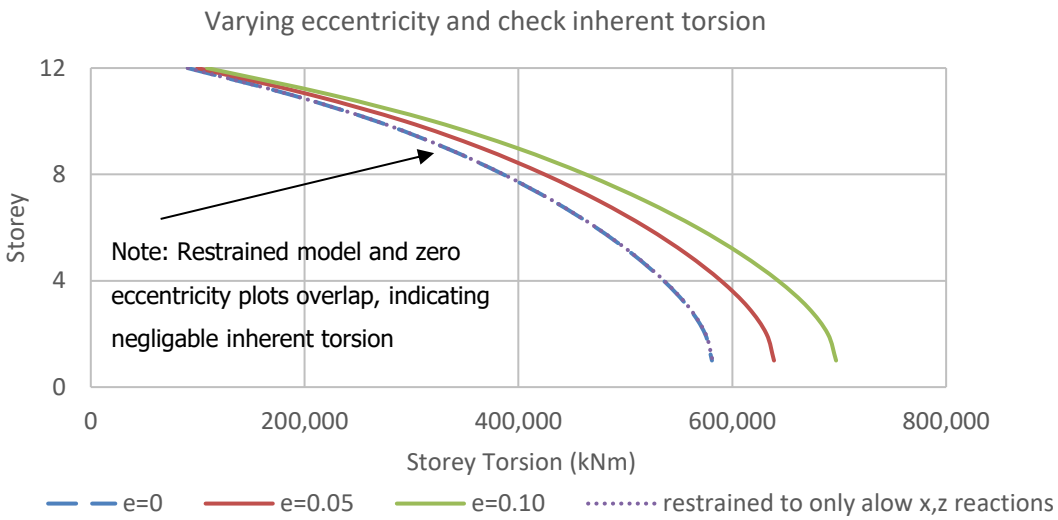

Figure 5-8 Varying eccentricities and inherent torsion

6. Convert from elastic to inelastic forces and pseudo-elastic displacements

Both elastic and scaled response spectrum x-direction storey shears are shown in Figure 5-9. The figure illustrates the impact of including ductility into seismic design by showing the magnitude of force reduction achieved. Figure 5-10 shows the scaling method for drift. Note that drift results were exceeding the specified drift limit for post disaster; therefore, design iteration was required.

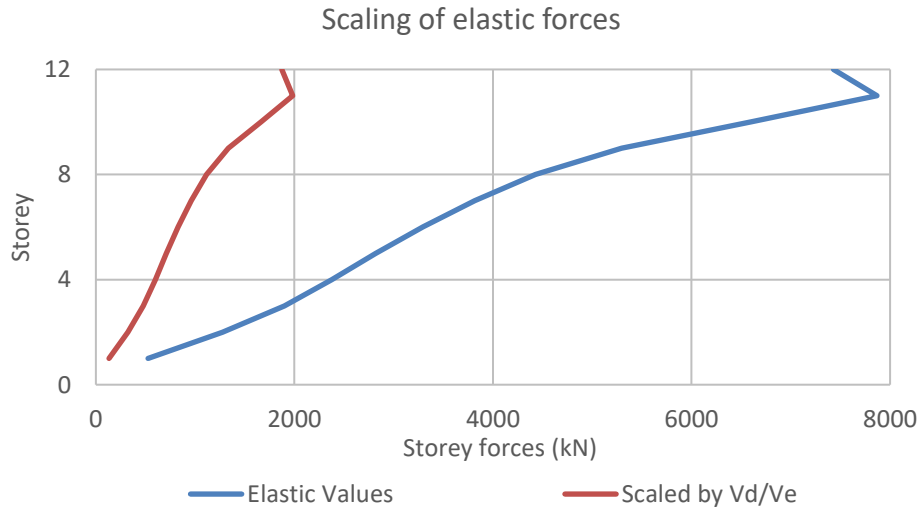

Figure 5-9 Scaling of elastic forces

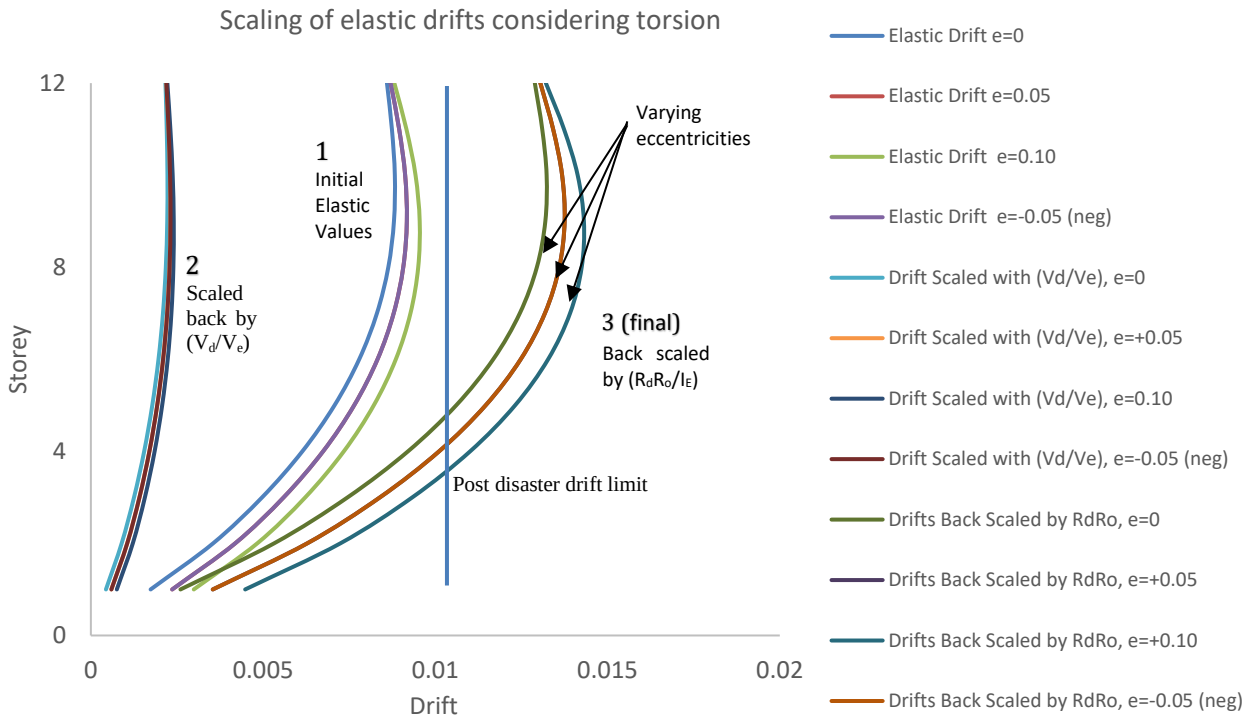

Figure 5-10 Scaling of drifts considering torsion

5.2.4 Selection and scaling of ground motions

The selection and scaling of ground motions for response history analysis following Method A, from the appendix of Commentary J in the NRC Structural Commentaries (2015), was applied for the site and structure as follows:

1. Determine the target response spectrum S(T)

The response spectrum S(T) used for ground motion selection and scaling procedures was the site modified, and low period detailed spectrum shown in Figure 5-11.

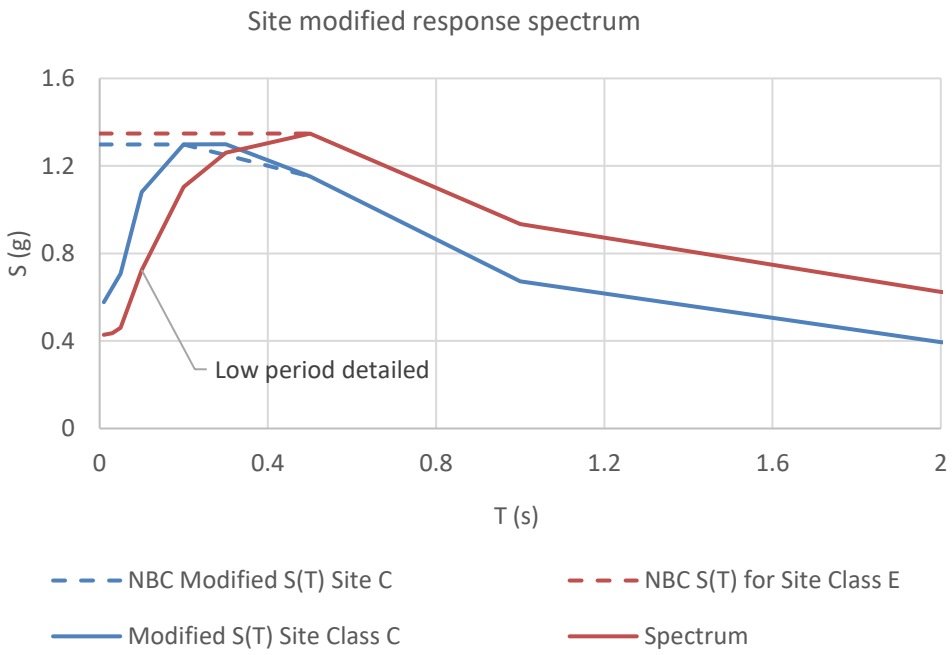

Figure 5-11 Response spectrum for selection and scaling of ground motions

2. Determine the period range of interest (T_R)

The period range of interest was governed by the 90 percent participating mass ratio on the low spectrum and the minimum upper limit for the high end of the spectrum. Participating mass ratios from contributing modes are shown in Table 5-10 and the resulting period range of interest is shown in Figure 5-12.

Table 5-10 Participating mass ratio's

		Participating mass ratio (%)			
Mode	T (s)	X	Y	Z	Mode
1	0.655	0%	34%	2%	X,1
2	0.608	28%	34%	13%	Y,1
3	0.577	32%	35%	83%	Z,1
4	0.193	33%	35%	92%	Z,2
5	0.154	72%	35%	92%	X,2
6	0.151	73%	67%	92%	Y,2
7	0.113	73%	68%	96%	X,3
8	0.080	73%	68%	97%	Y,3
9	0.074	86%	68%	98%	X,4
10	0.068	86%	80%	98%	Y,4
11	0.061	86%	80%	98%	Z,3
12	0.050	86%	80%	99%	Z,4
13	0.049	92%	80%	99%	X,5
14	0.043	92%	87%	99%	Y,5
15	0.042	92%	88%	99%	Z,5
16	0.037	95%	88%	99%	X,6
17	0.036	96%	88%	100%	X,7
18	0.032	96%	88%	100%	Z.6
19	0.030	96%	92%	100%	Y,6

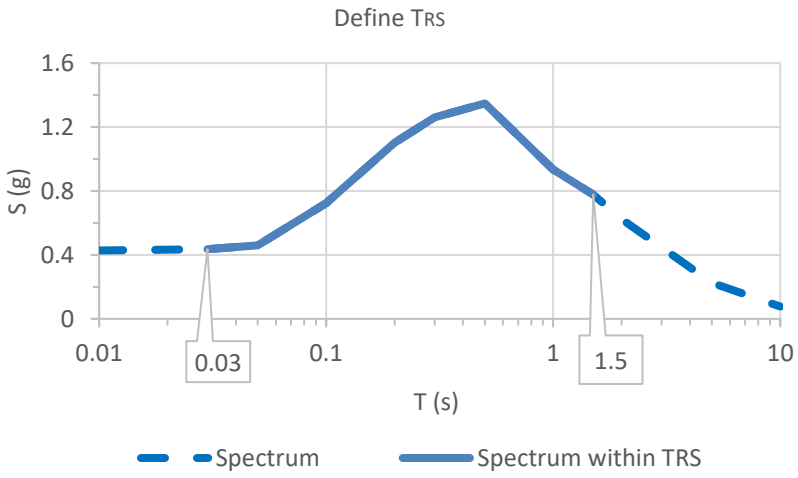

Figure 5-12 Period range of interest

3. Determine the seismo-tectonic regime

Because the site is located near the Cascadia subduction zone, three earthquake hazard scenarios were selected for the target ground motion suites; namely, crustal, in-slab and interface earthquakes. The nearest point from the earthquakes Canada hazard calculator (Natural Resources Canada, 2015) was referenced to choose the Latitude and Longitude to be matched with Open File 8090. Grid points are valid within about 10 km which is less than the closest grid point at 3.9 km away; therefore, there was no need to interpolate data file values. Data from Open File 8090 (Halchuk et al., 2016) was collated and plots were developed to demonstrate trends of the scenario-specific hazard contributions as shown in Figure 5-13 (a) and (b) with deaggregated spectra and relative contributions, respectively. Further, deaggregation plots requested from Earthquakes Canada and received via email (Canadian Hazards Information Service, 2017) were inspected to identify dominant scenarios. Selected deaggregation plots within the period range of interest and at the probability used in the 2015 NBC are provided in Figure A-1, Figure A-2, and Figure A-3 of Appendix A.

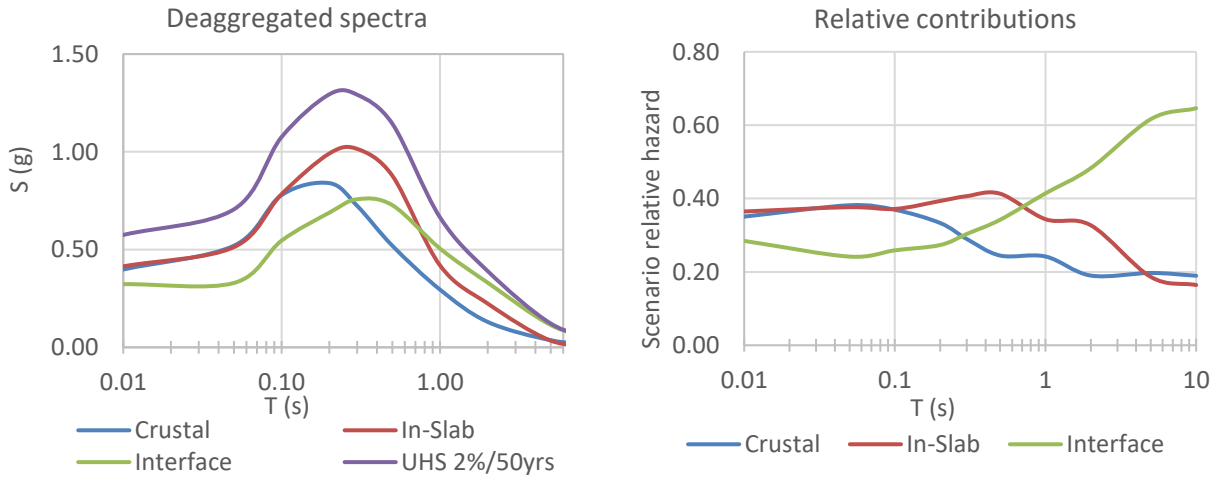

(a) (b)

Figure 5-13 Deaggregated hazard (a) deaggregated and uniform spectra, and (b) relative contributions of scenario-specific hazards

4. Define scenario-specific magnitude distance (M-R) relationships

The magnitude distance relationships for each scenario must be defined. These magnitude distance relations, along with soil parameter V_s30 formed the primary basis of ground motion record

selection while other secondary factors such as spectral shape, duration, and size of scale factor formed the secondary part of the ground motion selection process. To estimate the dominant magnitude-distance scenario's, global mode, global mean, and inspection of deaggregation plots methods were completed and are provided as additional information in Table A-1 and Table A-2 of Appendix A. The final target scenarios based on deaggregation inspection are presented in Table 5-11.

Table 5-11 Target scenario's

	M_w	R_{hyp} (km)	Vs30 (m/s)
Crustal	6.8	10	
In-slab	7.4	70	100-250*
Interface	9.0	50	

* Ideally Vs30 would be 0-180 m/s (site class E) but practically nothing below 100 m/s exists and some slightly over 180m/s may be well worth keeping as the values are not absolute; a strict interpretation of site class would be overly restrictive.

5. Scenario-specific period ranges of interest ($T_{RS,i}$)

With guidance not provided in the 2015 NRC Commentary on how exactly to develop scenario-specific period ranges, initially a 30 percent relative hazard assignment was attempted; however, this led to excessive scale factors due to maintaining not less than 90 percent of the mean over a longer segment of the period. Upon further literature review (Daneshvar, Bouaanani, Goda, & Atknison, 2016; Dehghani & Tremblay, 2016; Gonzalez, 2017; Monroy, Hull, & Atukorala, 2016; Shafiq, 2018; Tremblay et al., 2015) and review of deaggregated spectra dominant scenarios, the final scenario-specific period ranges of interest were adjusted with judgement to those shown in Table 5-12.

Table 5-12 Scenario-specific period range of interest

Scenario	Period range of interest
Crustal	$0.03\ s \leq T_{RS,crustal} \leq 0.40\ s$
In-slab	$0.03\ s \leq T_{RS,in\text{-}slab} \leq 0.80\ s$
Interface	$0.30\ s \leq T_{RS,interface} \leq 1.5\ s$

Exact methodology for defining the period range of interest was beyond the scope of the 2015 NRC Commentary but should be investigated further because the ground motion scale factors will directly affect the structural response.

6. Selection of ground motions

The selection of ground motions required utilization of multiple databases and supporting documentation on a scenario-specific basis. The PEER NGA-West2 database (Ancheta et al., 2018) provided records compatible with the crustal hazard. Using selection criteria of V_{s30} less than 180m/s, distance (R_{rup}) less than 50 km, and magnitude (M_w) of 5.5-7.5, initial selection was performed. To further reduce the number of ground motions, the design spectrum was considered to allow minimizing the mean square error. Duplicate records from the same event were removed and scale factors were minimized for scaling to $T_{rs,i}$. The K/KiK-Net database also contained an additional crustal record which made it into the final 11 selected records but was removed prior to the final three suites of five bi-directional ground motions (see Table A-3, Appendix A).

The K/KiK-Net (NIED, 2018) and Universidad de Chile (Departmento de Ingenieria Civil, 2018) databases were used to source subduction type events, including both in-slab and interface events. Flat files from Dawood, Rodriguez-Marek, Bayless, Goulet, & Thompson (2016) and Bastias & Montalva (2016) were used to assist with the selection processes for Japanese and Chilean earthquakes, respectively. For in-slab events, initial priority was given to soil parameter (V_{s30}) which resulted in the need to relax the magnitude and distance criteria. To increase the data pool, stochastic time histories from Atkinson (2009) M7 accelerograms were also considered; however, due to the preference of historical records and the criteria to minimize scale factors, these stochastic time histories were not included the final in-slab suite.

Ground motions originating from Japan's Kik-Net and Chile's Universidad de Chile databases were utilized for interface events. Retrieval of ground motion data was facilitated through COSMOS VDC (CESMD, 2018) as well as source databases. Simulated ground motions from Atkinson (2005) and Atkinson & Macias (2008) were also considered. The simulated ground motions were considered high quality for meeting the target magnitude distance scenario but lower quality compared to historical records in confidence of input time-acceleration values. None of the stochastic records made it to the final interface suite. Final selection of ground motions did not occur without going through the pre-processing and scaling procedures. The selection process was somewhat iterative as the final selected ground motions were refined by reviewing the magnitude of the required scale factors. Final selected ground motions are presented in Table 6-3 along with scaled mean spectra results are provided in Figure 6-13, on page 101.

7. Pre-processing of ground motions

Pre-processing requirements were primarily dependent on the source database. PEER NGA-West2 provided pre-processed accelerograms and any additional filtering was found to only distort the ground motions. Baseline correction was however at times required as integration of the accelerograms sometimes resulted in non-zero residual displacement trends. K/Kik-Net provided uncorrected (not pre-processed) accelerograms; therefore, filtering and baseline correction was always required. Universidad de Chile ground motion files were provided in both corrected and uncorrected formats. Where suitable, pre-processed ground motions were utilized. Where filtering was required, a Butterworth bandpass filter was used with frequency cut-offs at 0.1 Hz and 25 Hz for low and high frequency, respectively. When baseline corrections were required, a linear correction was first attempted; if the linear correction was not providing acceleration, velocity and displacement traces that best matched the original signature amplitude and phase, the filter order was increased to quadratic then cubic if required. Accelerogram timesteps varied from 0.004 to 0.01 seconds between different recording stations. All time steps were linearly interpolated (as required) to provide all ground motion accelerograms with a 0.01 second consistent time step maintaining duration characteristics of the original ground motion. Detailed pre-processing notes are provided in Table A-4 of Appendix A. It was reasonable not to rotate ground motions to fault normal and fault parallel directions because no target scenarios were within five km of the site; however, directionality effects still may impact the results; directionality effects have been left for future study.

8. Scaling of ground motions

Linear scaling over scenario-specific period ranges of interest was carried out. First, the geometric mean of bi-directional ground motions was calculated. Next, individual geometric means were linearly scaled by one divided by the average such that the record specific average was equal to the response spectrum average. Finally, the code limit of having the mean of geometric means not fall below 90 percent of the target spectrum was applied as a suite scale factor. The procedures of each scenario scaling are provided in Figure 5-14, Figure 5-15, and Figure 5-16 and the final mean spectrum results are presented in Figure 6-13.

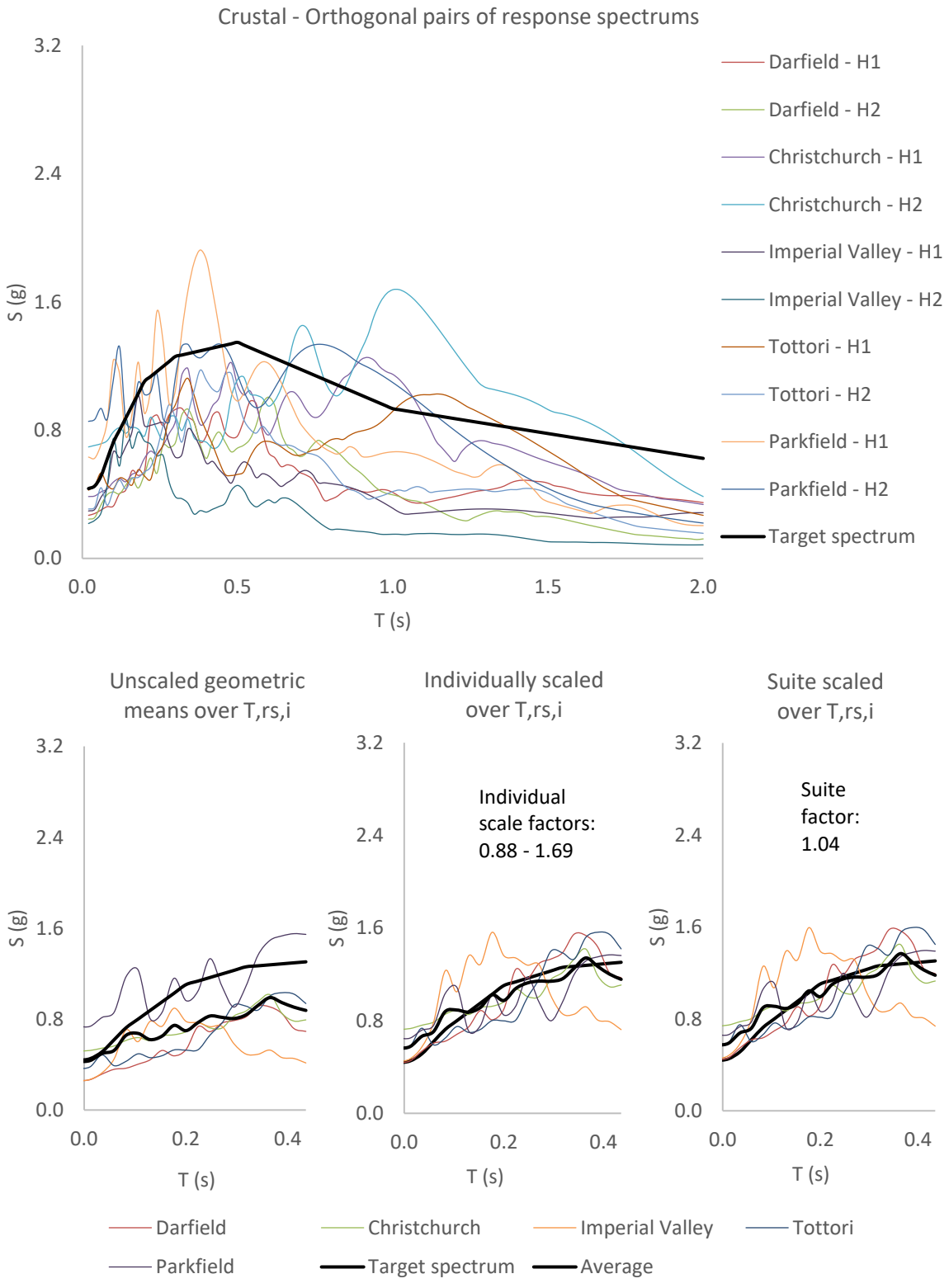

Figure 5-14 Crustal suite

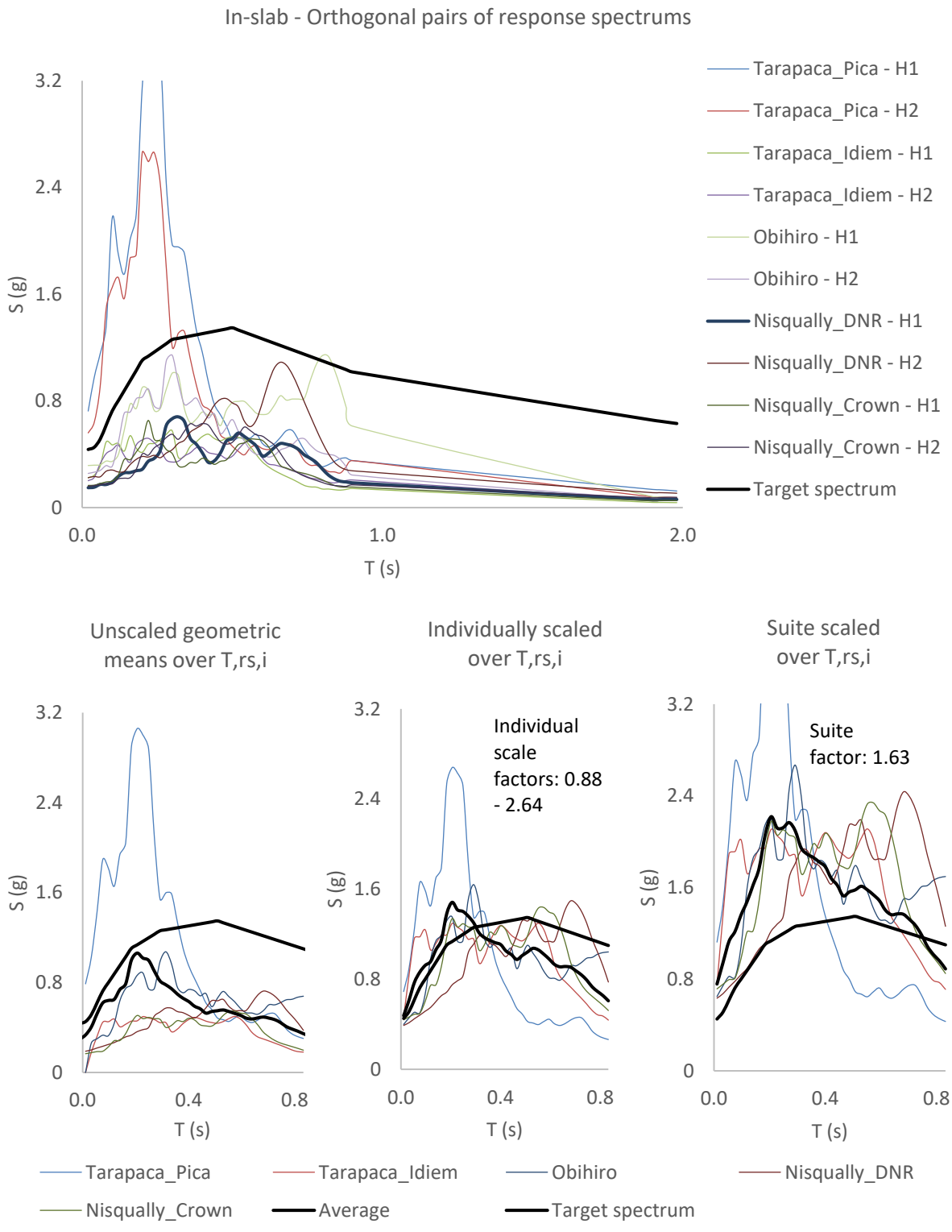

Figure 5-15 In-slab suite

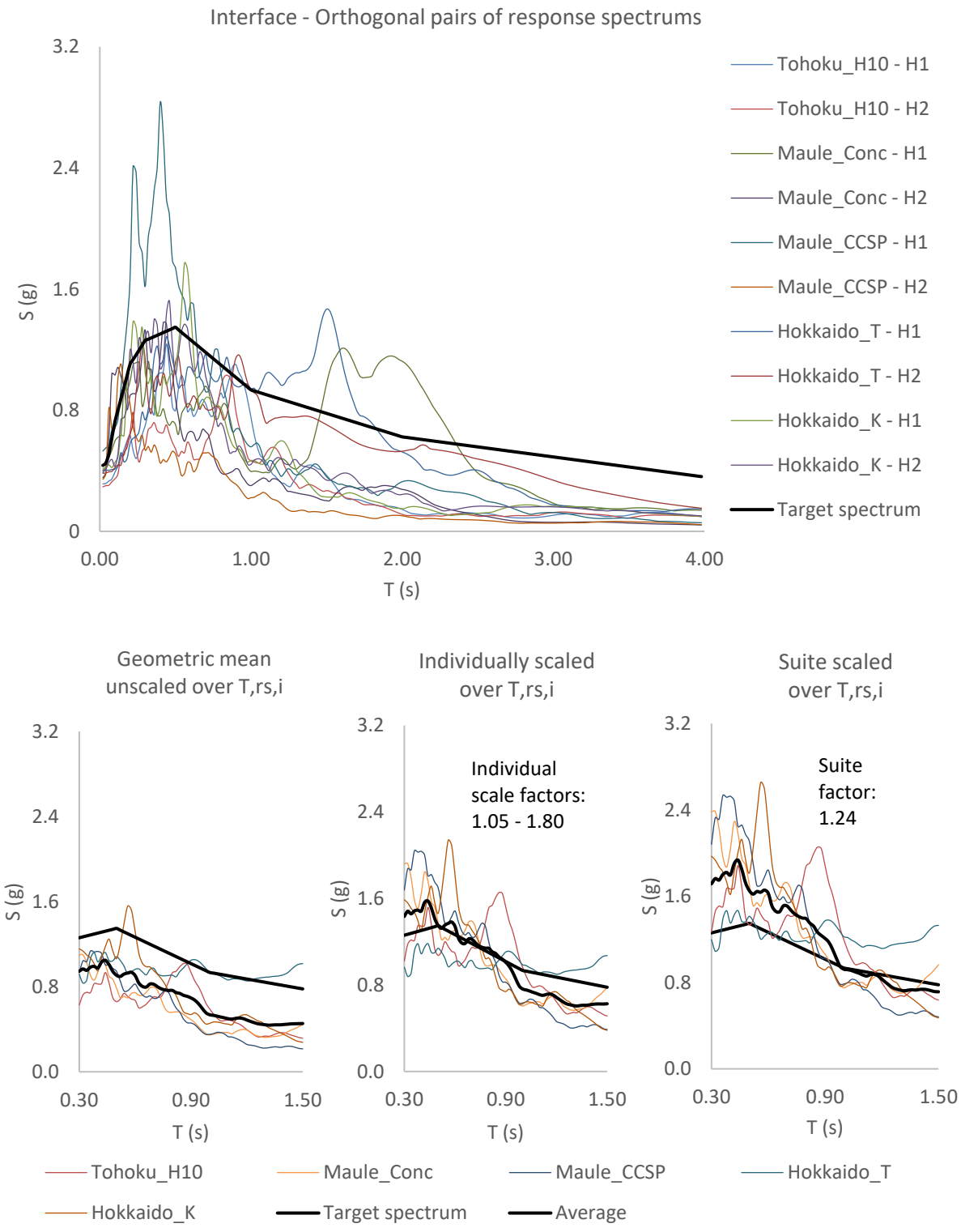

Figure 5-16 Interface suite

9. Application of ground motion pairs

While 4.1.8.8.(1) of the 2015 NBCC allows for a uni-directional analysis in each of the two primary orthogonal axis with orthogonal seismic force resisting systems, a simultaneous bi-directional analysis was instead selected. The 100:30 rule was applied such that each pair of orthogonal horizontal ground motions was simultaneously applied with 100 percent of one motion and 30% of the orthogonal motion in orthogonal directions. Next, each was rotated by 90 ° and the process was repeated. Vertical components were not included in the analysis. A simultaneous bi-directional or tri-directional analysis is more appropriate than a uni-directional analysis for response history analysis (Sherstobitoff, 2008). Also, for vertical elements that resist loads in both directions, such as columns or core walls, the effects of bi-directionality may become significant (Canadian Commission on Building and Fire Codes National Research Council of Canada, 2015); therefore, load cases were defined with the 100:30 rule for orthogonal pairs. This led to 60 load cases for the three scenario-specific suites of five pairs of orthogonal horizontal ground motions, allowing each of the two orthogonal ground motions to have 100 percent and 30 percent in each of the two primary orthogonal horizontal directions. Numerically, 3 x 5 x 2 x 2 = 60 load cases or 30 load cases for each of the two primary orthogonal directions. A sample of the notation for the load case definition is: CR-1-X-1 where CR indicates crustal, 1 indicates the first ground motion in the suite (Darfield), X indicated the primary direction (direction of 100 percent), and the 1, respectively, indicates that the 100 percent component is coming from the H1 component.

5.2.5 Linear response history analysis

For the linear response history analysis, a damping ratio of five percent of critical was assumed for all modes. The ground motions were scaled up for importance as

$$Input\ Ground\ Motion = (I_E) Design\ Ground\ Motion \quad (5\text{-}25)$$

The initial scale factor was Importance (I_E) multiplied by gravity (g) in terms of mm/s^2. Numerically, the scale factors for input accelerations were calculated as (9806)(1.5) = 14,709; due to a bi-directional analysis being carried out, the simultaneous orthogonal component scale factor was further reduced as (0.3)(14,709)=4,413. Note that the individual and suite factors were already applied during the selection and scaling of ground motions procedure. Back scaling was required for drift. Simultaneous bi-directional pairs were run with the 100:30 rule and the governing

response was identified from each pair having either H1 or H2 as primary orthogonal component (where H1 and H2 are arbitrary orthogonal components of ground motion) as the primary contributor. Governing combinations were identified and plotted as shown in Figure 5-17 (a), (c), and (e), and (b), (d), and (f) for x, and y-directions, respectively.

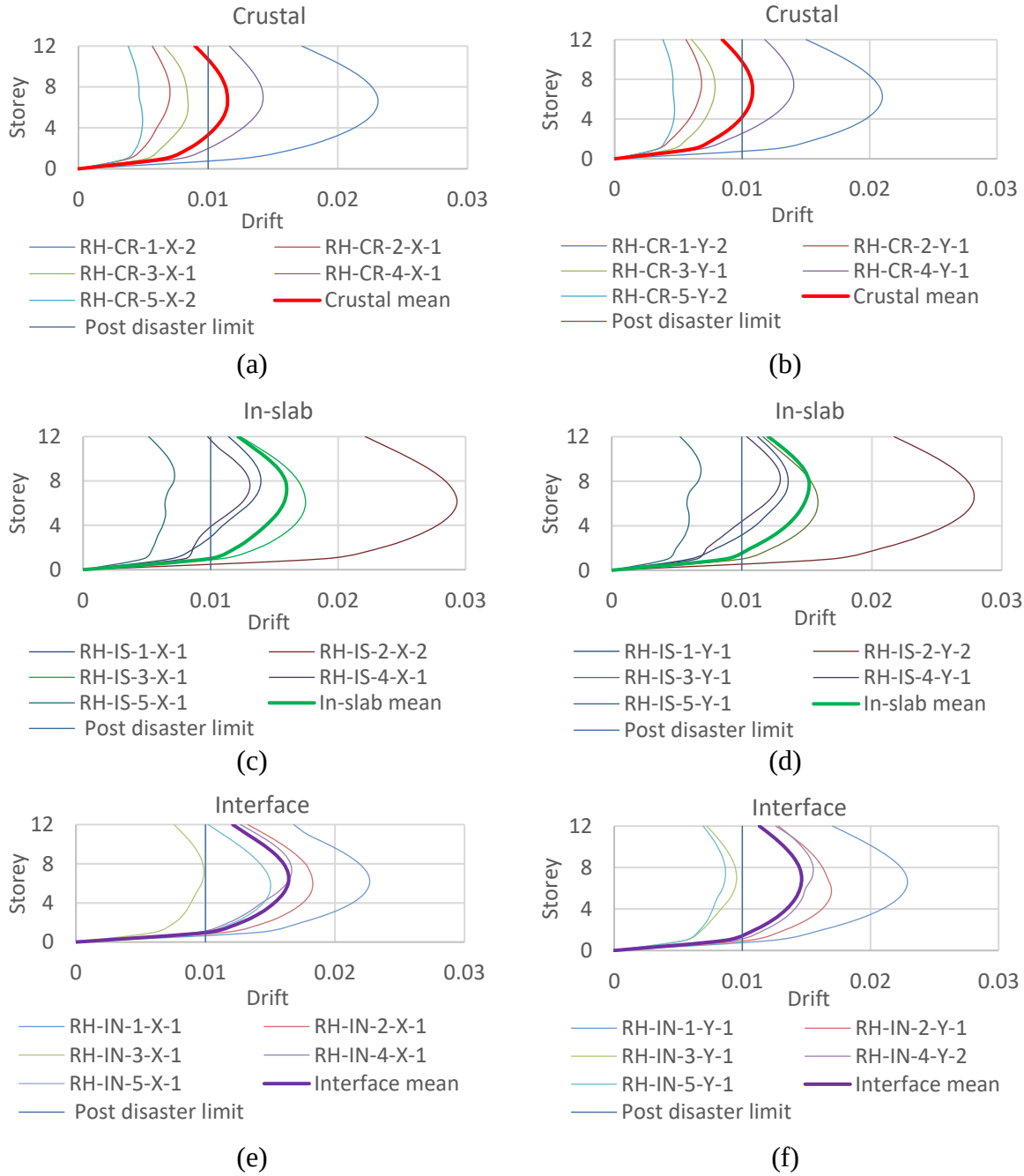

Figure 5-17 Governing maximum drift orthogonal pairs with suite average (a), (c), and (e) x-direction; (b), (d), (f) y-direction

Other global response parameters of storey shears and overturning were averaged in the same way; those results, along with the scenario drift combinations are presented in Chapter Six.

5.2.6 Non-linear response history analysis

Non-linear response history analysis was carried out much the same as the previous linear response history analysis except with overstrength, non-linearities, damping, and load cases updated. Overstrength was accounted for by increasing the modulus of elasticity properties by 20 percent as determined in the literature review section. Strain hardening was included into the reinforcing model as per the default for A615Gr60 rebar.

The inherent damping was set to 2.5 percent to be more aligned with experimentally measured values (see the literature review section 2.3.6 Damping), less than the maximum allowable of three percent under the 2015 NBCC, and greater than the minimum value recommended by the LATBC (2017). For further explanation of the damping selection.

Fast non-linear analysis (FNA) was used because it saves computational effort and time by separating the linear and non-linear components in the equation of motion. A Ritz modal case was defined for use with the FNA.

Dead and live loads were applied as linear static cases. A ramp function was defined with a rise time of seven seconds and a uniform time of seven seconds. This was to allow the non-seismic loads to be applied as fast non-linear analysis (FNA) case and then for the time history case to start after the gravity loads were applied. Damping for the ramp function was set to 99 percent of critical to allow the gravity loads to be applied and quickly stabilize.

The non-linear hinges included wall fiber hinges in all core walls and coupling beam hinges at each end of coupling beams in the coupled and double coupled core walls. Cantilever walls exist on gridline C, F, and H, while double coupled walls exist on grid line four and seven, and single coupled walls exist on gridline five and six. Note that the single coupled walls were added during design iterations with the modal response spectrum analysis. Timber connection non-linearities were omitted from the model to improve computational efficiency; these were previously shown to provide negligible lateral resistance compared with the core (see Section 4.2.2 ESFP). For the

concrete core, the non-linearity was captured as described in the review portion using both fiber model wall sections for the lower walls plastic hinge region and flexural hinges at coupling beams. Both hinges were automatically generated by ETABS based on ASCE-41-13 which is the relevant U.S. standard for seismic evaluation including aspects of performance-based design. Hinge reinforcing was automatically determined from the design carried out in ETABS. Figure 5-18 (a) shows the general arrangement in plan, (b) shows each basic type of core wall including coupled, double-coupled, and cantilever. Run times for the analysis varied by ground motion from about 30 minutes to over eight hours for the more intense, long duration motions. Post processing of global response parameters, including drift, storey shear and overturning moment, was completed in MS Excel.

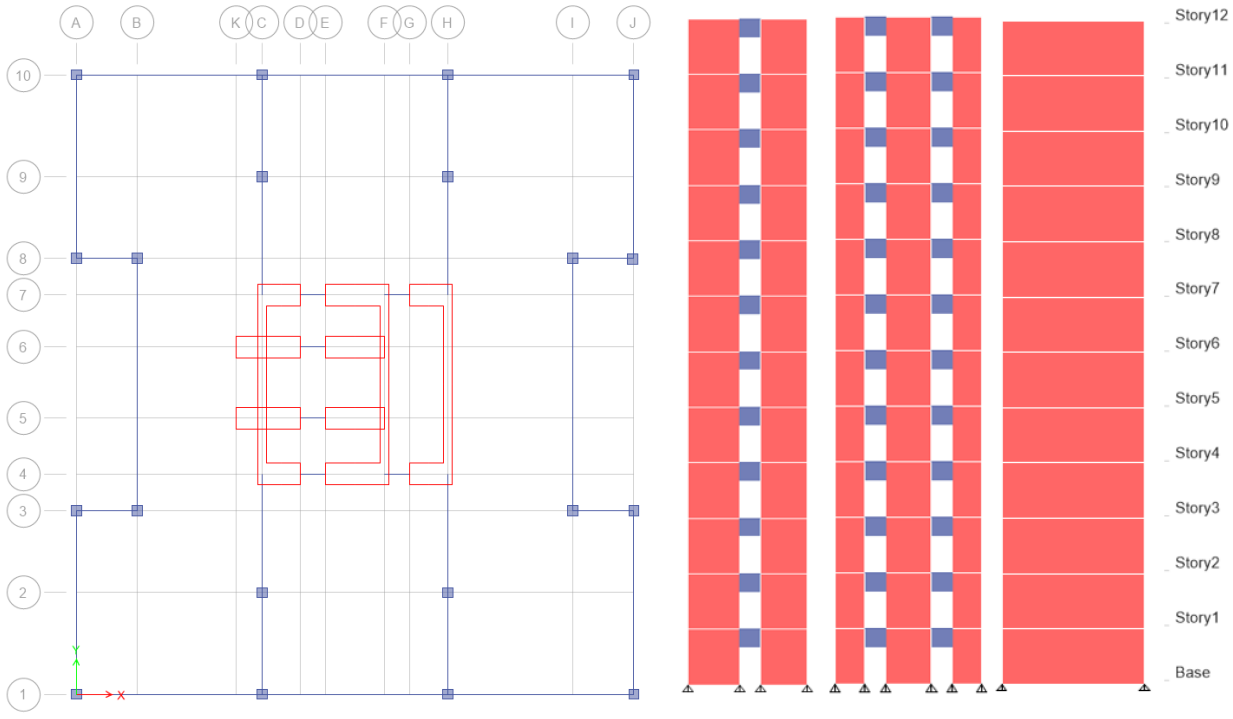

(a) (b)

Figure 5-18 General arrangement (a) plan view with core walls and gravity framing, and (b) elevations of basic coupled, double-coupled, and cantilever core walls

6 Results

Results of experimental verifications and the extended study are presented.

6.1 Experimental validations

Results of the one, two, and three-dimensional experimental verifications are presented.

6.1.1 One-dimensional study

The results of best fitting hysteretic connection models are provided in Figure 6-1. Figure 6-1 (a) and (b) show the beam to core connection for each axis of rotation while (c) and (d) show the beam-column and column-base connections, respectively. Aside from the less stiff reloading stiffness, the calibrated connection models provide a good visual trace to the experimental data. The strong axis of the beam to core connection Figure 6-1 (a) yields at around 25 kNm whereas the weak-axis (b) yields at around 7 kNm. With the same beam depth and connection arrangement, the beam to column connection (c) yields slightly lower than the connection to the core. This can be explained by the crushing of timber column in the perpendicular to grain orientation. The column to base connection (d) has a limited effective depth which provides yielding at similar levels to the weak axis beam connection.

Considering link rotational demand from ETABS during the extended study, a maximum rotation of 0.00181 radians was found. This was during elastic analysis. The rotational demand must therefore be scaled by (R_dR_o/I_E) equals (3.5*1.7/1.5)(0.00181) = 0.0072 radians as a maximum inelastic rotational demand. Checking the calibrated connection results, it can be seen that 0.0072 radians is less than both, beam-column at 0.01 radians to yield and beam-core at 0.05 radians to yield, connection capacities which makes the timber gravity system suitable for inclusion as a gravity load carrying system.

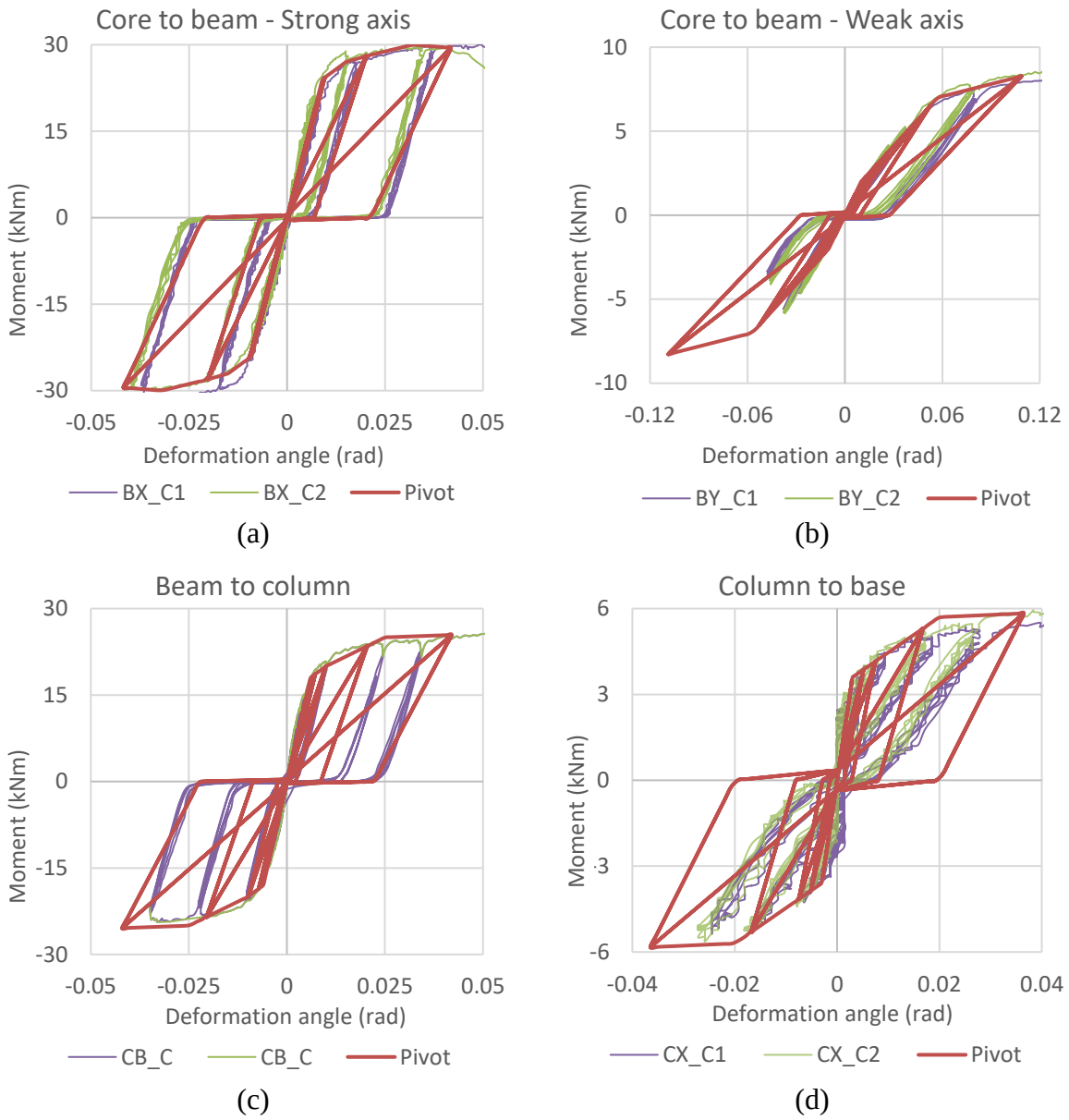

Figure 6-1 Calibrated Pivot hysteretic connection models (a) concrete core to timber beam – strong axis, (b) concrete core to timber beam – weak axis, (c) timber beam to timber column, and (d) timber column to base.

Table 6-1 summarizes results of the connection calibration obtained from the connections used in the 3D timber concrete hybrid model. The backbone parameters are typical between typical hysteretic models and can be used for various numerical connection models, besides just Pivot; whereas the non-linear parameters are specific to the Pivot model.

Table 6-1 Pivot connection parameters for tension bolt moment resisting connections

	Connection type			
Parameters	Core to beam – strong axis	Core to beam – weak axis	Beam to column	Column to base
Positive Backbone				
M_1 [kNm]	24	8.8	26	3.6
Θ_1 [radians]	0.009	0.16	0.065	0.003
M_2 [kNm]	27	8.3	25	5.7
Θ_2 [radians]	0.015	0.11	0.025	0.02
M_3 [kNm]	28	7	20	6.5
Θ_3 [radians]	0.020	0.057	0.02	0.12
M_4 [kNm]	30	2	18	5
Θ_4 [radians]	0.032	0.01	0.006	0.15
Negative Backbone				
M_{-4} [kNm]	-30	-2	-18	-5
Θ_{-4} [radians]	-0.032	-0.01	-0.006	-0.15
M_{-3} [kNm]	-28	-7	-20	-6.5
Θ_{-3} [radians]	-0.020	-0.057	-0.02	-0.12
M_{-2} [kNm]	-27	-8.3	-25	-5.7
Θ_{-2} [radians]	-0.015	-0.11	-0.025	-0.02
M_{-1} [kNm]	24	-8.8	-26	-3.6
Θ_{-1} [radians]	-0.009	-0.16	-0.065	-0.003
Stiffness [kNm/radian]	2667	160	2200	140
Non-Linear Parameters				
α_1	2.8	2.8	2.8	2.8
α_2	2.8	2.8	2.8	2.8
β_1	0.02	0.1	0.1	0.1
β_2	0.02	0.1	0.1	0.1
η	0	0	0	0

6.1.2 Two-dimensional study

Table 6-2 provides properties of calibrated connections from the two-dimensional study. The stiffnesses provided are valid for the specific timber connections studied and do not need to be used exclusively in the portal frame arrangement.

Table 6-2 Pivot parameters for lagscrewbolt connections

Parameters	Beam Connection			Column Connection		
	HTA 400	HTA 500	HTA 600	HCB 4	HCB 5	HCB 8
Positive Backbone						
M_1 [kNm]	52	50	80	10	25	25
Θ_1 [radians]	0.006	0.0025	0.004	0.0045	0.008	0.006
M_2 [kNm]	68	80	110	45	55	75
Θ_2 [radians]	0.015	0.008	0.008	0.02	0.025	0.035
M_3 [kNm]	72	115	110	55	70	95
Θ_3 [radians]	0.029	0.02	0.02	0.032	0.045	0.065
M_4 [kNm]	30	35	1	35	50	65
Θ_4 [radians]	0.065	0.08	0.063	0.046	0.063	0.08
Negative Backbone						
M_{-4} [kNm]	-30	-35	-1	-35	-50	-65
Θ_{-4} [radians]	-0.065	-0.08	-0.063	-0.046	-0.063	-0.08
M_{-3} [kNm]	-72	-35	-110	-55	-70	-95
Θ_{-3} [radians]	-0.029	-0.02	-0.02	-0.032	-0.045	-0.065
M_{-2} [kNm]	-68	-115	-110	-45	-55	-75
Θ_{-2} [radians]	-0.015	-0.008	-0.008	-0.02	-0.025	-0.035
M_{-1} [kNm]	-52	-80	-80	10	-25	-25
Θ_{-1} [radians]	-0.006	-0.0025	-0.004	-0.0045	-0.008	-0.006
Semirigidity [kNm/radian]	4,370	8,900	16,000	2,600	2,800	3,500
Non-Linear Parameters						
α_1	2.8	2.8	2.8	2.8	2.8	2.8
α_2	2.8	2.8	2.8	2.8	2.8	2.8
β_1	0.1	0.1	0.1	0.1	0.1	0.1
β_2	0.1	0.1	0.1	0.1	0.1	0.1
η	0	0	0	0	0	0

Pushover validations for the different types of column to base and beam to column connections are shown in Figure 6-2 (a) and (b), respectively. The component pushover curves show the numerical model fitting well to the experimental results. Next, the results of the portal frames with 400 mm and 500 mm deep beams are shown in Figure 6-3 (a), and (b), respectively.

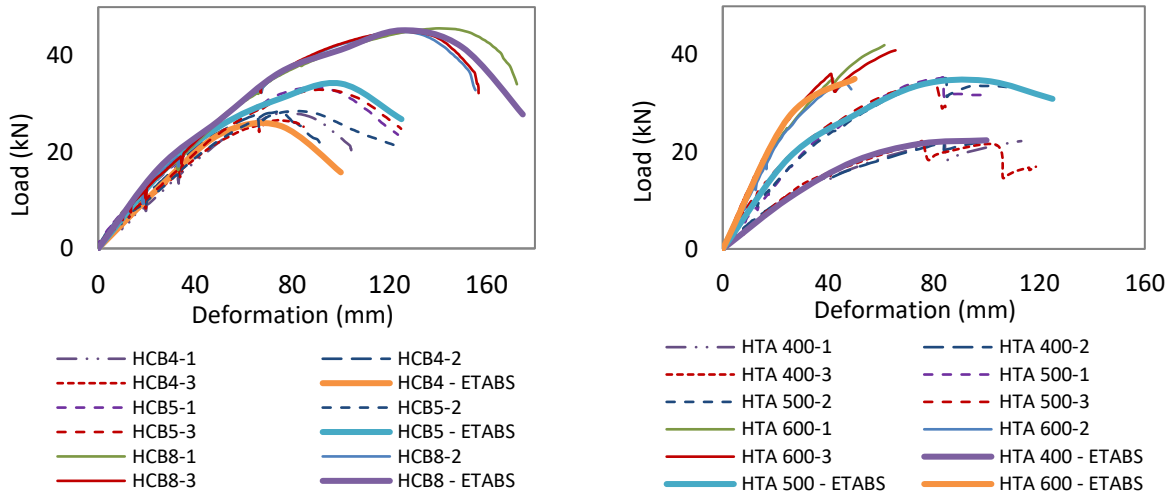

(a) (b)

Figure 6-2 Connection static pushover curves matched to experimental data (a) column to base, and (b) beam to column

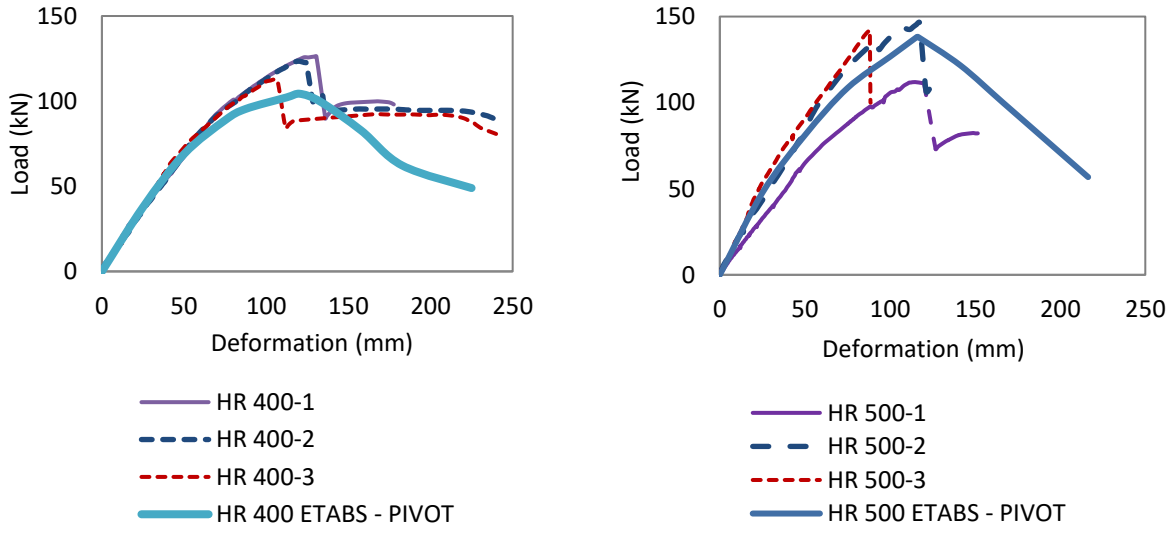

(a) (b)

Figure 6-3 Frame static pushover curves matched to experimental data (a) 400mm beam depth frame, and (b) 500mm beam depth frame

Results from the non-linear static pushover analysis of the portal frames fitted the experimental data well. This was achieved through iterations of connection stiffness at the connection level, then application of the validated hysteretic models to the portal frame models. Validation of the calibrated connection models to the portal frame models allowed for further confidence in the connection parameters presented in Table 6-2 as well as verified the modelling techniques used to develop the two-dimensional non-linear frame model.

6.1.3 Three-dimensional study

Best matching of floor acceleration and displacement are shown in Figure 6-4 and Figure 6-5, respectively.

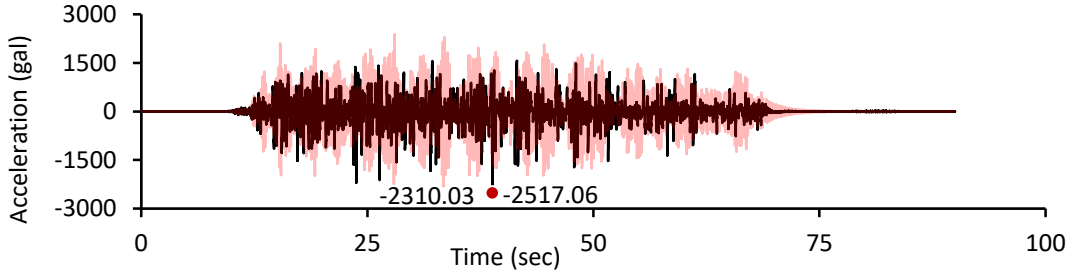

Figure 6-4 Best fit of maximum floor acceleration

Figure 6-4 shows peak values within eight percent, (2517-2310)/2517=0.08; however, the phase and alignment of peaks is not well fitted. Similarly, Figure 6-5 shows overall maximum floor displacements within 11 percent (15.95-17.80)/15.95=0.11 but not well fitted phase and alignment. The best simultaneous matching of floor acceleration and peak displacement occurred with damping set to around 2.2 percent and diaphragm stiffness was set to 12,000 MPa. The best individual matching of floor acceleration was achieved with very low damping of about 0.5 percent; however, it was apparent that this was not correct due to the rapid oscillations of the under-damped system. For individual matching of maximum displacement, diaphragm stiffness was reduced; however, the floor accelerations became far lower than the experimental values; therefore, the results were not considered representative of the real system. Another aspect that was not well matched was the experimental data which showed the maximum displacement occurring at the first storey. All numerical simulations in this study predicted maximum displacement in the upper storey. Perhaps some additional non-linearity occurred in the experiment

which was not accounted for in the numerical model; investigation of this has been left for future study.

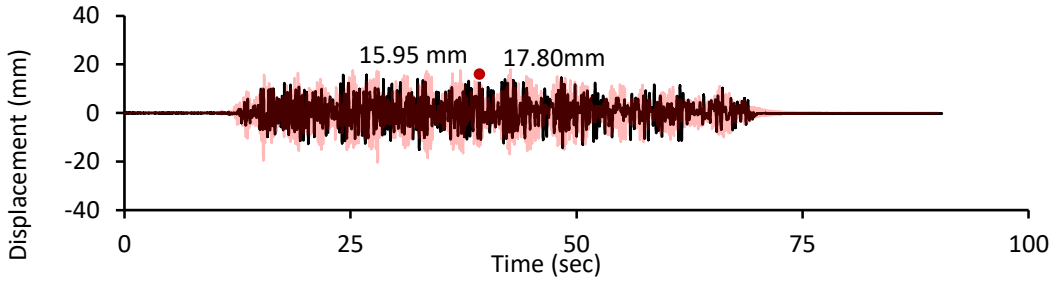

Figure 6-5 Best fit of maximum floor displacement

6.2 Extended study

Results from each analysis type and from the selection and scaling of ground motions are presented for the extended study of the 12-storey structure.

6.2.1 Equivalent static force

Final maximum drifts below the code specified one percent drift limit for post disaster structures was achieved through design iteration, including increasing thickness of coupling beams to 850mm (as shown in Figure 6-9), increasing concrete strength to 60 MPa, increasing core wall thickness as shown in Figure 6-9 and finally, the addition of two coupled blade walls, also as shown in Figure 6-9. The final drifts from equivalent static force procedure are plotted in Figure 6-6. As with the preliminary design, the softer coupled system in the x-direction is governing the drift response at approximately 0.90 percent while the stiffer, cantilevered shear wall system (in the y-direction) is at 0.85 percent. For both directions, the maximum interstorey drift occurs just beyond the mid-height of the structure. The increase in concrete volume required to achieve passing design for the coupling beams and shear wall piers in the coupled-direction was significant. The increase over the base structure results presented in Figure 4-11 on page 47 of this Thesis can be explained by the increase in strength demand and reduced drift allowance due to high importance; as well as, the amplified response spectrum due to soft soil. Further, the increase in self weight of the core due had a feedback effect that further increased the design requirements.

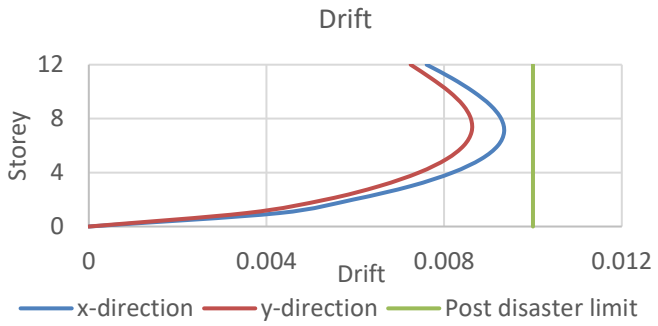

Figure 6-6 Equivalent static drift

Storey shears plotted in Figure 6-7 show uncoupled (y-direction) results with higher shear forces due to the stiffer system compared to the coupled (x-direction) system. Similarly, higher overturning is shown for the stiffer (un-coupled) system in Figure 6-8.

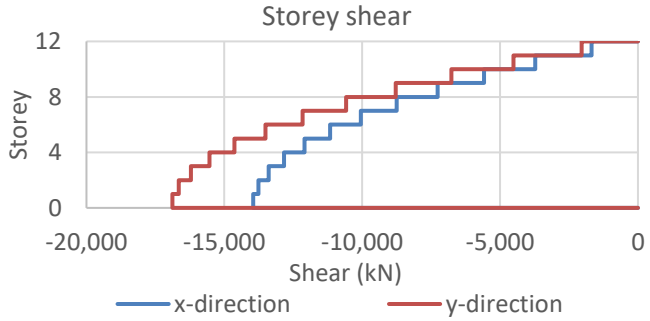

Figure 6-7 Equivalent static storey shear

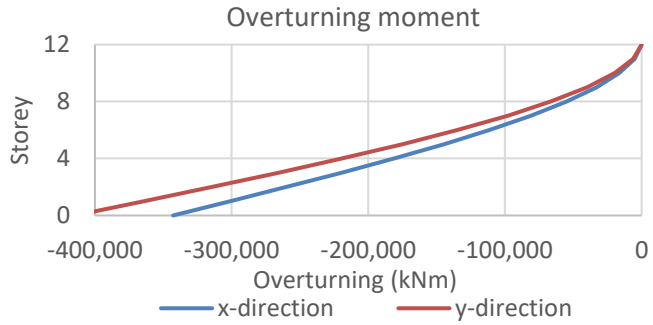

Figure 6-8 Equivalent static overturning moment

Final reinforced concrete core section and elevation reinforcing, as developed with ETABS, are provided in Figure 6-9. The results show that it was necessary to add two blade walls to maintain drifts of less than one percent. This design option was selected in order to not change the overall core dimensions and it was seen as a way to achieve a passing design without disrupting the overall flow excessively. Alternate design options were not investigated but may prove to be more practical. The thicker walls in the coupled direction are aligned with findings of other researchers (CSCE, 2008) in that shear demand in coupling beams is critical and that dimensional iterations are often required to reduce demand and/or increase capacity.

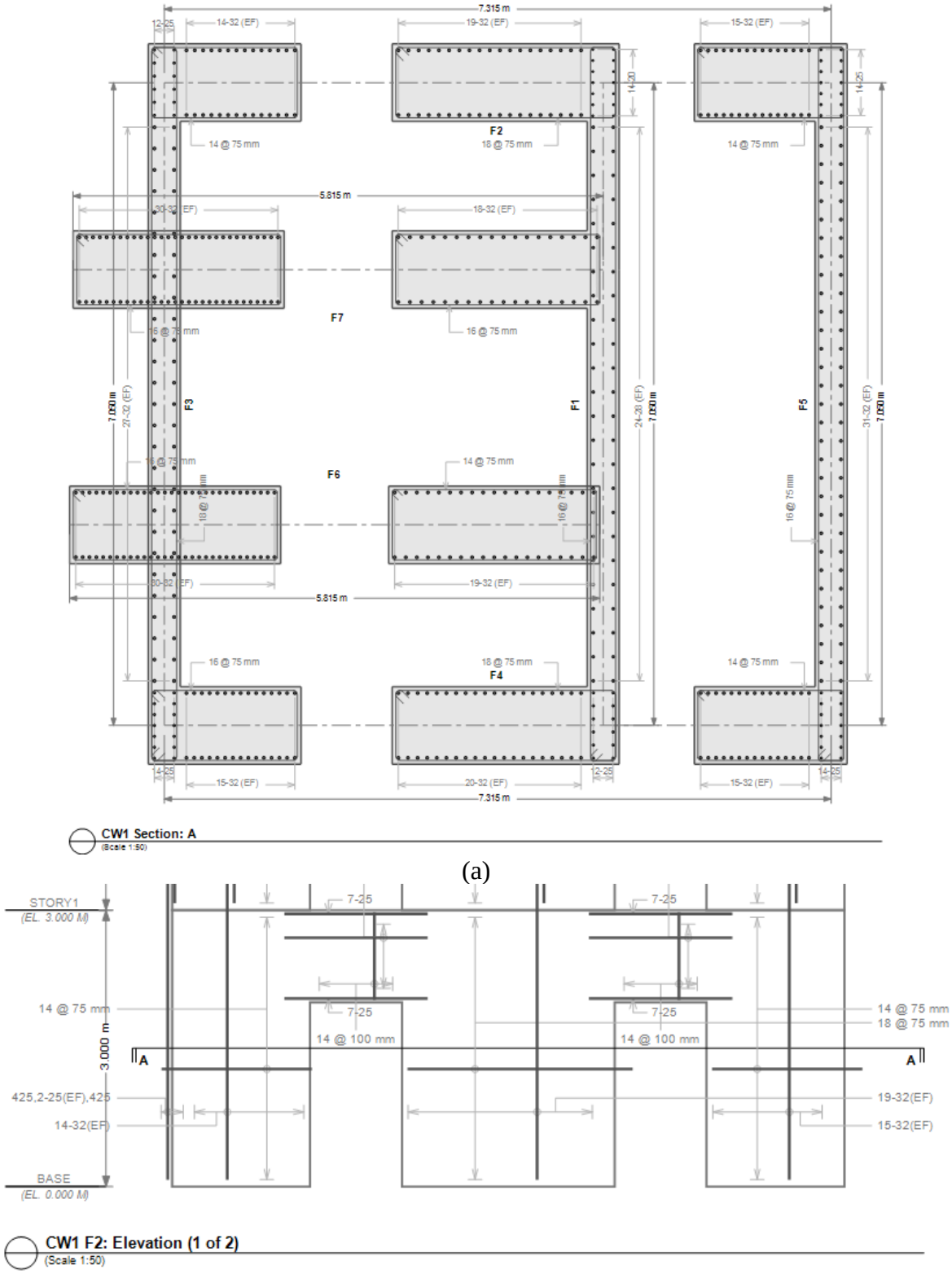

Figure 6-9 Concrete core (a) section, and (b) elevation

6.2.2 Response spectrum

Final drift plots are provided in Figure 6-10; note that the x-direction appears to slightly exceed the limit; however, within the required significant figures, the drift is at the limit and acceptable.

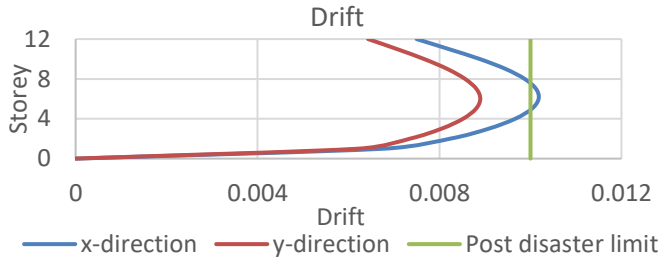

Figure 6-10 Response spectrum drift

Storey shears plotted in Figure 6-11 align well with the ESFP results maintaining higher relative demand of the stiffer y-direction system.

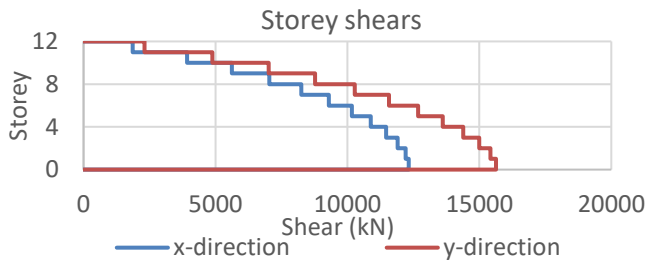

Figure 6-11 Response spectrum storey shear

Overturning plotted in Figure 6-12 shows lower overall demand compared to the ESFP overturning, indicating influence of higher modes in the vertical distribution of seismic loads.

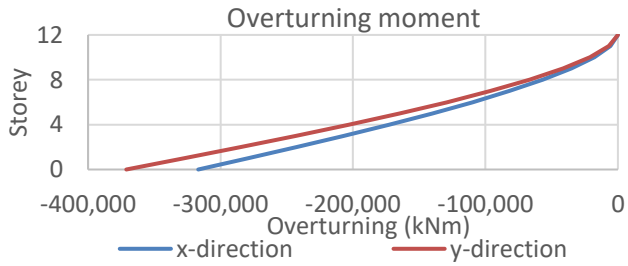

Figure 6-12 Response spectrum overturning moment

6.2.3 Selection and scaling of ground motions

Results of the selection and scaling of ground motions are provided in Table 6-3 and the scaled mean spectra is provided in Figure 6-13.

Table 6-3 Final selected suites of ground motions

Scenario	Earthquake	Year	Site	Mw	R (km)	Vs30 (m/s)	Individual scale factor	Suite scale factor
Crustal	Darfield, NZ	2010	Resthaven	7.0	19	141	1.64	1.04
	Christchurch, NZ	2011	Resthaven	6.2	5	141	1.38	
	Imperial Valley, CA	1979	E.C.A.-3	6.5	13	163	1.69	
	Tottori, Japan	2010	TTR008	6.6	7	139	1.48	
	Parkfield, CA	2004	P.F.Z.-1	6.0	3	178	0.88	
In-slab	Tarapaca, Chile	2005	Pica	7.8	125	492	0.88	1.63
	Tarapaca, Chile	2005	Idiem	7.8	144	386	2.61	
	Obihiro, Japan	2013	TKCH07	6.9	107	140	1.53	
	Nisqually, WA	2001	Crown	6.8	78	285	2.07	
	Nisqually, WA	2001	DNR	6.8	56	300	2.64	
Interface	Tohoku, Japan	2011	IBRH10	9.0	338	144	1.63	1.24
	Maule, Chile	2010	Conc	8.8	69	223	1.75	
	Maule, Chile	2010	CCSP	8.8	70	236	1.8	
	Hokkaido, Japan	2003	TKCH07	8.0	125	140	1.05	
	Hokkaido, Japan	2003	KSRH02	8.0	150	219	1.37	

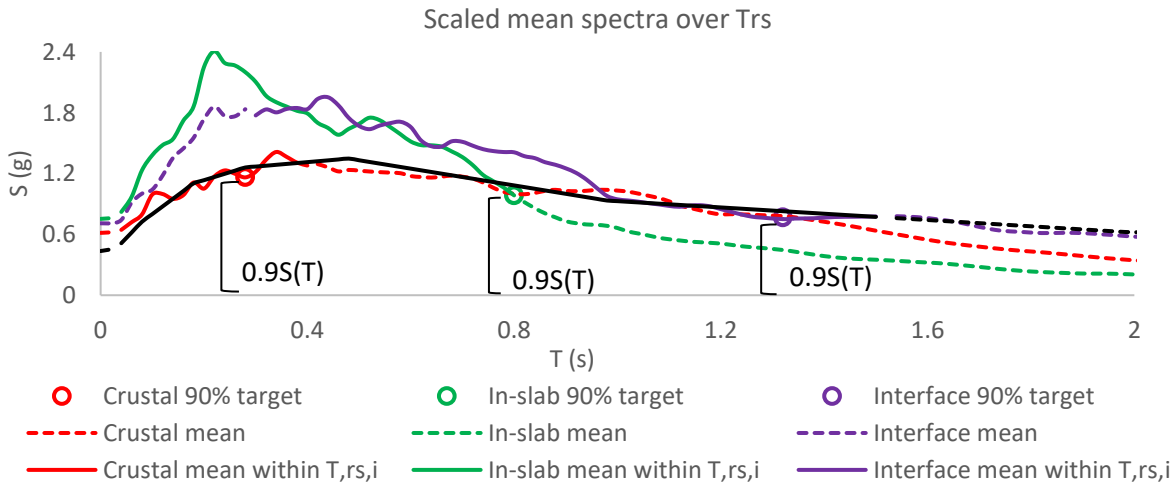

Figure 6-13 Scaled mean spectra

Limited historical records made finding high quality matches difficult. The ground motions, along with their scaled mean spectrum results are aligned with findings of Tremblay et al. (2015). Increased demand is evident due to short period over scaling resulting from the default linear scaling method of the guideline.

6.2.4 Linear response history

Scenario-specific average maximum results from the simultaneous bi-directional linear response history analysis are provided. Figure 6-14 provides interstorey drift results which are not passing for the post-disaster limit; however, they are well below high and normal importance limits. The drifts exceeding the limit was not a surprise as the scaled mean spectrum for each suite of ground motions is above the target spectrum. The response history analysis is beyond the code requirement and serves to better predict and understand structural response; therefore, design iterations were not carried out.

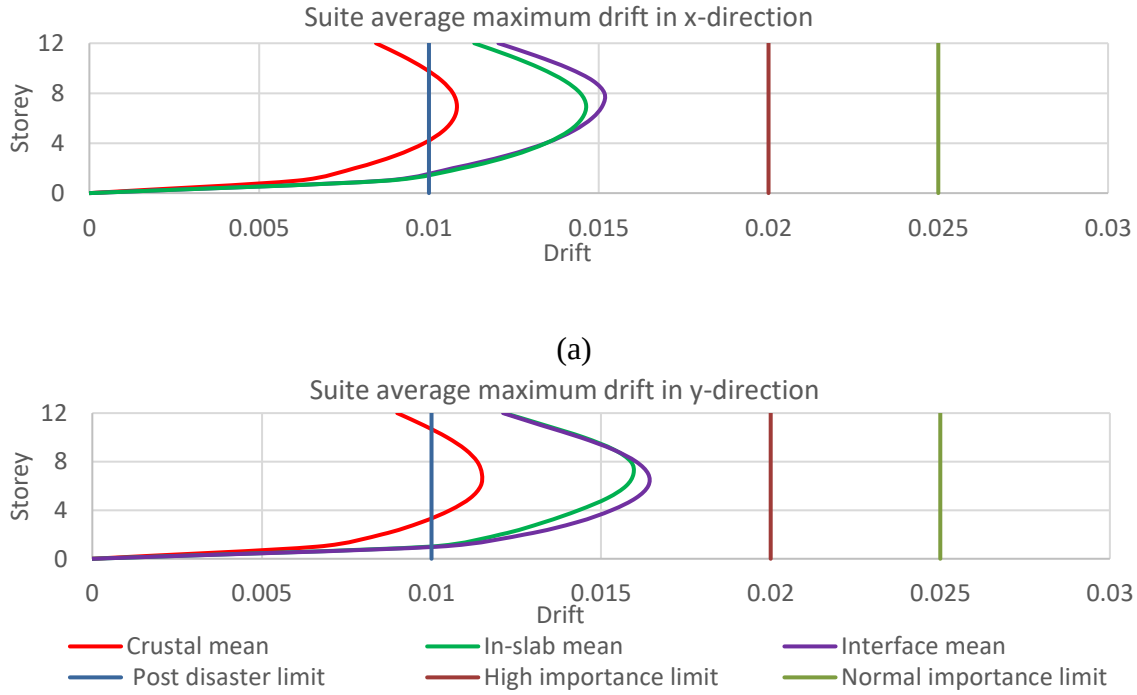

Figure 6-14 Linear response history suite average maximum drift (a) x-direction, and (b) y-direction

Scenario-specific shear demand is provided in Figure 6-15. Both subduction-type hazards (in-slab and interface) govern the demand at all storeys. Similarly, shows overturning dominated by subduction hazards. Figure 6-16 shows both major and minor bending due to the 100:30 load application. It can be seen that the minor subduction overturning is approximately equal to the crustal major overturning.

The results demonstrate a benefit of response history analysis; that is the unique positive and negative time varying response to allow more realistic load combinations to be generated. Further, the simultaneous bi-directional response history analysis allowed determination of simultaneous minor axis loading concurrent with the major axis loading.

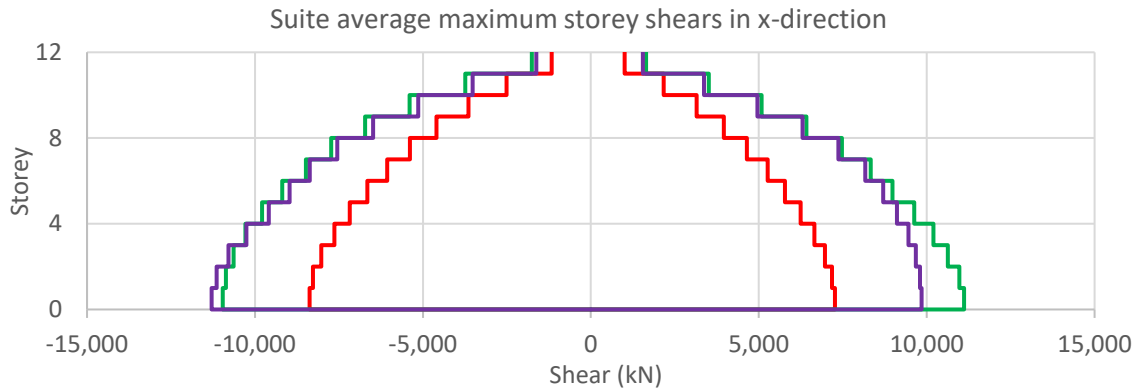

(a)

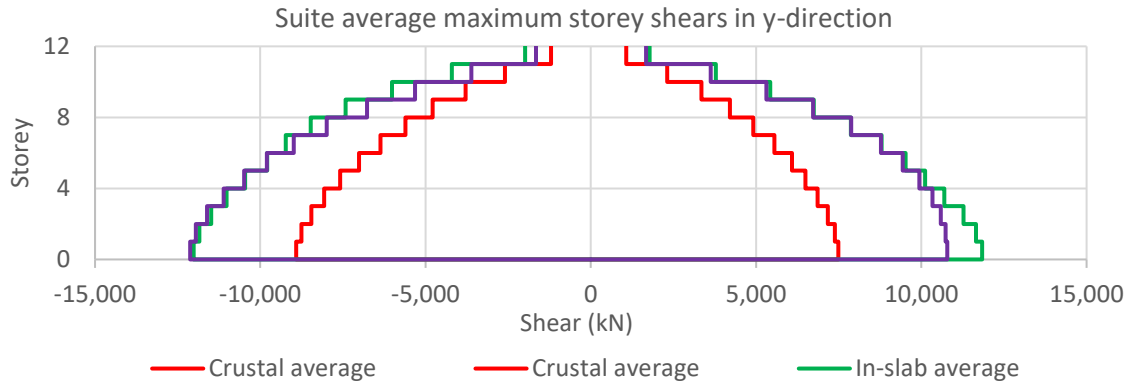

(b)

Figure 6-15 Linear response history suite average maximum storey shear (a) x-direction, and (b) y-direction

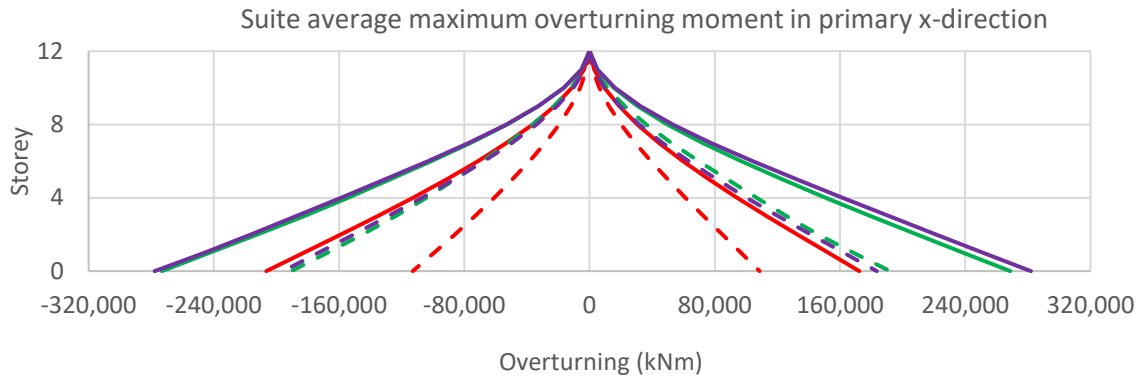

(a)

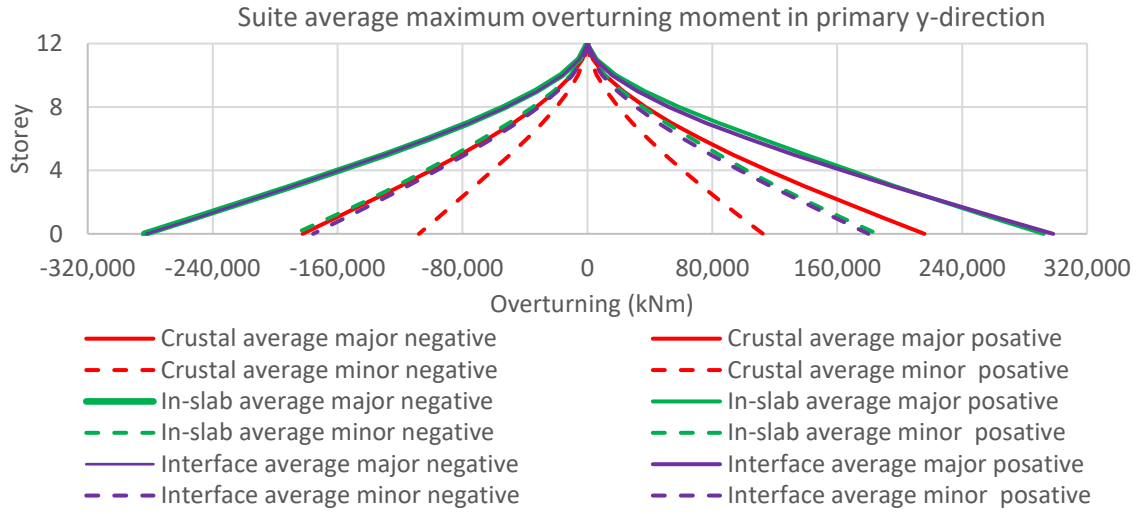

(b)

Figure 6-16 Linear response history suite average maximum major and minor overturning moment (a) x-direction, and (b) y-direction

Member forces for the base of a lower storey pier are provided from a linear response history analysis which used preliminary ground motions. The results are meant to convey load combinations rather than be used for a specific design. Tension and compression are uniquely handled for load cases (due to the non-uniformity of reinforced concrete materials and sections behavior under tensile and compressive loading). Also, it is shown that the maximum axial load is not concurrent with the maximum shear and bending values. First, the results were averaged then each of the averaged load cases for x- and y-direction inputs were applied (as a set) either entirely negative or entirely positive. The averaged output results and resulting four load cases (for seismic loading) are shown in Table 6-4.

Table 6-4 Member design forces from preliminary ground motions

Case	Axial (kN)	Shear (kN)	Shear (kN)	Torsion (kNm)	Moment (kNm)	Moment (kNm)
Case 1 and 2 (+/-)	320	1701	0	24	0	29668
Case 3 and 4 (+/-)	8719	285	42	25	101	1224

Case one (1) and two (2) represent input load functions where the primary function is in-plane stiffness. Case three (3) and four (4) represent out-of-plane loading (relative to the SFRS primary direction). The large axial forces are due to the flanging effect that occurs when in-plane SFRS walls are loaded in their weak axis but they are fully shear connected to the in-plane walls. The out-of-plane elements provide negligible base moment resistance but they resist significant moment by coupling effects between opposite flanges of an in-plane SFRS component. This member design force example illustrates a benefit of a linear response history analysis rather than a linear modal response spectrum analysis as it allows signs to be preserved and timewise variation in loads which allows for more realistic load combinations. All further post-processing of results and design of elements was left for future study.

6.2.5 Non-linear response history

Scenario-specific average maximum results from the simultaneous bi-directional non-linear response history (NL-RH) analysis are provided. Figure 6-17 provides interstorey drift results which again show the subduction-type seismic events dominating the response. Drifts are reasonably aligned with the linear response history results which is as should be expected according to National Research Council (2015). As typical, the interface and in-slab dominate the response; however, the dynamic response of coupled versus uncoupled systems were uniquely excited in the non-linear analysis which shows them alternately dominating the drift response. Storey shears for each primary direction are presented in Figure 6-18. Overturning moment results in Figure 6-19 (a) show typical results of subduction events dominating the response in the coupled direction; however, in the cantilever (y) direction, the response to crustal dominates over in-slab scenarios in Figure 6-19 (b). Because this response was not evident in any linear analysis conducted nor in the cantilever (y) direction, the coupling beam non-linearity may have contributed to the enhanced response to the crustal suite of ground motions. The non-linear results

show excessively high shear and overturning results; however, the drift results are in-line with the other analysis method results. The high shear and overturning values indicate that insufficient non-linear response is being achieved and force demand is not being reduced to the extent that the structural system has been designed. This may be a result of the strict drift limitation of one percent imposed by the high importance classification of the structure which in turn made the structure unable to achieve ductility in the anticipated range or it may be that hinge properties need to be refined. Further and detailed investigation of non-linear hinge properties used at coupling beams and in wall segments has been left for future study but should be investigated further, as discussed in the conclusion chapter of this thesis.

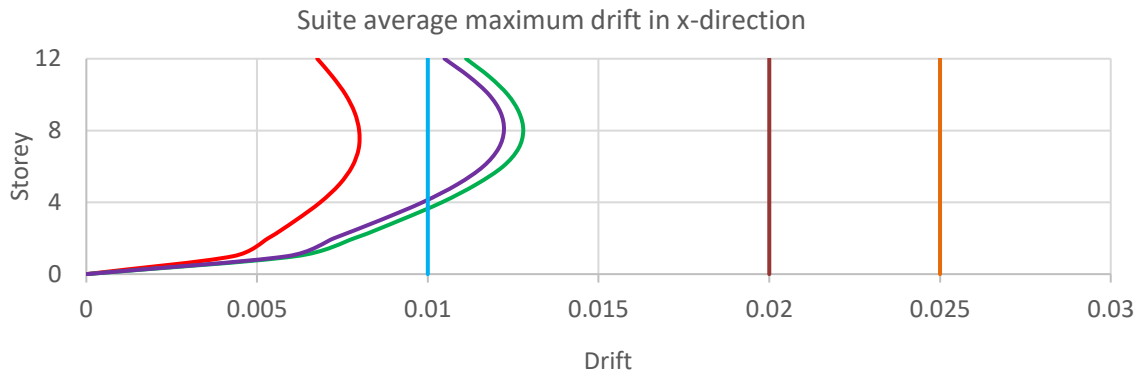

(a)

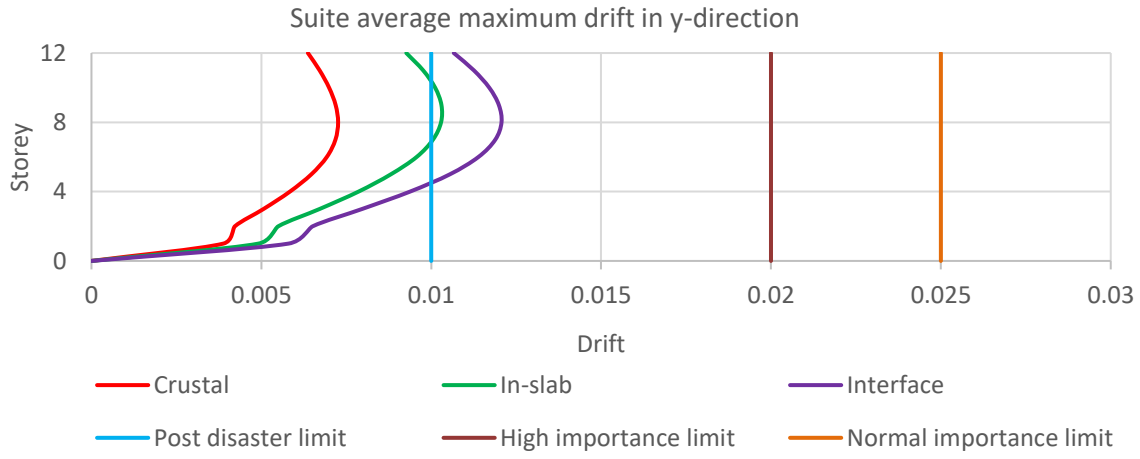

(b)

Figure 6-17 Non-linear response history suite average maximum drift (a) x-direction, and (b) y-direction

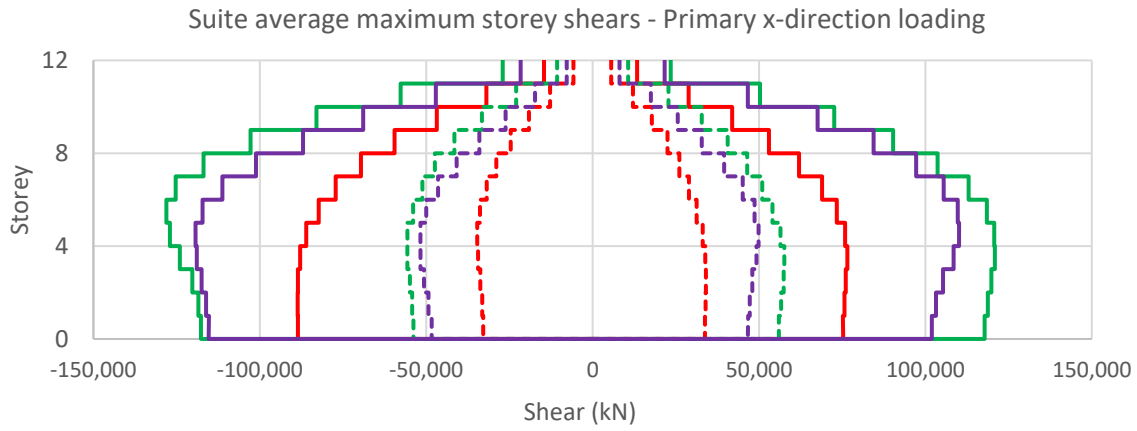

(a)

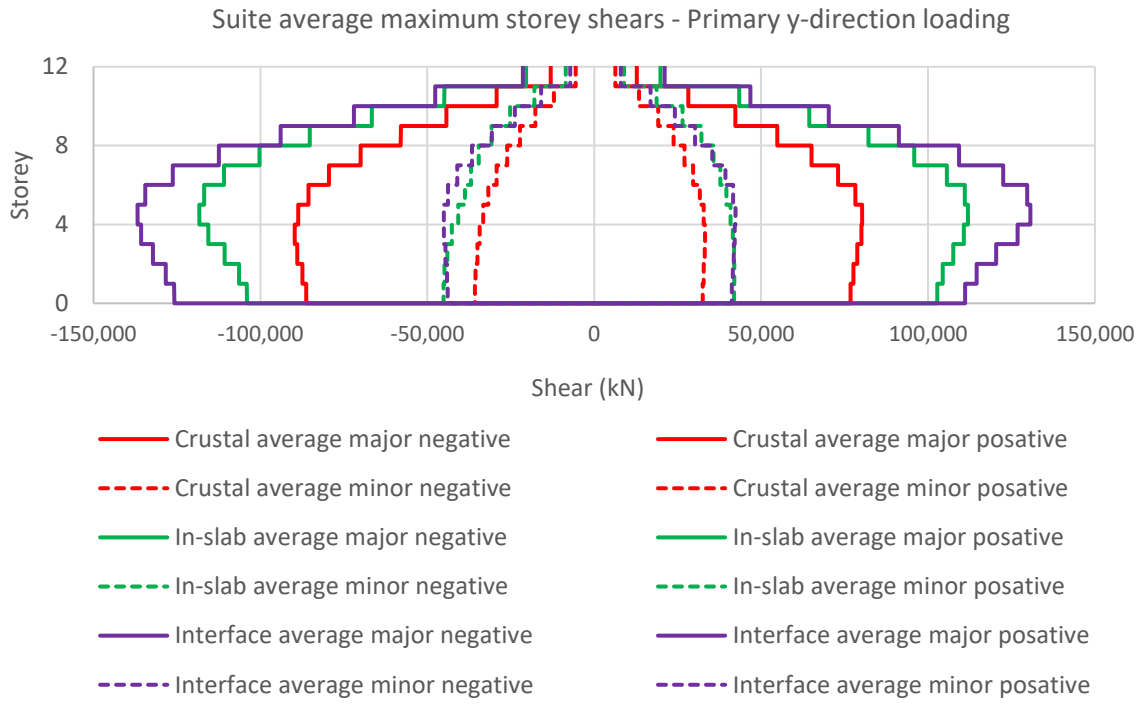

(b)

Figure 6-18 Non-linear response history suite average maximum storey shear (a) x-direction, and (b) y-direction

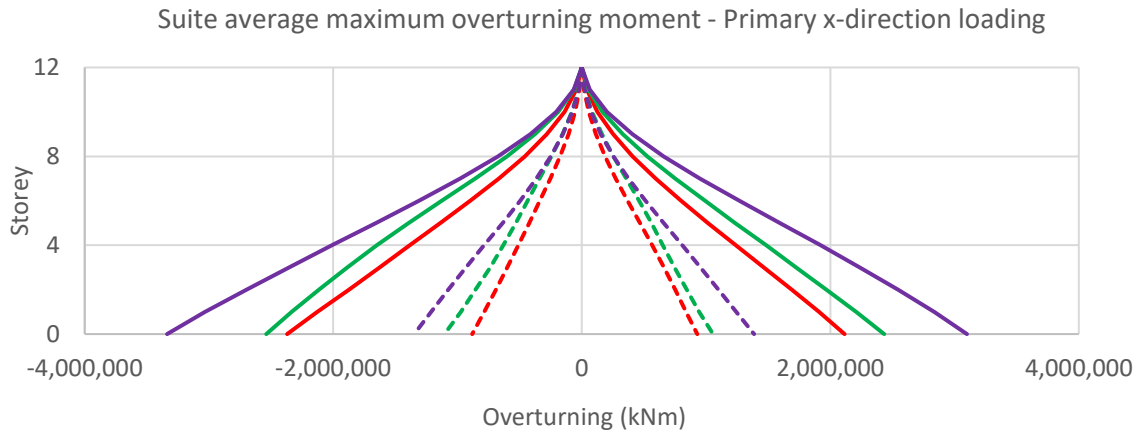

(a)

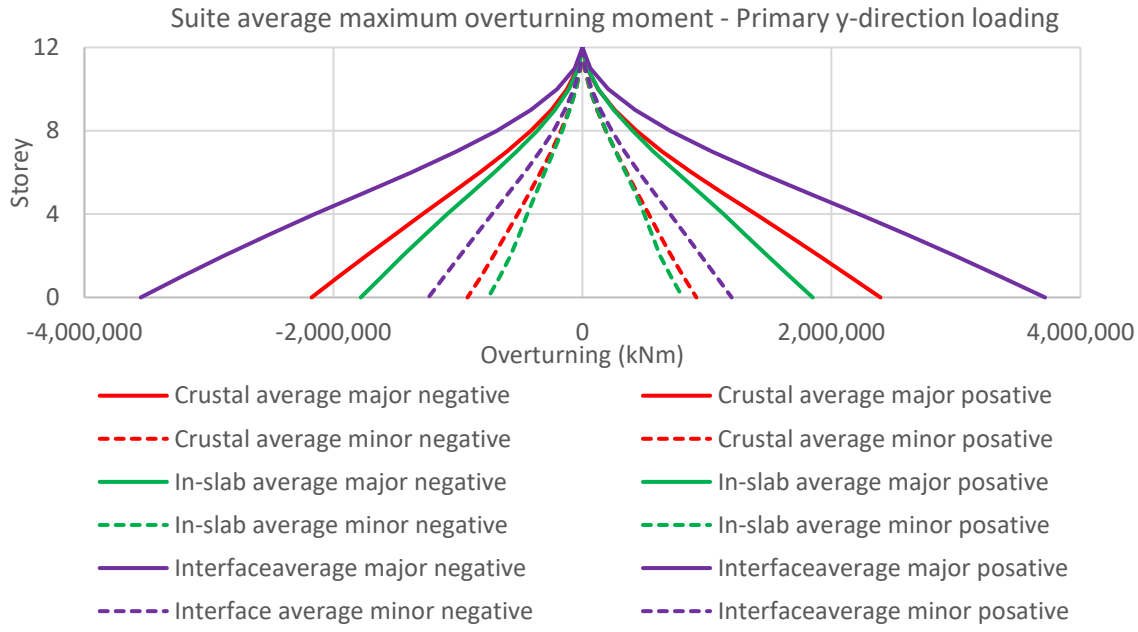

(b)

Figure 6-19 Non-linear response history suite average maximum overturning moment (a) x-direction, and (b) y-direction

7 Conclusions

Conclusions from the experimental validations and extended study are provided.

7.1 Experimental validations

Conclusions from the one, two and three-dimensional studies are presented.

7.1.1 One-dimensional study

Hysteresis matching with the Pivot model was used to validate non-linear parameters of specific timber and timber-concrete hybrid connections. The Pivot model provided traces that fit generally well; however, limitations are noted along with the contributions of this research.

The key limitation of this research and the Pivot model was that accurate initial reloading stiffness for the timber and concrete-timber hybrid connections could not be realized. Regardless of non-linear parameter definitions, the initial reloading stiffness was less stiff in the Pivot model compared to the experimental. The Pivot model restricted initial reloading stiffness to be more gradual, gaining strength steadily from the axis of zero displacement. The pivot point (at the axis of zero displacement) was often not representative of actual connection performance. This can be explained by the wood crushing due to previous excursions and subsequent lack of stiffness until new contact is realized. This results in underprediction of the energy dissipation per hysteretic loop in the Pivot model (based on the area enclosed in the hysteretic loop) compared to the energy dissipation occurring in reverse cyclic load tests.

The second limitation of this research is along unloading stiffness trace which degraded more in the Pivot model compared to that of the reverse cyclic testing. This was only slightly apparent even near four times the yield rotation. The slight loss of unloading stiffness does not appear to be significant; however, quantification of this limitation was beyond the scope of this study.

The first contribution of this research is the observation that non-linear parameters of the Pivot hysteresis model did not vary significantly between all connections calibrated. This indicates that basic assignment of the non-linear parameters may be valid for similar connection types which

would leave the user to only update backbone curve parameters, simplifying the utility of the connection model.

The second contribution of this research is the recommendation to use the Pivot model for timber connections in timber and concrete-timber hybrid structures until such a time that an improved model is provided.

The third contribution of this research is the provision of validated hysteretic connection models for the four connection types that were tested. It is recommended to use the linear and non-linear parameters of the calibrated connections as provided in the results section of this study for timber and concrete-timber hybrid connections the same as those validated.

The fourth contribution of this research is the application of hysteretic validation in both major and minor axis flexure for the beam to core connection. This type of validation will foster use of the validated connection model in a three-dimensional system. Where connections are not validated for weak axis flexure, connection model parameters would be left as free to rotate and not provide and stiffness to the system nor would the effects of hysteretic energy dissipation be captured due to weak axis flexure.

The fifth contribution of this research was recognition of the fact that improved unloading and reloading stiffness capabilities of the Pivot model in ETABS would improve accuracy in terms of energy dissipation and trace-characteristics of the hysteresis. The best fitting model that was currently available was Pivot. If the model could maintain very little stiffness until the rotation from the previous cycle was obtained, a better fit may be achieved.

Expanding on the fifth and final contribution is a recommendation for inclusion of an additional Pivot parameter to shift the positive and negative pivot points respectively in the opposite directions along the rotational (x) axis of the hysteretic, moment-rotation plot to improve the Pivot connection model. The additional parameter could allow for definition of a factor, normalized between zero and one (0-1), where zero would provide a result exactly as the present Pivot model (where reloading stiffness begins to ramp up as soon as rotation becomes non-zero. When the proposed parameter approaches one, the ramping up or reloading stiffness would hold until the previous cycle rotation was achieved. The additional parameter could be defined for the negative

side of the model with another separate parameter, allowing for unique behaviour when subjected to positive compared to negative flexural stress.

This one-dimensional study was based on four connection types tested not less than twice each; increased sample size and connection type testing, as well as increased number of hysteretic models validated (beyond just Pivot) would increase applicability and allow more broad conclusions to be drawn.

7.1.2 Two-dimensional study

Non-linear static pushover analysis and hysteresis matching were used to validate the portal frame connections and portal frame global drift response which demonstrated good fit to experimental results.

The first limitation of this research is same as in the one-dimensional study, related to the fit of the Pivot model. Please refer to the one-dimensional study for full explanation related to hysteretic matching.

The second limitation of this research is that the two-dimensional study does not include three-dimensional effects; therefore, any influence of minor axis flexure is not captured in the two-dimensional pushover analysis.

The first contribution of this research is the provision of validated Pivot connection model parameters for a series of post to beam and post to base connections. These connection models may be used in timber or concrete-timber hybrid structures.

The second contribution of this research is the capture of non-linear response using non-linear static pushover analysis on a two-dimensional frame with validated hysteretic connections oriented in two unique global directions. This shows a practical application of using validated connection models which is not a new concept; however, the specific connection and frame arrangement has not previously been demonstrated with the Pivot connection model.

This research was based on three experimental tests of each frame, beam depth and connection type; increased sample size and increased overall testing scheme would allow wider application of

the results. Further parametrization of timber frame types and timber connection methods, with connections to ensure ductile failure modes, would improve the implementation of semi-rigid timber portal frames in practice.

7.1.3 Three-dimensional study

Full scale shake table testing was used to validate the three-dimensional numerical model. This three-dimensional study fostered confidence in extension to the more advanced numerical modelling required for the extended study. The targeted non-linear response parameters were captured using a lumped plasticity approach with the Pivot hysteretic connection models previously validated in the one-dimensional study. Contributions and limitations of the three-dimensional validation are discussed.

The first and more general limitation of this research is that the full dynamic response of the two-storey, three-dimensional structure was not fully captured. While great efforts were made to validate key parameters of non-linear connections, damping, diaphragm stiffness and core stiffness, the model simply did not provide in-phase response of the shake table results.

A second limitation of this work is that peak displacements of the shake table work occurred in the first storey; whereas, in the three-dimensional model, the peak displacements occurred in the upper storey. This may indicate either additional non-linearity in the first storey or a contribution of higher mode effects to the dynamic response.

The main contribution of this research is that damping was found to fit best at 2.2 percent based on simultaneous matching of peak floor accelerations and displacement as well as review of the response history trace for frequency of oscillations. The value of 2.2 percent seems to be an appropriate estimate (for use with non-linear analysis of hybrid concrete-timber structures) because it fits well within the range of experimental and recommended values as discussed in this study.

The secondary contribution of this research is the demonstration of application of validated hysteretic connection models to a three-dimensional numerical model. Biaxial hysteretic connection parameters were used which demonstrated a method that could be used by designers

to evaluate demand on timber connections, particularly in a torsionally sensitive structure, during non-linear response history analysis of timber or concrete-timber structures.

Data from a single shake table experiment formed the basis of this study; further numerical validations of the other parametrized structures could be used to refine modelling aspects and develop innovative solutions for hybrid concrete timber structures. If appropriate ductility and overstrength factors could be established for a hybrid timber concrete lateral force resisting system, then, where feasible, the timber semi-rigidities could be attributed to the seismic force resisting system.

For future work to improve three-dimensional model validation results, it is recommended to thoroughly review all aspects of the shake table experiment and compare with numerical model parameters to identify any potential discrepancies.

7.2 Extended study

Conclusions from the extended study of a 12-storey hybrid structure, including limitations and contributions, are presented.

The first limitation of the extended study is that only a single structure was studied with only a few design iterations carried out and foundation system was neglected. Options such as increasing the concrete core size or adding additional shear walls further from the centre of rigidity could significantly reduce material volumes. Further, analysis and design of the required foundation system to allow overall structure performance to be verified should also be included.

The second limitation of this research is that the concrete hinge property definition was not explored in great detail but instead defined based on current design. The non-linear response history analysis demonstrated that at the low target drift of one percent, minimal non-linear behaviour was occurring in the concrete hinges which explains the large forces observed in the non-linear analysis results compared with those of the linear response history analysis. This may indicate that when the structure is designed to such stringent drift criteria, there is less non-linearity occurring than the ductility factor would suggest. Alternately, the large forces may also be due to incorrect hinge property definition. Iteration of hinge properties was beyond the scope of this research.

The third limitation of this research, realized during the selection and scaling of ground motions procedure, was the limited availability of historical ground motion records. This well-documented concern has led to various solutions including developing synthetic ground motions and relaxing ground motion selection criteria. In this study, the limited availability of historical records was overcome by relaxing the criteria for either the soil type, magnitude, or distance in order to meet the guideline criteria of getting multiple unique records; however, this relaxation did not come without cost. Relaxing the soil criteria to allow stiffer soils contributed to the eventual over scaling in the short period range due to the increased low frequency content (spectral shape) of stiffer soil sites. Conversely, excessive relaxing of the magnitude or distance criteria resulted in increased scale factors (at times beyond recommended values). Potential inclusion of synthetic record was also considered; however, these were eventually eliminated from final selection due to lack of guidance for inclusion within suites under the guideline and perceived general preference of historical records based on the literature review.

The first contribution of this research is the identification of the primary structural components of the lateral and gravity systems and their interaction within the hybrid structure. The primary lateral system components include vertical and horizontal elements which are the reinforced concrete core and the cross laminated timber diaphragms, respectively. The primary gravity system components include the timber post and beam framing as well as the cross laminated timber floor panels. Identification of the structural components to be included in the primary lateral system required checking the contribution of timber frame semi-rigidities to the first mode period as well as consideration of the impact on the resulting lateral design load requirements. For the impact on the first mode period, the timber frame semi-rigidities were found not to contribute, causing only a two percent decrease in the first mode period. According to the national building code of Canada (2015), if the influence is less than 15 percent, the contribution may be neglected during the lateral design. For the impact on the lateral force demand, inclusion of the timber frame semi-rigidities would require reduced ductility and overstrength factors which would increase the design load and be a detriment on the system; therefore, the timber semi-rigidities were not included in the lateral system. Once it was determined that the timber frames were not to be included in the lateral system, their interaction with the gravity system was considered. It was required to check if they could accommodate movements expected under the design ground motion movement. The timber frames were found to be able to accommodate the expected lateral movements for the drift limit of one

percent as required for the post disaster drift limit imposed on this structure. For future work, ductility and overstrength factors for hybrid structural systems should be developed to better reflect the actual design base shear that should be considered for respective systems so that current worst-case overstrength and ductility factors would not be required when combining lateral system components from unique classifications of seismic force resisting systems.

The second contribution of the research is the preliminary design of the vertical component of the lateral system; namely, the concrete core, including cantilever walls and coupled cantilever walls. Design iterations were required from the initial structure which was based on significantly less loading. Design iterations resulted in the addition of coupled blade walls to control drift and an increase in wall thickness and concrete strength primarily to meet strength requirements. Future work should aim to reduce concrete volumes by increasing effective depth of core walls or; alternately, changing the concrete core to a lighter, perhaps mass timber core may be suited to further investigation.

The third contribution of this research is the selection and scaling of ground motions for the soft soil site of Victoria, B.C. Three suites of five ground motions were selected and scaled for the site and structure type. This facilitated a response history analysis with inputs, developed in accordance with the building code guideline, that could be reasonably expected for the site. The specific ground motions could be used for other structures with similar period ranges of interest, soil type, and location.

A fourth contribution of this research is identification of three aspects of the guideline for selection and scaling of ground motions which did not provide adequate guidance to ensure consistent application. These are 1) definition of the period range of interest, 2) identification of target scenarios, and 3) the relative importance of ground motion selection criteria - magnitude, distance, and soil type. The most critical of the three is definition of a period range of interest. This is because the defined period range of interest directly affects the ground motion scale factors which impact the resulting structural response. The second aspect is the relative importance or weighting of magnitude, distance and soil type criteria during the ground motion selection process. Guidance here would reduce variability in ground motion selection results which would in-turn reduce variability in predicted structural response. The third area of the guideline identified as needing attention was in the definition of target scenarios. Definition of target scenarios was attempted

from a few perspectives in this research including global mean, global mode, and inspection of deaggregation plots. The deaggregation data that was used was certainly critical to developing the scenarios that were developed in this work; however, there was still some judgement required in determining scenario-specific magnitude and distance targets. Improved guidance on the definition of target scenarios is seen as a less critical task because the exact target scenarios did not have a significant impact on ground motion selection due to the limited availability of historical records and the resulting required relaxation of scenarios for selection. Still, a consistent approach provided in the guideline would be beneficial and the inclusion of scenario specific means within deaggregation data would be helpful in achieving consistent target scenario selection.

The final contribution of this research is the provision of four methods of analysis from the building code to the hybrid concrete-timber structure. These methods allow for comparison of results from each method as well as provide for confidence in the results of more complex analysis methods. Further, use of the dynamic analysis methods allows a savings in force demand compared with the static approach which results in design savings. The response spectrum method allowed for improved estimation of vertical force distribution within the structure which improves the quality of the response prediction. The linear response history method provides opportunity to develop ground motion selection and scaling procedures as well as create load combinations that are not possible in the response spectrum method. The non-linear response history method is beyond the code requirement for normal structures but where special studies are required such as in developing innovative hybrid structural systems, non-linear response history analysis can provide a better prediction of the structural response. In this structure, the non-linear results appear to need refining to be reliable as they should produce similar results as the previous analysis methods. This refinement of non-linear results is left for future study.

References

Abeysekera, I. (2015). Dynamic response of tall timber buildings. *Institute of Structural Engineers,* (May, Issue 101)

Adebar, P., Mutrie, J., & DeVall, R. H. (2005). Ductility of concrete walls: The Canadian seismic design provisions 1984 to 2004. *Canadian Journal of Civil Engineering, 32*, 1124-1137.

Ancheta, T., Darragh, R., Stewart, J., Seyhan, E., Silva, W., Chiou, B., . . . Donahue, J. (2018). PEER NGA-West2 database. Retrieved December 10, 2017 from https://ngawest2.berkeley.edu/

Applied Technology Council. (2009). *FEMA 695: Quantification of building seismic performance factors.* (No. 695). Redwood City, California: FEMA.

Archila, M., & Ventura, C. (2012). (2012). Effect of ground motion directionality on seismic response of tall buildings. Paper presented at the *15th World Conference of Earthquake Engineering,* Lisboa.

Association of professional engineers and geoscientists of British Columbia (APEGBC). (2015). *Technical and practice bulletin 5 and 6 storey wood frame residential building projects (mid-rise).* Canadian Wood Council.

Association of professional engineers and geoscientists of British Columbia (APEGBC). (2016). APEGBC professional practice guideline: Sustainability. *Volume 1.*

Atkinson, G. (2009). Earthquake time histories compatible with the 2005 NBCC uniform hazard spectrum. *Canadian Journal of Civil Engineering, 36*, 991-1000.

Atkinson, G., & Macias, M. (2008). Predicted ground motions for great interface earthquakes in the Cascadia subduction zone. *Bulletin of the Seismological Society of America* 1-60.

Baker, J. W. (2011). Conditional mean spectrum: Tool for ground-motion selection. *Journal of Structural Engineering, 137*(3), 322-331. doi:10.1061/(ASCE)ST.1943-541X.0000215

Bartlett, S. (2014). *Processing of time histories.* Department of Civil and Environmental Engineering, University of Utah.

Bastias, N., & Montalva, G. (2016). Chile strong ground motion flatfile. *Earthquake Spectra,* (Preprint)

Binational Softwood Lumber Council. (2017). In Holt R., Luthi, T. and Dickof, C. (Eds.), *Nail-laminated timber: Canadian design and construction guide v1.1* (1st ed.). Vancouver, BC: Binational Softwood Lumber Council and Forestry Innovation Investment Ltd.

Boivin, Y., & Paultre, P. (2012). Seismic force demand on ductile reinforced concrete shear walls subjected to western North American ground motions: Part 1 - parametric study. *Canadian Journal of Civil Engineering,* (39), 723-737. doi:10.1139/L2012-043

Boore, D. (2005). On pads and filters: Processing strong-motion data. *Bulletin of the Seismological Society of America, 95*(2), 745-750. doi:10.1785/0120040160

Booth, E., & Key, D. (2006). Timber. *Earthquake design practice for buildings* (second ed., pp. 219). Heron Quay, London: Thomas Telford.

Boroschek, R., & Yanez, F. (2000). Experimental verification of basic analytical assumptions used in the analysis of structural wall buildings. *Engineering Structures, 22*(6), 657-669.

Braconi, A., Salvatore, W., Tremblay, R., & Bursi, O. S. (2007). Behaviour and modelling of partial-strength beam-to-column composite joints for seismic applications. *Earthquake Engineering & Structural Dynamics, 36*(1), 142-161. doi:10.1002/eqe.629

Canadian Commission on Building and Fire Codes National Research Council of Canada. (2015). *Structural commentaries (users guide - NBC 2015: Part 4 of division B)* NRC - National Research Council Canada.

Canadian Hazards Information Service. (2017). In correspondence from Halchuk, S. (Ed.), *Seismic hazard deaggregation* Natural Resources Canada.

Canadian Wood Council and American Wood Council. (2016). *User guide: For U.S. design office 10 and Canadian design office 9* Canadian Wood Council.

CESMD. (2018). Strong motion virtual data center (VDC). Retrieved on April 12, 2018 from http://strongmotioncenter.org/vdc/scripts/about.plx

Chang, W., Shanks, J., Kitamori, A., & Komatsu, K. (2009). The structural behavior of timber joints subjected to bi-axial bending. *Earthquake Engineering & Structural Dynamics, 38*(6), 739-757. doi:10.1002/eqe.854

Charney, F. (2015). (2015). Linear response history analysis procedure for the 2015 NEHRP recommended provisions and for ASCE 7-16. Paper presented at the *American Society of Civil Engineers Structures Congress*, Portland, Oregon. 2467-2482.

Computers and Structures Inc. (2015). *ETABS Volume 15*

Computers and Structures Inc. (2016). Rigid vs. semi-rigid. Retrieved on June 30, 2017 from https://wiki.csiamerica.com/display/etabs/Rigid+vs.+Semi-rigid+diaphragm

Computers and Structures, I. (2015a). *CSI analysis reference manual*. Berkeley, California: Computers and Structures, Inc.

Computers and Structures, I. (2015b). *CSI analysis reference manual: For SAP2000, ETABS, SAFE, and CSIBridge.* (No. July).

COSMOS. (2005). *Guidelines and recommendations for strong-motion record processing and commentary.* (No. CP-2005/01). California: COSMOS.

CSA - CSA Standards. (2014a). CSA CAN/CSA-A23 Design of concrete structures

CSA - CSA Standards. (2014b). CSA CAN/CSA-O86 Engineering design in wood.

CSA - CSA Standards. (2014c). CSA CAN/CSA-S16 Design of steel structures.

CSCE. (2008). (2008). Time history analysis. Paper presented at the *Time History Analysis Presented by CSCE*, UBC Vancouver. 1-5.

CSI Inc. Generation of spectrum-compatible time-history functions by modifying a reference time series in the frequency/time domain. Retrieved from http://docs.csiamerica.com/helpfiles/etabs/Menus/Define/Functions/Time_History_Functions/Time_History_Matched_to_Response_Spectrum.htm

Daneshvar, P., Bouaanani, N., Goda, K., & Atknison, G. (2016). Damping reduction factors for crustal, in-slab, and interface earthquakes characterizing seismic hazard in southwestern British Columbia, Canada. *Earthquake Spectra, 32*(1), 45-74.

Dawood, H., Rodriguez-Marek, A., Bayless, J., Goulet, C., & Thompson, E. (2016). A flatfile for the KiK-net database processed using an automated protocol. *Earthquake Spectra, 32*(2), 1281-1309.

Dehghani, M., & Tremblay, R. (2016). Robust period-independent ground motion selection and scaling for effective seismic design and assessment. *Journal of Earthquake Engineering, 20*(2), 185-218. doi:10.1080/13632469.2015.1051635

Departmento de Ingenieria Civil. (2018). Terremotos de Chile. Retrieved on April 15, 2018 from http://terremotos.ing.uchile.cl/

Dias, A. M. P. G. (2012). Analysis of the nonlinear behavior of timber-concrete connections. *Journal of Structural Engineering (New York, N.Y.), 138*(9), 1128; 1128-1137; 1137.

Dias, A. M. P. G., Van de Kuilen, J. W., Lopes, S., & Cruz, H. (2007). A non-linear 3D FEM model to simulate timber–concrete joints. *Advances in Engineering Software, 38*(8–9), 522-530. Retrieved on August 02, 2017 from http://dx.doi.org.ezproxy.library.ubc.ca/10.1016/j.advengsoft.2006.08.024

Filliatrault, A., Tremblay, R., Christopoulos, C., Folz, B., & Pettinga, D. (2013). *Elements of earthquake engineering and structural dynamics* (Third ed.) Presses Internationales Polytechnique.

Fox, M., Sullivan, T., & Beyer, K. (2014). (2014). A case study in the capacity design of RC coupled walls. Paper presented at the *Second European Conference on Earthquake Engineering and Seismology,* Istanbul. 1-12.

FP Innovations. (2012). CLT handbook. *FP Innovations, Canadian Edition*

Fragiacomo, M. (2003). Design of bilinear hysteretic isolation systems. *Earthquake Engineering & Structural Dynamics, 32*(9), 1333; 1333-1352; 1352.

Fragiacomo, M. (2011). Elastic and ductile design of multi-storey Crosslam massive wooden buildings under seismic actions. *Engineering Structures, 33*(11), 3043; 3043-3053; 3053.

Gonzalez, M. (2017). *Seismic response of tall buildings using ground motions based on national building code of Canada 2015* (Master of Applied Science).

Government of British Columbia. (2009). Wood first act. *BCLaws.*

Green, D., Winandy, J., & Kretchmann, D. (1999). Mechanical properties of wood. *Wood handbook - wood as an engineering material* (pp. 4-1). Madison, WI: U.S. Department of Agriculture, Forest Service.

Guorui, H., & Toa, L. (2015). Review of baseline correction of strong-motion accelerogram. *International Journal of Science, Technology and Society, 3*(6), 309-314.

Halchuk, S., Adams, J., & Allen, T. I. (2016). Fifth generation seismic hazard model for Canada: Crustal, in-slab, and interface hazard values for southwestern Canada. *Geological Survey of Canada, Open File 8090,* doi:1 .zip file. doi:10.4095/299244

He, M., Li, S., Guo, S., & Ni, C. (2011). The seismic performance in diaphragm plane of multi-storey timber and concrete hybrid structure. *Procedia Engineering, 14*, 1606-1612. Retrieved

on November 15, 2017 from http://dx.doi.org.ezproxy.library.ubc.ca/10.1016/j.proeng.2011.07.202

Hehl, S., Tannert, T., Meena, R., & Vallee, T. (2014). Experimental and numerical investigations of groove connections for a novel timber-concrete-composite system. *Journal of Performance of Constructed Facilities, 28*(6), A4014010; A4014010.

Ibarra, L. F., Medina, R. A., & Krawinkler, H. (2005). Hysteretic models that incorporate strength and stiffness deterioration. *Earthquake Engineering & Structural Dynamics*, *34*(12), 1489-1511. doi:10.1002/eqe.495

Irvine, T. (2016). Damping properties of materials. Retrieved on June 06, 2017 from www.vibrationdata.com

Isoda, H., Kawai, N., Koshihara, M., Araki, Y., & Tesfamariam, S. (2016). Timber-reinforced concrete core hybrid system: Shake table experimental test. *ASCE Journal of Structural Engineering,* doi:10.1061/(ASCE)ST.1943-541X.0001631, 04016152.

Isoda, H., & Tesfamariam, S. (2016). Connections for timber-concrete hybrid building: Experimental and numerical model results. *ASCE Journal of Performance of Constructed Facilities, R1v2* doi:10.1061/(ASCE)CF.1943-5509.0000849, 04016024

Kalkan, E., & Chopra, A. (2010). *Practical guidelines to select and scale earthquake records for nonlinear response history analysis of structures*. U.S. Department of the Interior U.S. Geological Survey.

Khorsandnia, N. (2015). Coupled finite element-finite difference formulation for long-term analysis of timber-concrete composite structures. *Engineering Structures, 96*, 139; 139-152; 152.

Klemenic, R., Fry, J. A., & Hooper, J. (2007). Performance-based design of tall reinforced concrete ductile core wall systems. *ASCE Structures Congress - Structural Engineering Research Frontiers,*

Kleven, M., & Noras, R. (2011). *Finite element based simulation of diaphragm action on light weight composite plywood to sheet metal roof element* (Master).

Kremer, P., & Symmons, M. (2015). Mass timber construction as an alternative to concrete and steel in the Australia building industry: A PESTEL evaluation of the potential. *International Wood Products Journal, 6*(3), 138-147. doi:10.1179/2042645315Y.0000000010

Latour, M., & Rizzano, G. (2015). Cyclic behavior and modeling of a dissipative connector for cross-laminated timber panel buildings. *Journal of Earthquake Engineering,* doi: 10.1080/13632469.2014.948645

Li, Z., He, M., Lam, F., Li, M., Ma, R., & Ma, Z. (2014). Finite element modeling and parametric analysis of timber–steel hybrid structures. *Structural Design of Tall and Special Buildings,* doi: 10.1002/tal.1107

Los Angeles Tall Buildings Structural Design Council. (2017). *An alternative procedure for seismic analysis and design of tall buildings located in the Los Angeles region: A consensus document.* Los Angeles: LATBSDC.

Lowes, L., Mitra, N., Altoontash. (2004). A beam-column joint model for simulating the earthquake response of reinforced concrete frames. *Pacific Earthquake Engineering Research Center. Retrieved on October 16, 2017 from* http://peer.berkeley.edu/publications/peer_reports/reports_2003/0310.pdf

Lu, X., Cui, Y., Liu, J., & Gao, W. (2015). Shaking table test and numerical simulation of a 1/2-scale self-centering reinforced concrete frame. *Earthquake Engineering and Structural Dynamics,* doi: 10.1002/eqe

Meleki, H., Asiz, A., Smith, I., Gagnon, S., & Mohammad, M. (2011). Differential movements in a timber multi-storey hybrid building. *Procedia Engineering, 14,* 1613-1620. Retrieved on March 02, 2017 from http://dx.doi.org.ezproxy.library.ubc.ca/10.1016/j.proeng.2011.07.203

MGB Architecture, and Equilibrium Consulting. (2012). *Tall wood*.

Michaud, D., & Léger, P. (2014). Ground motions selection and scaling for nonlinear dynamic analysis of structures located in eastern North America. *Canadian Journal of Civil Engineering, 41*, 232–244. doi: dx.doi.org/10.1139/cjce-2012-0339

Monroy, M., Hull, A., & Atukorala, U. (2016). *Technical memorandum: Massey tunnel replacement project.* (No. 14-1447-0012-008-TM-Rev0). Vancouver, BC: Golder Associates Ltd.

Mori, T., Nakatani, M., & Tesfamariam, S. (2015). Performance of semi-rigid timber frame with lagscrewbolt connections: Experimental, analytical, and numerical model results. *International Journal of Advanced Structural Engineering (IJASE), 7*(4), 387-403. doi:10.1007/s40091-015-0107-4

Mousseau, S., Paultre, P., & Mazars, J. (2008). Seismic performance of a full-scale, reinforced high-performance concrete building. part II: Analytical study. *Canadian Journal of Civil Engineering, 35*, 849-862. doi:10.1139/L08-019

Natural Resources Canada. (2015). Determine 2015 national building code of canada seismic hazard values. Retrieved on June 12, 2017 from http://www.earthquakescanada.nrcan.gc.ca/hazard-alea/interpolat/index_2015-en.php

Naumoski, N., Saatcioglu, M., Lin, L., & Amiri-Hormozaki, K. (2006). Evaluation of the effects of spectrum compatible seismic excitations on the response of medium-height reinforced concrete frame buildings. *Canadian Journal of Civil Engineering, 33*, 1304-1319.

NIED. (2018). K-net and KiK-net strong-motion seismograph network. Retrieved on February 22, 2018 from http://www.kyoshin.bosai.go.jp/kyoshin/quake/index_en.html

NRC - National Research Council Canada. (2010). National building code of Canada.

Panneton, M., Leger, P., & Tremblay, R. (2006). Inelastic analysis of a reinforced concrete shear wall building according to the national building code of Canada 2005. *Canadian Journal of Civil Engineering, 33*, 854-871.

Park, R., & Paulay, T. (1975). Reinforced concrete structures. *USA: John Wiley and Sons.,*

Paulay, T. (2001). Seismic response of structural walls: Recent developments. *Canadian Journal of Civil Engineering, 28*, 922-937.

Paulay, T., & Preistley, N. (1992). *Seismic design of reinforced concrete and masonry buildings* John Wiley and Sons, Inc.

Popovski, M., Mohammad, M., Ni, C., Rezai, M., Below, K., Malczyk, R., & Sherstobitoff, J. (2014). Design and construction of tall wood buildings: Input data, testing and advanced analysis.

Reyes, J., & Kalkan, E. (2012). (2012). Relevance of fault-normal/parallel and maximum direction rotated ground motions on nonlinear behaviour of multi-story buildings. Paper presented at the *World Conference on Earthquake Engineering*, Lisboa.

Robert Drysdale. (2014). In email correspondence to Chris Pieper (Ed.)

Rogers, G., Halchuk, S., Adams, J., & Allen, T. (2015). 5th generation (2015) seismic hazard model for southwest British Columbia. Paper presented at the *11th Canadian Conference on Earthquake Engineering Paper 94197,*

Saaticioglu, M., & Humar, J. M. (2003). Dynamic analysis of buildings for earthquake-resistant design. *Canadian Journal of Civil Engineering*, 338. doi:10.1139/L02-108

Schneider, J., Shen, Y., Stiemer, S. F., & Tesfamariam, S. (2015). Assessment and comparison of experimental and numerical model studies of cross-laminated timber mechanical connections under cyclic loading. *Construction and Building Materials, 77*, 197-212. Retrieved on July 22, 2017 from http://dx.doi.org.ezproxy.library.ubc.ca/10.1016/j.conbuildmat.2014.12.029

SeismoSoft. (2014). SeismoStruct user manual. *SeismoStruct, Version 7.0*

Shafiq, A. (2018). *Performance-based seismic design and evaluation of eccentrically braced frames with tubular links as bridge bents* (Master of Applied Science).

Shen, Y., Schneider, J., Tesfamariam, S., Stiemer, S. F., & Mu, Z. (2013). Hysteresis behavior of bracket connection in cross-laminated-timber shear walls. *Construction and Building Materials, 48*, 980-991. Retrived on December 12, 2016 from http://dx.doi.org.ezproxy.library.ubc.ca/10.1016/j. conbuildmat2013.07.050

Sherstobitoff, J. (2008). (2008). Time history versus response spectrum analysis. Paper presented at the *Time History Analysis Presented by CSCE,* UBC Vancouver. 9-47.

Structurlam. (2016). *Crosslam CLT technical design guide*. Penticton, BC: Structurlam.

Tesfamariam, S., & Goda, K. (2017). Impact of earthquake types and aftershocks on loss assessment of non-code conforming buildings: Case study with Victoria, British Columbia. *Earthquake Spectra, Preprint*

Tremblay, R., Atkinson, G. M., Bouaanani, N., Daneshvar, P., Leger, P., & Koboevic, S. (2015). Selection and scaling of ground motion time histories for seismic analysis using NBCC 2015. Paper presented at the *11th Canadian Conference on Earthquake Engineering: Canadian Association for Earthquake Engineering,* Victoria, B.C. Canada.

Tremblay, R., Leger, P., & Tu, J. (2001). Inelastic seismic response of concrete shear walls considering P-delta effects. *Canadian Journal of Civil Engineering, 28*, 640-655.

Ventura, C. (2005). *Lecture 04 dynamic analysis of buildings.* Unpublished manuscript.

Wallace, J. (2012). Behavior, design, and modeling of structural walls and coupling beams – lessons from recent laboratory tests and earthquakes. *International Journal of Concrete Structures and Materials, Vol.6*(No.1), 3-18. doi:10.1007/s40069-012-0001-4

Xu, B. H., Bouchaïr, A., Taazount, M., & Vega, E. J. (2009). Numerical and experimental analyses of multiple-dowel steel-to-timber joints in tension perpendicular to grain. *Engineering Structures, 31*(10), 2357-2367. Retrieved on July 18, 2017 from http://dx.doi.org.ezproxy.library.ubc.ca/10.1016/j.engstruct.2009.05.013

Yasumura, M., Kobayashi, K., Okabe, M., Miyake, T., & Matsumoto, K. (2015). Full-scale tests and numerical analysis of low-rise CLT structures under lateral loading. *Journal of Structural Engineering, E4015007-1* doi: 10.1061/(ASCE)ST.1943-541X.000

Yeoh, D. (2011). State of the art on timber-concrete composite structures: Literature review. *Journal of Structural Engineering (New York, N.Y.), 137*(10), 1085; 1085-1095; 1095.

Zhang, C. (2015). Timber-concrete composite systems with ductile connections. *Journal of Structural Engineering (New York, N.Y.), 141*(7)

Zhang, X., Fairhurst, M., & Tannert, T. (2015). Ductility estimation for a novel timber–steel hybrid system. *Journal of Structural Engineering, E4015001-2*

Appendices

Appendix A – Additional information for selection of ground motions

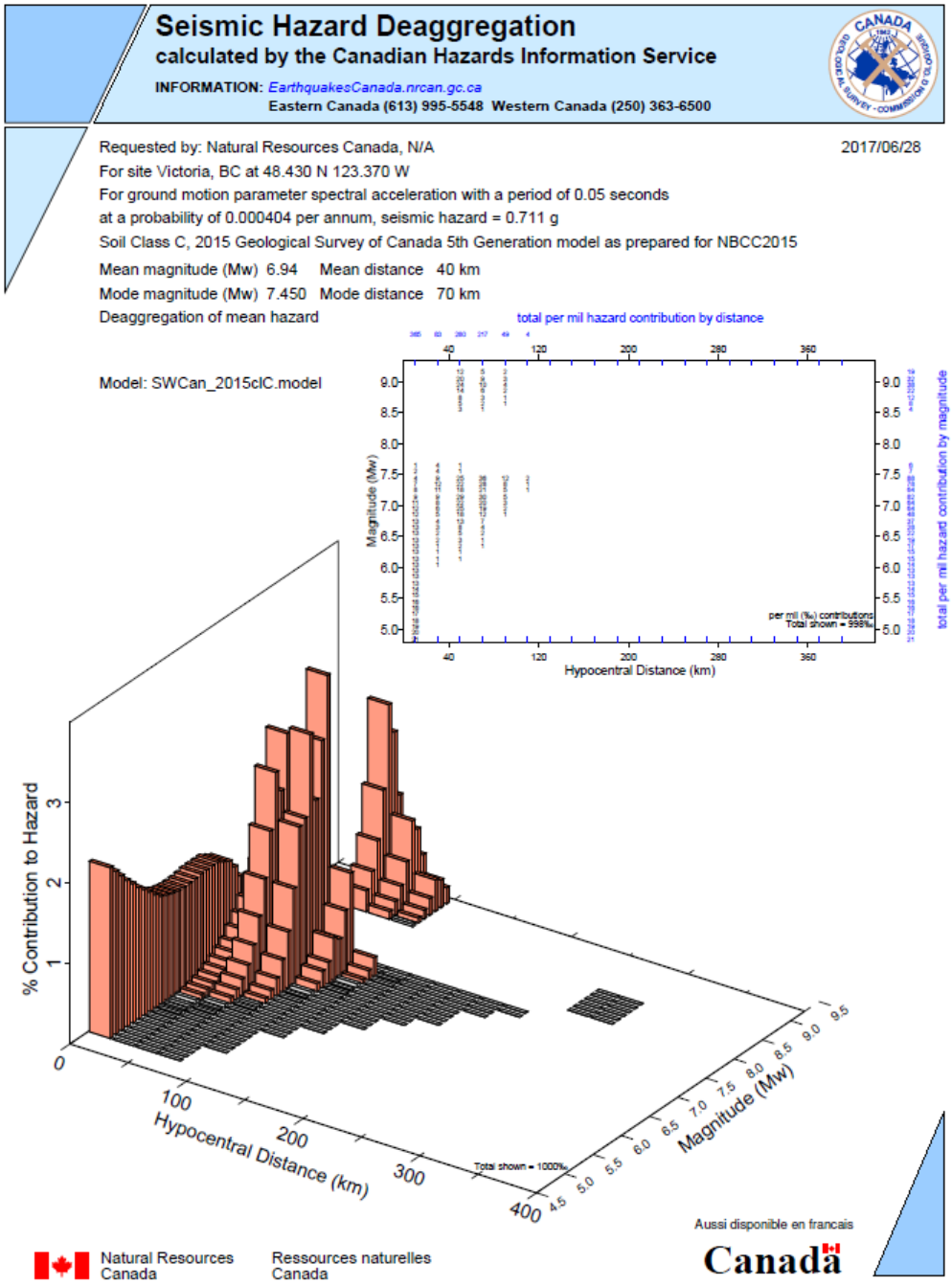

Figure A-1 Deaggregation at 0.05 seconds – Significant contribution from crustal events however in-slab dominating and interface is significant as well [(Canadian Hazards Information Service, 2017) © with permission from publisher. This reproduction is a copy of an official work that is published by the Government of Canada and the reproduction has not been produced in affiliation with, or with the endorsement of the Government of Canada]

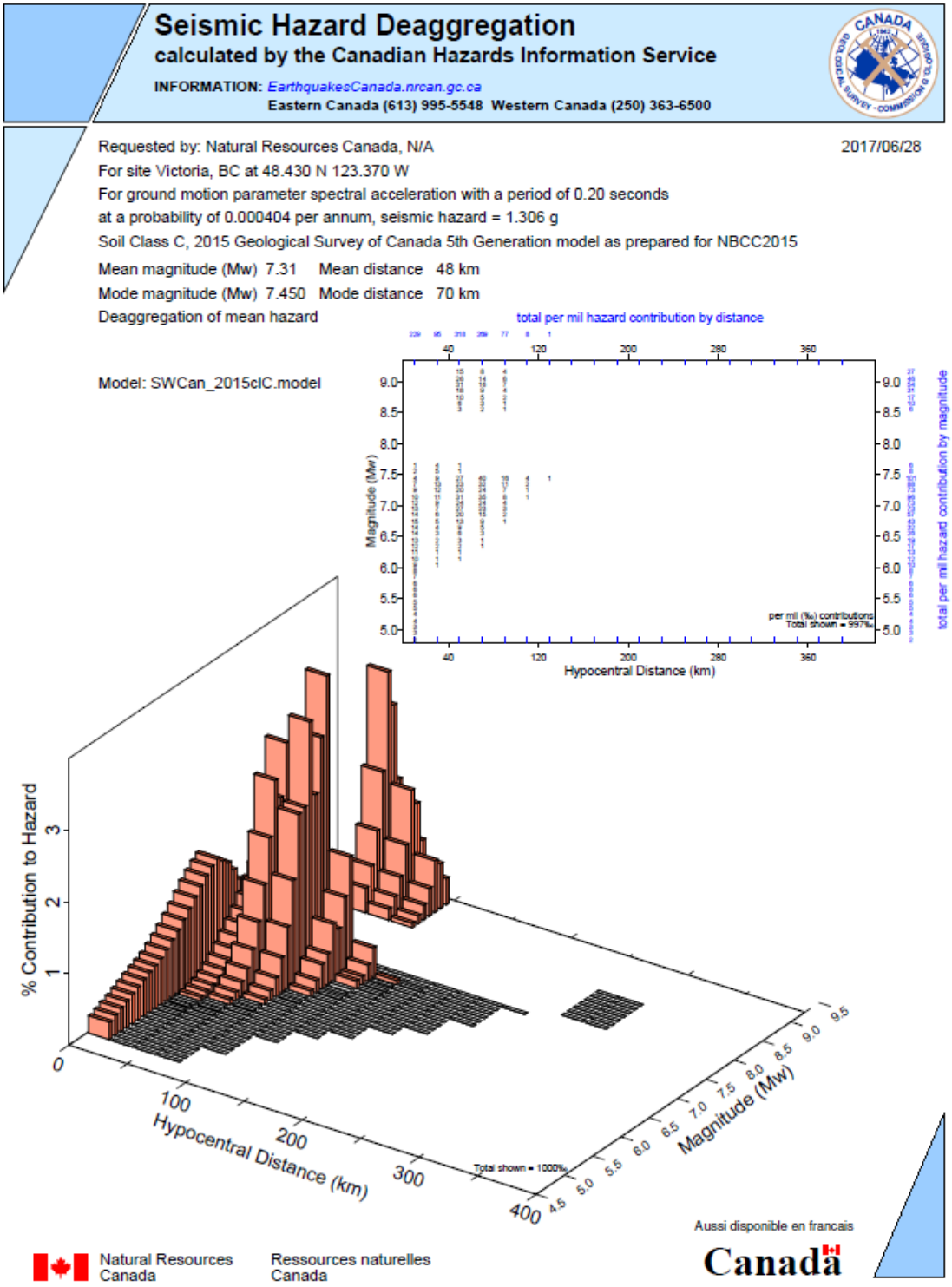

Figure A-2 Deaggregation at 0.2 seconds – In-slab dominates with crustal reducing in importance and interface increasing [(Canadian Hazards Information Service, 2017) © with permission from publisher. This reproduction is a copy of an official work that is published by the Government of Canada and the reproduction has not been produced in affiliation with, or with the endorsement of the Government of Canada]

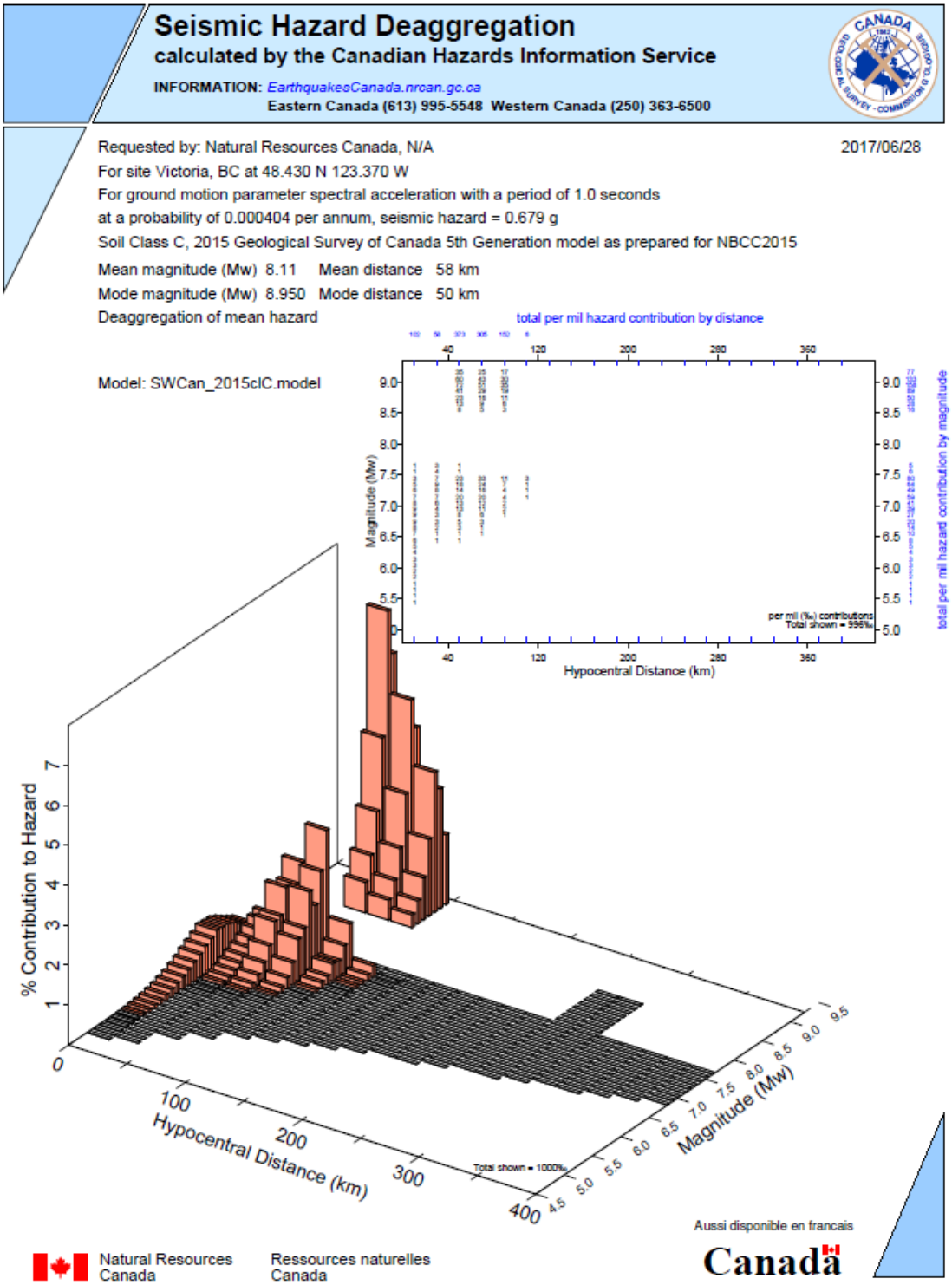

Figure A-3 Deaggregation at 1.0 seconds – Interface events increasingly dominate [(Canadian Hazards Information Service, 2017) © with permission from publisher. This reproduction is a copy of an official work that is published by the Government of Canada and the reproduction has not been produced in affiliation with, or with the endorsement of the Government of Canada]

Table A-1 Scenarios based on global mode and mean methods

Measure	Mean		Mode*		
	Mw	R (km)	Mw	R (km)	Scenario
PGV	7.88	60	7.45	70	In-Slab
PGA	7.27	45	8.95	50	Interface
0.05	6.94	40	7.45	70	In-Slab
0.10	7.04	42	7.45	70	In-Slab
0.20	7.31	48	7.45	70	In-Slab
0.30	7.5	53	7.45	70	In-Slab
0.50	7.68	56	8.95	50	Interface
1.00	8.11	58	8.95	50	Interface
2.00	8.38	62	8.95	50	Interface
5.00	8.73	64	8.95	50	Interface
10.00	8.81	66	8.95	50	Interface

*Mode is sensitive to bin size but still a reasonable estimate. When compared to Tremblay et al. (2015) it seems reasonable considering distance between Vancouver and Victoria is about 90 km's and somewhat orthogonal to the subduction zone fault. The mode is certainly a better estimate than the mean which is clearly skewed by multi-scenario contributions.

Table A-2 Scenarios based on inspection of deaggregation plots

	Crustal		In-slab		Interface		Comments
	M	R	M	R	M	R	
PGV	7.1	10	7.4	70	9	50	Target scenario's may be further refined by having access to source specific deaggregation mode and mean values. The global mode and means do not present the crustal source as the most significant hazard at any period; however, the crustal motions do contribute to the hazard so a suite of crustal ground motions will be obtained. Values within the period range of interest shown in bold. Only these values contribute to the averages.
PGA	6.8	10	7.4	70	9	50	
0.05	6.8	10	7.4	70	9	50	
0.1	6.8	10	7.4	70	9	50	
0.2	6.8	10	7.4	70	9	50	
0.3	6.8	10	7.4	70	9	50	
0.5	6.8	10	7.4	70	9	50	
1	6.9	10	7.4	70	9	50	
2	7.0	20	7.4	70	9	50	
5	7.3	20	7.4	60	9	50	
10	7.3	20	7.4	60	9	50	
Target	6.8	10.0	7.4	70.0	9.0	50.0	

Table A-3 Preliminary selection of three (3) suites of 11 ground motions

Crustal				**Target Scenario:**	**6.8**	**10**	**<1200**
Record	**Database**	**Earthquake**	**Date (dd/mm/yyyy)**	**Station**	**Magnitude (Mw)**	**Hypocentral distance (km)**	**Soil (Vs30) (m/s)**
1	PEER-NGA-West2	El Mayor-Cucapah, Mexico	2010	El Centro Array #3	**7.2**	**41**	**163**
2	PEER-NGA-West2	Darfield, New Zealand	2010	Christchurch Resthaven	**7.0**	**19**	**141**
3	PEER-NGA-West2	Loma Prieta, USA	1989	Foster City - APEEL 1	**6.9**	**44**	**116**
4	PEER-NGA-West2	Iwate, Japan	2008	MYG006	**6.9**	**30**	**147**
5	PEER-NGA-West2	Northridge-01, USA	1994	Carson - Water St	**6.7**	**50**	**161**
6	PEER-NGA-West2	Tottori, Japan	2000	TTR008	**6.6**	**7**	**139**
7	PEER-NGA-West2	Superstition Hills-02, USA	1987	Imperial Valley WLA	**6.5**	**24**	**179**
8	PEER-NGA-West2	Imperial Valley-06, USA	1979	El Centro Array #3	**6.5**	**13**	**163**
9	PEER-NGA-West2	Christchurch, New Zealand	2011	Christchurch Resthaven	**6.2**	**5**	**141**
10	PEER-NGA-West2	Parkfield-02, USA	2004	Parkfield - Fault Zone 1	**6.0**	**3**	**178**
11	KiK-Net/K-Net	Fukushima-Hamadori, Japan	11/4/2011	IBRH10	**6.7**	**11**	**144**
In-slab				**Target Scenario:**	**7.4**	**70**	**<200**
Record	**Database**	**Earthquake**	**Date (dd/mm/yyyy)**	**Station**	**Magnitude (Mw)**	**Hypocentral distance (km)**	**Soil (Vs30) (m/s)**
1	University of Chile / u.chile	Tarapaca, Chile	13/06/2005	TARA05R (Pica)	**7.8**	**125**	**492**
2	University of Chile / u.chile	Tarapaca, Chile	13/06/2005	TARA09R (IDEM)	**7.8**	**144**	**386**
3	Seismotoolbox.ca	Stochastic, Atkinson 2005	r20/04/2018	M7wnaE1_1_2	**7.5**	**70***	**180**
4	Seismotoolbox.ca	Stochastic, Atkinson 2005	r20/04/2018	M7wnaE1_3_4	**7.5**	**70***	**180**
5	KiK-Net/K-Net	Tohoku-Aftershock, Japan	11/3/2011	AOMH13	**7.4**	**144**	**154**
6	University of Chile / u.chile	Punitaqui, Chile	14/10/1997	Illapel	**7.1**	**112**	**502**
7	KiK-Net/K-Net	Hokkaido Aftershock_1, Japan	6/12/2004	NMRH04	**6.9**	**77**	**168**
8	KiK-Net/K-Net	Obihiro, Japan	2/2/2013	TKCH07	**6.9**	**107**	**140**
9	PNSN / COSMOS VDC	Nisqually, Olympia, USA	28/02/2001	DNR Bldg / near 7054	**6.8**	**56**	**300**
10	PNSN / COSMOS VDC	Nisqually, Olympia, USA	28/02/2001	Crown Plaza/ near 7040	**6.8**	**78**	**285**
11	KiK-Net/K-Net	2001 Geiyo, Japan	24/03/2001	EHMH04	**6.7**	**65**	**254**
Interface				**Target Scenario:**	**9**	**50**	**<200**
Record	**Database**	**Earthquake**	**Date (dd/mm/yyyy)**	**Station**	**Magnitude (Mw)**	**Hypocentral distance (km)**	**Soil (Vs30) (m/s)**
1	KiK-Net/K-Net	Tohoku, Japan	11/3/2011	IBRH10	**9.0**	**338**	**144**
2	KiK-Net/K-Net	Tohoku, Japan	11/3/2011	IBRH07	**9.0**	**328**	**107**
3	Seismotoolbox.ca	Stochastic, Atkinson 2005	r20/04/2018	M9wnaE1_1	**9.0**	**60**	**180**
4	Seismotoolbox.ca	Stochastic, Atkinson & Macias 2008	r20/04/2018	amp-vic_1	**9.0**	**60**	**760**
5	University of Chile / u.chile	Maule, Chile	2/27/2010	CONC	**8.8**	**69**	**223**
6	University of Chile / u.chile	Maule, Chile	2/27/2010	CCSP	**8.8**	**70**	**236**
7	Seismotoolbox.ca	Modified Tokachi, Atkinson & Macias 2008	r20/04/2018	vic_084ew	**8.5**	**72**	**760**
8	KiK-Net/K-Net	Kuril, Japan	15/11/2015	NMRH04	**8.4**	**790**	**180**
9	University of Chile / COSMOS VDC	Valparaiso, Chile	3/3/1985	RANC01S (Rapel)	**8.0**	**85**	**108**
10	KiK-Net/K-Net	Hokkaido (Tokachi-Oki), Japan	26/09/2003	TKCH07	**8.0**	**125**	**140**
11	KiK-Net/K-Net	Hokkaido (Tokachi-Oki), Japan	26/09/2003	KSRH02	**8.0**	**150**	**219**

Table A-4 Detailed notes for final ground motion suites (continues horizontally on next page)

Basic identification				Pre-processing					Target for selection					
Hazard and range	**Earthquake**		**Date (DD/MM/ YYYY)**	**Time step initial (s)**	**Time step Inter-polated (s)**	**Baseline correction applied**	**Filter applied**	**D,o (s)**	**Magnitude target (Mw)**	**Magnitude (Mw)**	**Distance target (km)**	**Distance (km)**	**Soil target (m/s)**	**Soil site (m/s)**
Crustal 0.03 < Trs < 0.40	**Darfield, NZ**	H1	September 4, 2010	0.005	0.010	Quadratic	Pre-processed by others (no update req'd.)	149.995	6.8	7.0	10	19	Site class E (V<180m/s) but practically 100<V<200 is a realistic target range	141
		H2						149.980						
	Christchurch, NZ	H1	February 22, 2011			Linear		50.000		6.2		5		
		H2												
	Imperial Valley, CA, USA	H1	October 15, 1979					39.590		6.5		13		163
		H2												
	Tottori, Japan	H1	October 6, 2010	0.010		Cubic		299.970		6.6		7		139
		H2						299.960						
	Parkfield, CA, USA	H1	September 28, 2004	0.005		Linear		20.970		6.0		3		178
		H2												
In-slab 0.03 < Trs < 0.80	**Tarapaca, Chile**	Pica - H1	June 13, 2005	0.005		Quadratic	Butterworth (0.1 - 25 Hz Bandpass)	251.980	7.4	7.8	70	125		492
		Pica - H2						55.800				144		386
		Idiem - H1												
		Idiem - H2												
	Obihiro, Japan	H1	February 2, 2013	0.010		Linear		299.980		6.9		107		140
		H2												
	Nisqually, WA, USA	Crown - H1	February 28, 2001	0.005		no update req'd.	no update req'd.	95.980		6.8		78		285
		Crown - H2				Linear								
		DNR - H1				no update req'd.		151.980				56		300
		DNR - H2												
Interface 0.30 < Trs < 1.50	**Tohoku, Japan**	H1	March 11, 2011	0.010		Quadratic	Butterworth (0.1 - 25 Hz Bandpass)	262.480	9.0	9.0	50	338		144
		H2												
	Maule, Chile	Conc - H1	February 27, 2010	0.005				141.670		8.8		69		223
		Conc - H2												
		CCSP - H1				Cubic		143.260				70		236
		CCSP - H2												
	Hokkaido, Japan	T - H1	September 26, 2003			Linear		299.990		8.0		125		140
		T - H2												
		K - H1										150		219
		K - H2												

Table A-4 Detailed notes for final ground motion suites (concluded)

Basic identification				Linear scaling results			Detailed identification				
Hazard and range	**Earthquake**		**Date (DD/MM/ YYYY)**	**Individual scale factor**	**Suite scale factor**	**Comments**	**Station and Channel**	**Recording site**	**Data base**	**Data retrieval**	**Flatfile/documentation**
Crustal 0.03 < Trs < 0.40	**Darfield, NZ**	H1	September 4, 2010	1.64	1.04	Balance minimizing scale factor with M-R relationships and soil conditions	RSN6959_DARFIELD_REHSN02E	Resthaven	PEER NGA West2		
		H2					RSN6959_DARFIELD_REHSS88E				
	Christchurch, NZ	H1	February 22, 2011	1.38			RSN8123_CCHURCH_REHSN02E				
		H2					RSN8123_CCHURCH_REHSS88E				
	Imperial Valley, CA, USA	H1	October 15, 1979	1.69			RSN178_IMPVALL.H_H-E03140	E.C.A #3			
		H2					RSN178_IMPVALL.H_H-E03230				
	Tottori, Japan	H1	October 6, 2010	1.48			RSN3965_TOTTORI_TTR008EW	TTR008			
		H2					RSN3965_TOTTORI_TTR008NS				
	Parkfield, CA, USA	H1	September 28, 2004	0.88			RSN4107_PARK2004_COW090	Parkfield FZ 1			
		H2					RSN4107_PARK2004_COW360				
In-slab 0.03 < Trs < 0.80	**Tarapaca, Chile**	Pica - H1	June 13, 2005	0.88	1.63	Relaxed soil matching criteria;	PICA S/N 2799 - CHAN 1: EW	Pica	Universidad de Chile - Renadic		Bastias et al (2016)
		Pica - H2					PICA S/N 2799 - CHAN 2: NS				
		Idiem - H1		2.61			IQUIQUE IDIEM S/N 7051 - CHAN 1: EW	Iquique Idiem			
		Idiem - H2					IQUIQUE IDIEM S/N 7051 - CHAN NS				
	Obihiro, Japan	H1	February 2, 2013	1.53			TKCH071302022317 - EW	TKCH07	K-Net/KiK-Net		Dawood et al (2016)
		H2					TKCH071302022317 - NS				
	Nisqually, WA, USA	Crown - H1	February 28, 2001	2.07		Not free-field	7010g	Seattle Crown Plaza	USGS / PNSN	COSMOS VDC	Filliatrault et al (2011); ESCWEB (r2018)
		Crown - H2					77010j				
		DNR - H1		2.64			7015a	DNR			
		DNR - H2					7015c				
Interface 0.30 < Trs < 1.50	**Tohoku, Japan**	H1	March 11, 2011	1.63	1.24	Relax soil criteria	IBRH101103111446 - EW	IBRH10	K-Net/KiK-Net		Dawood et al (2016)
		H2					IBRH101103111446 - NS				
	Maule, Chile	Conc - H1	February 27, 2010	1.75			Concepcion1002271 S/N 5003 - CHAN 1 L	Conc	Universidad de Chile - Renadic		Bastias et al (2016)
		Conc - H2					Concepcion1002271 S/N 5003 - CHAN 2				
		CCSP - H1		1.8			Constitucion1002271 - S/N 4598 - CHAN 01 L	Cons			
		CCSP - H2					Constitucion1002271 - S/N 4598 - CHAN 2				
	Hokkaido, Japan	T - H1	September 26, 2003	1.05			TKCH070309260450 - EW	TKCH07	K-Net/KiK-Net		Dawood et al (2016)
		T - H2					TKCH070309260450 - NS				
		K - H1		1.37			KSRH020309260450 - EW	KSRH02			
		K - H2					KSRH020309260450 - NS				